# USE OF TIME-DOMAIN REFLECTOMETRY TO CHARACTERIZE THERMAL AND HYDRAULIC PROPERTIES OF UNSATURATED SANDS

by

XUELIN WANG

DISSERTATION

Submitted in partial fulfillment of the requirements
for the degree of Doctor of Philosophy at
The University of Texas at Arlington
December 2020

Arlington, Texas

Supervising Committee:

Xinbao Yu, Supervising Professor
Laureano Hoyos
MD. Sahadat Hossain
Saibun Tjuatja
Dong-Jun Seo

# ACKNOWLEDGMENTS

This dissertation would not have been possible without inspiration and encouragement of many extraordinary individuals. I sincerely offer my thanks and acknowledgment to all of them for being part of this journey and making this dissertation accessible.

As a Ph.D. candidate, I was grateful to have Dr. Xinbao Yu as a mentor, adviser, and supervisor. Dr. Yu was always there to keep me on track, hold me responsible, and provide academic support. I appreciate his concern, time, and discipline. His patience and support have been an inspiration, and I sincerely value his fellowship. He encouraged me when we both faced obstacles and always conveyed a trust and optimism, which helped me overcome the obstacles.

I would like to thank the members of my committee, Dr. Laureano Hoyos, Dr. MD. Sahadat Hossain, Dr. Dong-Jun Seo, and Dr. Saibun Tjuatja for their invaluable feedback and encouragement. I would also like to thank Dr. Haiying Huang, Dr. Jungchih Chiao, Dr. Aravind Pedarla, Dr. Aritra Banerjee, and Dr. Tejo V. Bheemasetti for sharing with me their experience and extensive knowledge through their courses of study and laboratory works.

I am forever thankful to my colleagues in Dr. Yu's research group throughout the years we worked together. I offer sincere thanks to Dr. Nan Zhang, Saurav Sinha, Christian Gonzales, Nice Kaneza, Dr. Teng Li, Gang Lei, Sandesh Gautam, and Omid Habibzadeh for their friendship and support and for providing a dedicated working environment. I am also grateful for all the visiting scholars in Dr. Yu's research group: Dr. Xiang Chen, Dr. Yankai Wu, and Dr. Chunxiang Wang. I will always be thankful for their prominent help, encouragement, and heartfelt compliments.

Finally, I genuinely thank my family for their uninterrupted and incomparable help, love, and support. I am forever grateful to my parents for giving me the opportunities and experiences that have made me who I am. They altruistically encouraged me to discover new directions in life and seek my destiny. This journey would not be possible without them, and I dedicate this dissertation to my parents.

December 01, 2020

TABLE OF CONTENTS

LIST OF ILLUSTRATIONS

LIST OF TABLES

ABSTRACT

USE OF TIME-DOMAIN REFLECTOMETRY TO
CHARACTERIZE THERMAL AND HYDRAULIC PROPERTIES OF
UNSATURATED SANDS

Xuelin Wang, Ph.D.

The University of Texas at Arlington, 2020

Supervising Professor: Xinbao Yu

Unsaturated soil is an essential consideration for many geotechnical engineering fields, for example, soil bearing capacity, soil lateral earth pressure, slope stability analysis, and seepage-related problems. Thermal-hydro-mechanical (THM) processes govern the behavior of unsaturated soils. Therefore, it is critical to simultaneously measure soil moisture, density, and thermal properties to better study THM processes.

A thermo-time-domain reflectometry (thermo-TDR) sensor, a dual-probe for both soil moisture and thermal properties, is improved (based on its previous design) and fully calibrated through various soils at different soil moisture circumstances. Nine different chemical reagents with known dielectric constant were utilized to perform calibration of the dielectric constant. Potassium chloride and sodium chloride solutions of different concentrations were used to implement the calibration of electrical conductivity. The effective sampling area for the thermo-

TDR sensor was determined using the COMSOL Multiphysics and MATLAB based on the transverse electromagnetic (TEM) propagation mode. The thermo-TDR sensor tested eight types of sands and clays compacted at different moisture contents. The accuracy and precision of thermal properties measurement were evaluated by comparing and analyzing the measurement results from a KD2 Pro thermal properties analyzer. Validation of temperature effects for dielectric constant and electrical conductivity was performed with sand and distilled water.

A modified hanging column device (MHCD) furnished with a lab-built thermo-TDR sensor, a T5x tensiometer, and a KD2 Pro thermal properties analyzer with a TR-1 thermal needle were used to test three sands at the laboratory (24 °C) and environmental chamber (10 °C and 2 °C). The measured data indicate that the hydraulic and thermal properties are functions of the drainage and evaporation processes. The measured results, thermal conductivity dry-out curves (TCDC), and soil-water characteristic curve (SWCC) were determined from the measured results. The effect of sand type and temperature on the TCDC and SWCC curves are evaluated.

The validation of the soil-water characteristic curve (SWCC) via the MHCD test method was performed using three SWCC models developed by Brooks and Corey (1964), van Genuchten (1980), and Fredlund and Xing (1994). The fitted curves' performance using the Fredlund and Xing model was better than the other two models (Brooks and Corey and van Genuchten models).

Numerical models are developed to model the sand dry-out processes (drainage and evaporating) during the MHCD test. The developed models will help to understand the coupled THM processes of sands.

# CHAPTER 1 INTRODUCTION

## 1.1 Background

Water plays a significant role in the behavior of unsaturated soils. For example, a person can easily walk on wet sand beach at low tide and sink at high tide. This example shows the beach sand to have a higher strength during drainage and a lower strength at saturation. This observation inspires the exploration of unsaturated soils' working mechanism subject to drainage and dry-out processes. In addition to the hydro process, temperature also plays an essential role in the hydraulic process, such as the moisture flux induced by a thermal gradient. In recent years, the development of active thermal earth-structures and thermal energy storage has necessitated the study of temperature effects on unsaturated soil behavior.

While the growth of mechanisms and techniques in unsaturated soil mechanics requires principles extracted from hydraulics, interfacial physics, and mechanics, it is expedient to categorize the numerous geotechnical engineering problems which make up the three general phenomena for unsaturated soil, i.e., the flow phenomena, stress phenomena, and deformation phenomena. The flow phenomena primarily involve the application of hydraulics and interfacial physics principles. Many seepage-related problems may be effectively treated by applying thermodynamic potential theory with tiny or no solid mechanics in unsaturated soil mechanics. The stress phenomena require both mechanical and chemical equilibrium. Terzaghi's effective stress, which is the foundation of soil mechanics at saturation, is either inappropriate or ineffective when it comes to completely explaining the failure conditions or stress distributions in unsaturated soil. The theory depicting used to depict the situation of stress and failure in unsaturated soil involves the attention of pore water thermodynamic properties according to soil suction, grain size distribution, the degree of saturation, and the resultant interparticle forces. The deformation

phenomena require physical changes to qualify large deformation or strains. This deformation is frequently caused by changes in the moisture situation in the unsaturated soil (Lu and Likos 2004).

In general, there are three regimes conceptualized when soil is transitioning from saturation to dry, as shown in Figure 1.1. The capillary fringe zone is a saturated regime. The continuous capillary or funicular zone is an unsaturated regime, and the residual or pendular zone is an isolated, discontinuous water phase regime.

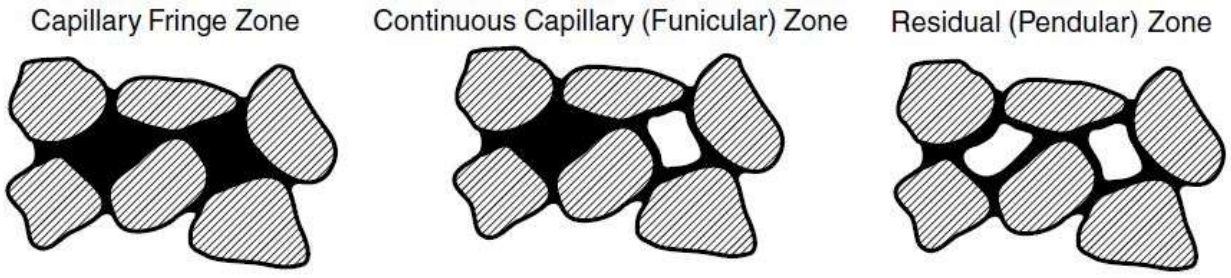


Figure 1.1 Schematic diagram of the unsaturated soil zone (Lu and Likos 2004)

Childs (1969) assumed a theoretical cross-section cross a soil sample that further elucidate ink-bottle hysteresis, as shown in Figure 1.2. The soil system is initially saturated in the figure, with the air-water interface located above the soil surface in Stage 1. The pore pressure is positive at this stage, having a magnitude equal to hydrostatic pressure dominated by the standing water's height. The solid-lines, corresponding to Stages 2 - 6, indicate promotes air-water interface positions. The pore pressure is sequentially decreased into a negative regime, thereby inducing the pore water to withdraw into increasingly smaller pore narrowings with the soil sample. The air-water interface's curvature describes the matric suction at each stage, which gets harsher as the drainage changes, and the pore-water withdrawal continues inside the increasing suction. The dashed-lines indicate Stages 7 - 9 the air-water interface positions experience a succeeding refilling process (i.e., the conduct stages shown in Fig. 1.2). In order to refill the pore structure, the air-

water interface must continue to undergo the extensive pore narrowing as shown inside the surroundings of Stages 8 and 9. The suction should facilitate a decrease of the narrowing to a point low enough to establish an equilibrium with the curvature so the filling process can proceed as the curvature within this pore narrowing becomes progressively less severe. The net effect is that the system's moisture content during the refilling process is methodically less than that shown based on the same magnitude of suction during the drainage process.

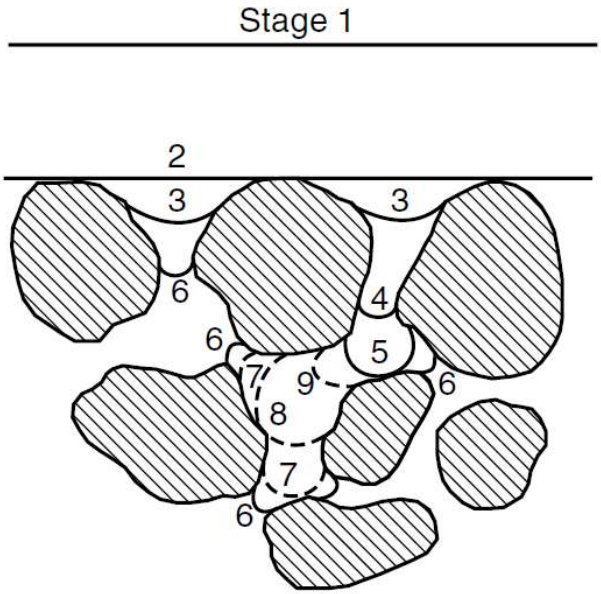


Figure 1.2 Theoretical unsaturated soil system at conduct stages of drainage and rewetting (Childs 1969)

In the study of unsaturated soil drainage and evaporation, temperature effects are an essential condition that must be considered. The temperature effects on soil properties are contingent on hydraulic conductivity, stress history, and thermal history (Burghignoli et al. 2000; Hueckel et al. 2009). Uchaipichat and Khalili (2009) reported temperature changes can cause volume change in unsaturated soils. Nevertheless, for unsaturated soils, the critical state shear strength envelope is not dependent on temperature change (Alsherif and McCartney 2016). A pore

pressure difference or temperature gradient could induce water migration. However, matric suction decreases with the temperature at a steady water content, and the water content decreases with the temperature at a steady matric suction. The cause could be ascribed to a reduction in the surface tension of water and a thermal-induced variation in the contact angle at the water soil particle interface (Bachmann and van der Ploeg 2002).

## 1.2 Problem Statement

This research focuses on understanding the soil thermal and hydraulic properties of sands during dry-out processes by determining how the temperature affects the soil-water characteristics curve (SWCC). Sensors are needed to measure the soil thermal conductivity and hydraulic properties (moisture and density) accurately over the complete saturation regime and account for the effect of temperature. However, there are no verified sensors that can provide accurate soil moisture measurements and density when the soil is subjected to moisture loss from saturation to dry and significant density changes. Experimental techniques for precise simultaneous measurement of soil suction, water content, and thermal properties were attempted. The soil-water characteristic curve (SWCC) and thermal conductivity dry-out curve (TCDC) are recognized methods used to present a relationship between soil matric suction and moisture content. However, very few efforts were found in the geotechnical literature, which directly and simultaneously measures the volumetric moisture content, soil matric suction, and thermal conductivity. Moreover, studies on soil volume change during drainage are minimal. The research presented in this dissertation attempts to narrow the information gap in all of these areas of study.

## 1.3 Research Objectives

This research's primary objective is to accurately measure soil moisture, density, and thermal conductivity of sands undergoing the dry-out process. The research tasks used to accomplish the above research objective are listed below.

1. Develop a calibration model for thermo-TDR to accurately measure moisture and density for unsaturated and nearly saturated soils.
2. Measure thermal conductivities of soils for compacted sands and clay.
3. Measure thermal conductivities and suction of sands using the modified hanging column device (MHCD) under different temperatures.
4. Develop a numerical model to predict the dry-out process in the MHCD test.

## 1.4 Dissertation Outline

This dissertation consists of six chapters: introduction (Chapter 1), literature review (Chapter 2), design, fabrication, and evaluation of Thermo-TDR sensors (Chapter 3), modified hanging column device (MHCD) test (Chapter 4), development of SWCC and TCDC models (Chapter 5), and summary, conclusions, and recommendations (Chapter 6).

Chapter 1 introduces this research, including a research background that facilitates understanding of thermal and suction changes in sands during dry-out processes. The problem statement comes from former research and the research objectives for this research.

Chapter 2 demonstrates a summary of former research through an: (1) introduction, (2) soil moisture measurements, (3) time-domain reflectometry (TDR) techniques, (4) SWCC and TCDC, (5) soil thermal properties and applications, and (6) prediction models.

Chapter 3 demonstrates the design, fabrication, and evaluation of thermo-TDR sensors. Sensor calibrations include dielectric constant and electrical conductivity. The sensor evaluations

include in-depth analyses of moisture content, dry density, and thermal properties. The effective sampling area for the thermo-TDR sensor is in this chapter as well.

Chapter 4 demonstrates modified hanging column device tests and comparable results for unsaturated soil exploration.

Chapter 5 demonstrates the development of models during sand dry-out processes. The developed models facilitate understanding of the coupled THM processes of sands. A series of discrete data points contain the relationship between soil matric suction and volumetric moisture content provided from experimental techniques to measure the soil-water characteristic curve (SWCC). A thermal conductivity dry-out curve (TCDC) model was predicted from related experimental results.

Chapter 6 provides a relevant summary and conclusions of this research as well as recommendation for future work.

# 2 CHAPTER 2 LITERATURE REVIEW

## 2.1 Introduction

This chapter summarizes previous literature concerning the research objective of this dissertation. The review is, therefore divided into five parts: (1) soil moisture measurements, (2) the time-domain reflectometry technique, (3) the soil-water characteristic curve (SWCC) and the thermal conductivity dry-out curve (TCDC), (4) soil thermal properties and applications, and (5) prediction models.

## 2.2 Soil Moisture Measurement

Soil moisture is an essential part of the soil's three-phase system (air, moisture, and solids) (Craig 2004; Das and Sobhan 2013). Earlier researchers developed some techniques for soil moisture measurement, for example, dielectric techniques such as capacitance, frequency domain reflectometry, and time-domain reflectometry (TDR) (Arulanandan 1991; Bhat and Singh 2007; Campbell 1990; Ferré et al. 1998; Gaskin and Miller 1996; Hilhorst et al. 2001; Jacobsen and Schjønning 1993; Mittelbach et al. 2012; Rao and Singh 2011; Rinaldi and Francisca 1999; Robinson and Dean 1993; Rohini and Singh 2004; Schwartz et al. 2008; Selig and Mansukhani 1975; Topp et al. 1982; Whalley et al. 1992), neutron scattering (Amoozegar et al. 1989; Elder and Rasmussen 1994; Evett 2000; Huang et al. 2011; Jayawardane et al. 1984; Li et al. 2003), soil resistivity (Sreedeep et al. 2004; Zazueta and Xin 1994), and thermal gravimetric analysis (ASTM 2008; Hillel 2013; Terhoeven-Urselmans et al. 2008).

Elimination of moisture from the soil specimen via chemical reaction or evaporation is a classical technique for soil moisture measurement (SU et al. 2014). Electrical properties of the soil (capacitance, dielectric constant, impedance, and soil resistivity), infrared rays, soil moisture

potential, and radioactive techniques (gamma attenuation, neutron scattering, and optical techniques are modern soil moisture measurement techniques (Lekshmi et al. 2014).

The capacitance technique, frequency-domain reflectometry (FDR), and time-domain reflectometry (TDR) are the practical techniques used to determine the soil's dielectric property for measuring soil moisture content (Lekshmi et al. 2014). The inappreciable fluctuations of temperature on electrical permittivity measurements make the FDR and TDR more accurate in determining soil moisture in shallow soils (Hilhorst 2000; Topp et al. 1982). TDR has become widely recognized for attaining the soil moisture content measurement (Hilhorst 2000; Ledieu et al. 1986; Robinson et al. 2008; Rohini and Singh 2004; Topp et al. 1980).

TDR determines the dielectric permittivity of the soil mass by measuring the delay in time between an incident and reflected electromagnetic pulses (Arulanandan 1991; Campbell 1990; Jacobsen and Schjønning 1993; Kupfer et al. 2007; Selig and Mansukhani 1975; Topp et al. 1982; Topp et al. 2000). A capacitance-based technique has an oscillation circuit and a sensing part embedded in the soil. This technique obtains the dielectric permittivity of a medium by the charge time measurement of a capacitor (Gardner et al. 1998; Minet et al. 2010; Robinson and Dean 1993; Whalley et al. 1992). The capacitor works with the oscillator to form a resonant circuit, and changes in soil moisture content are detected by changes occurring in the operating frequency (Lekshmi et al. 2014).

An electrical impedance sensor consists of probes that use coaxial impedance dielectric reflectometry to measure the dielectric constant of the soil. Subsequently, the dielectric constant will measure the amplitude of the reflected and incident signals in volts. The volt is related to the impedance and dielectric permittivity for soil moisture content measurement (Gaskin and Miller 1996; Rinaldi and Francisca 1999). Soil moisture content measurements also include ground

penetrating radar (GPR) (Robert 1998), micro electro mechanical system (MEMS) (Jackson et al. 2008), and soil resistivity sensor (Robinson et al. 2008).

## 2.3 Time-Domain Reflectometry (TDR) Technique

The time-domain reflectometry (TDR) technique has high multifunctionality, precision, relatively low completion costs, and the possibility of accomplishing continuous real-time measurements. TDR also makes the performance of continuous real-time measurements possible. An extra advantage is that TDR can be automated, and through multiplexers, it can use several sensors simultaneously with a single measurement device. For instance, Campbell Scientific manufactures the TDR200 time-domain reflectometer with one SDM8X50 50-ohm coaxial multiplexer that can measure eight channels simultaneously (Persico et al. 2019).

One another primary application for TDR is the dielectric characterization of materials. Moreover, TDR has been primarily used in water content measurements. TDR is widely used in field monitoring of soil moisture content. Several theoretical and empirical models have been exploited to deduce soil moisture content by TDR measurements over the years. Furthermore, geotechnical engineers use TDR to assess distributed pressure profiles, monitor liquefaction of soils and detect organic pollutants in sandy soils. Landslide monitoring is also an application for TDR.

The principles of the TDR technique are used to measure soil moisture content, as described in this section.

### 2.3.1 What is TDR?

The microwave reflectometry measurement must be taken before introducing TDR. Generally, two primary components are included in the measurements of microwave reflectometry.

One is the measurement cells found in the tested material by using the probe. Another one is the device for electromagnetic signal generation and reception. Frequency-domain reflectometry (FDR) and time-domain reflectometry (TDR) are two methods used to perform microwave-reflectometry-based measurements. In general, FDR instrumentation is more expensive than TDR instrumentation (Persico et al. 2019).

A TDR operates like a radar. A fast rise pulse is shot into the coaxial cable system near the end. As the pulse proceeds down the coaxial cable, any characteristic impedance variation will cause some of the incoming signals to reflect towards the source. The reflected pulse constituent will be positive or negative depending on if the reflection is plotted against time on a device display, such as an oscilloscope (Hernandez-Mejia and Perkel 2016).

### 2.3.2 Configuration of TDR Sensors

A two-probe sensor with an impedance-matching transformer has been widely used, as shown in Figure 2.1(B). Some researchers have used a two-probe sensor without an impedance-matching transformer and have had corresponding soil moisture content measurement (Kelly et al. 1995; Ledieu et al. 1986; Malicki et al. 1992; Malicki and Skierucha 1989; Rajkai and Ryden 1992; Stein and Kane 1983). However, Stein and Kane (1983) warned against risking confrontation with stray currents and voltages that could increase measurement precariousness when an impedance-matching transformer is not employed.

Zegelin et al. (1989) presented a multi-probe sensor imitating a coaxial cell, like the sensors Fellner-Feldegg (1969) and Topp et al. (1980) used. Therefore, a multi-probe sensor not required an impedance-matching transformer. The schematic diagram for a three-probe sensor is shown in Figure 2.1(A), which is useful for regular use.

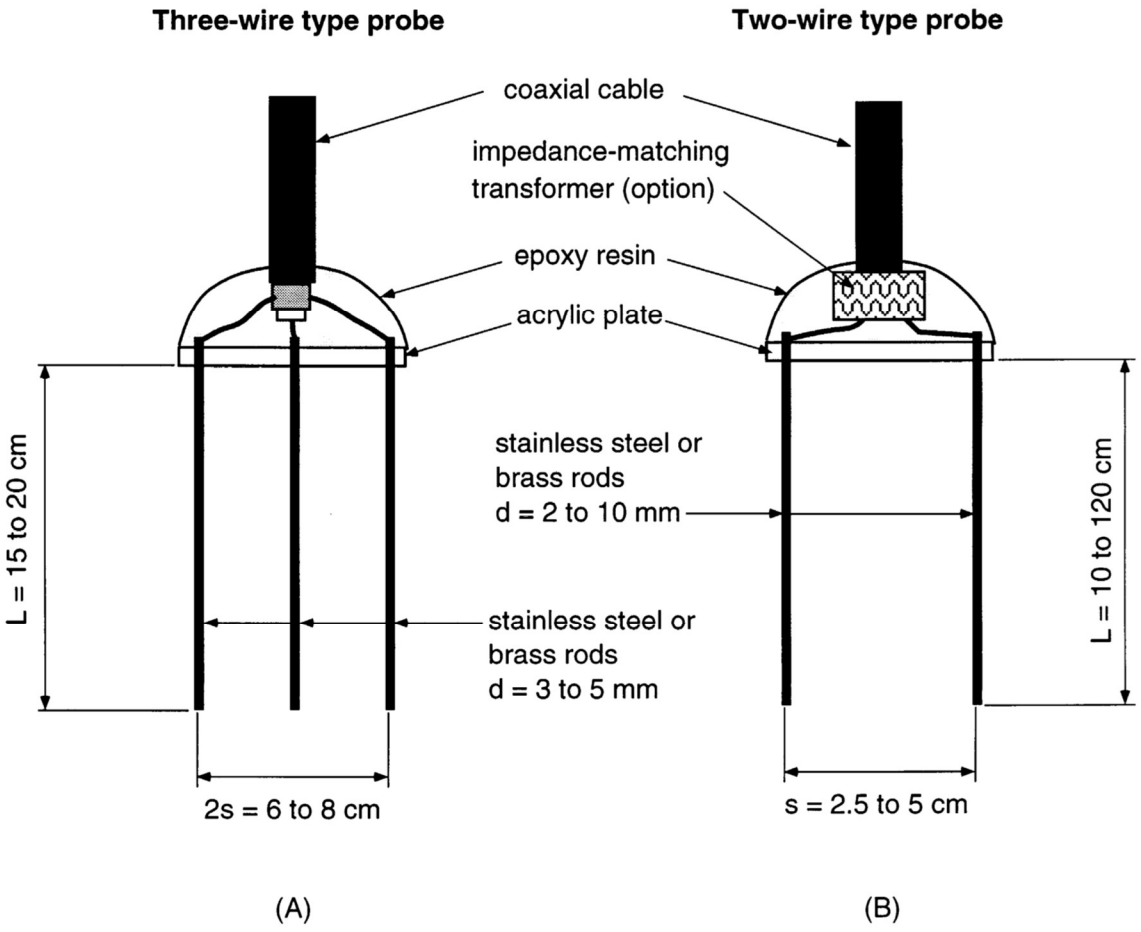


Figure 2.1 Schematic diagram of typical sensors: (A) three-probe sensor, and (B) two-probe sensor

Another type of sensor is presented to precisely measure soil volumetric moisture content (Selker et al. 1993). The sensor is a rectangular shape, as shown in Figure 2.2(A).

Recently, stainless steel rods have been the predominant material for sensors; however, brass rods were preferred earlier. Davis (1979) introduced polyvinyl chloride pipes covered with longitudinal, variable-width aluminum strips as an electric pole, shown in Figure 2.2(B).

A sensor with multiple rod diameters was linked together, as shown in Figure 2.2(C).

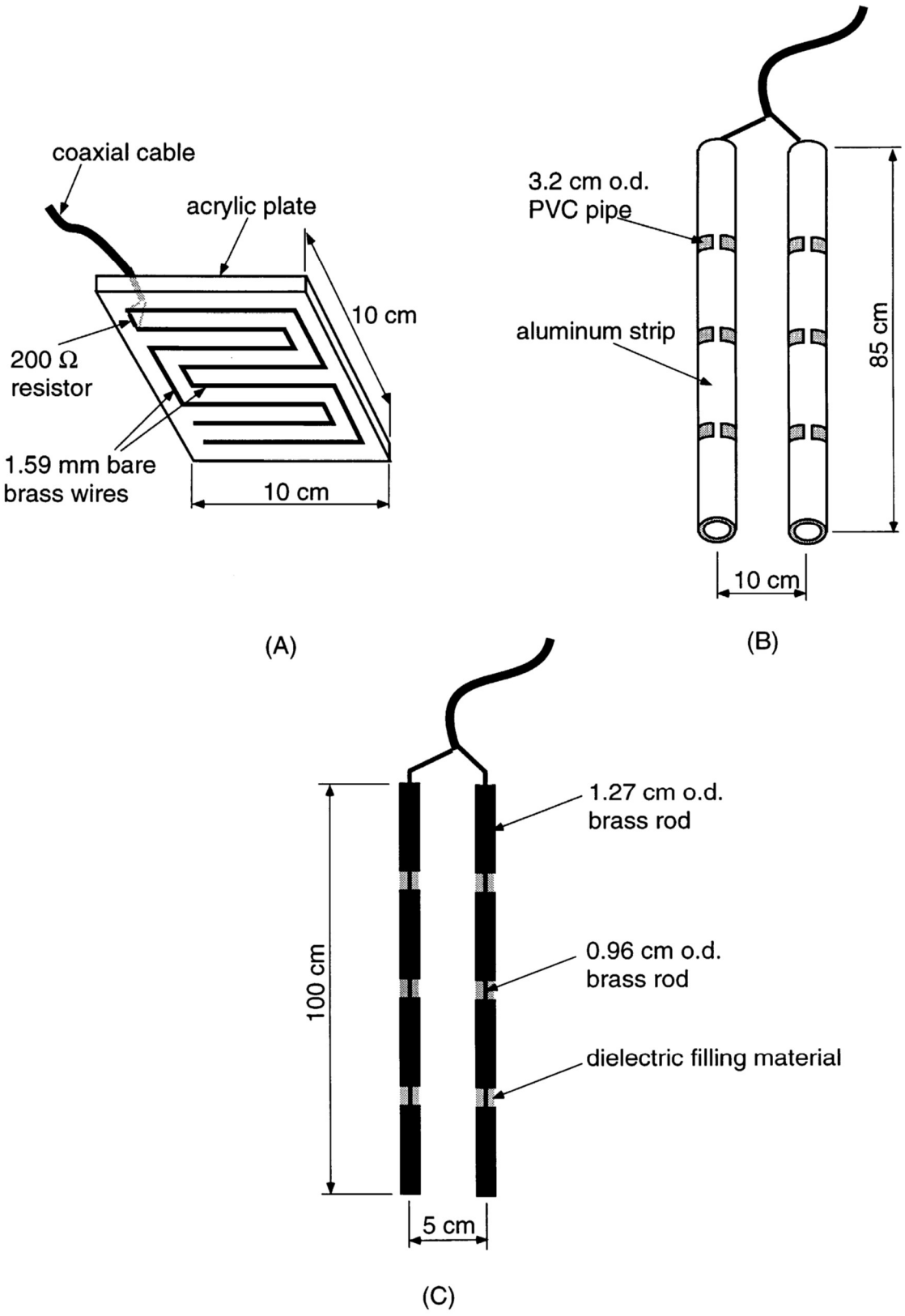


Figure 2.2 Schematic diagram of three different types of sensors (Davis 1979; Selker et al. 1993)

### 2.3.3 Soil Moisture Content Measurement by TDR

TDR obtains the dielectric constant ($K_a$) by recording electromagnetic waves' travel time sent from a cable tester (Figure 2.3) thrust in a medium. Electromagnetic waves transmit via a coaxial cable to a TDR sensor, generally a stainless steel or brass rod. The portion of an incoming electromagnetic wave is reflected at the probe's head because of the cable and probe impedance difference. The residual of the wave transmits via the sensor until it attains the probe's end, at which the wave is reflected.

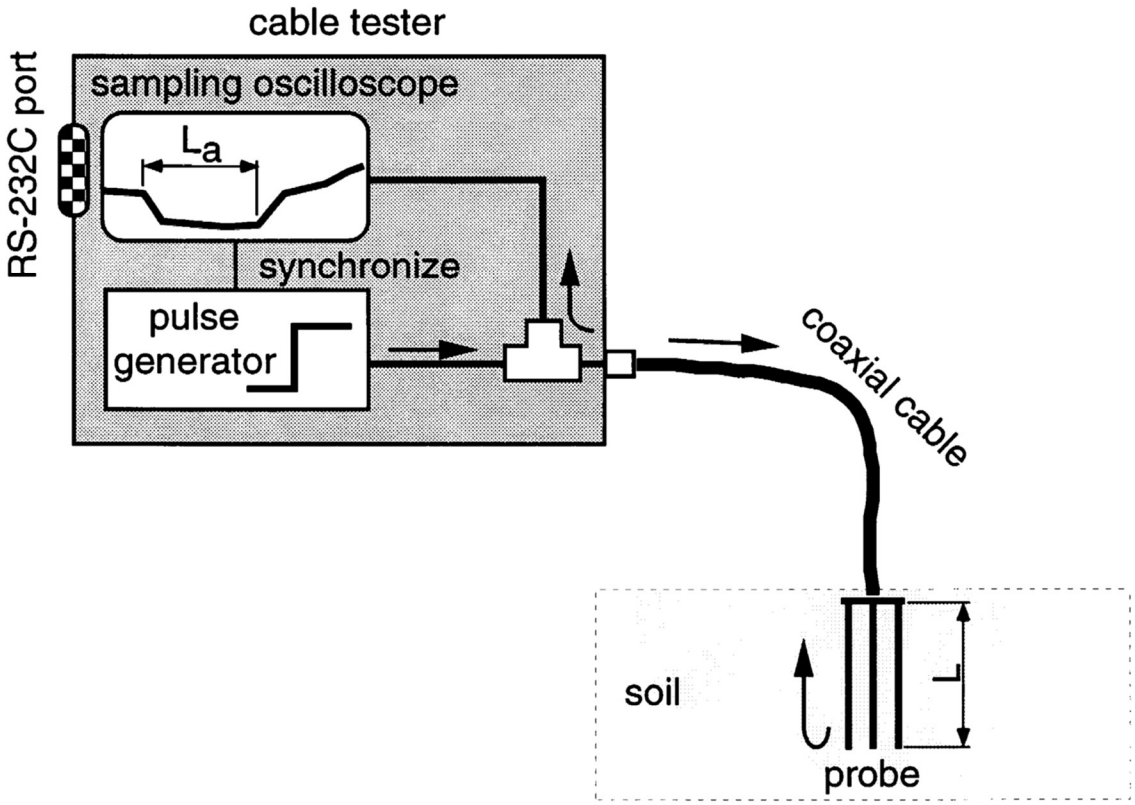


Figure 2.3 Schematic diagram of TDR to measure dielectric constant and the bulk electrical conductivity of soil (Noborio 2001)

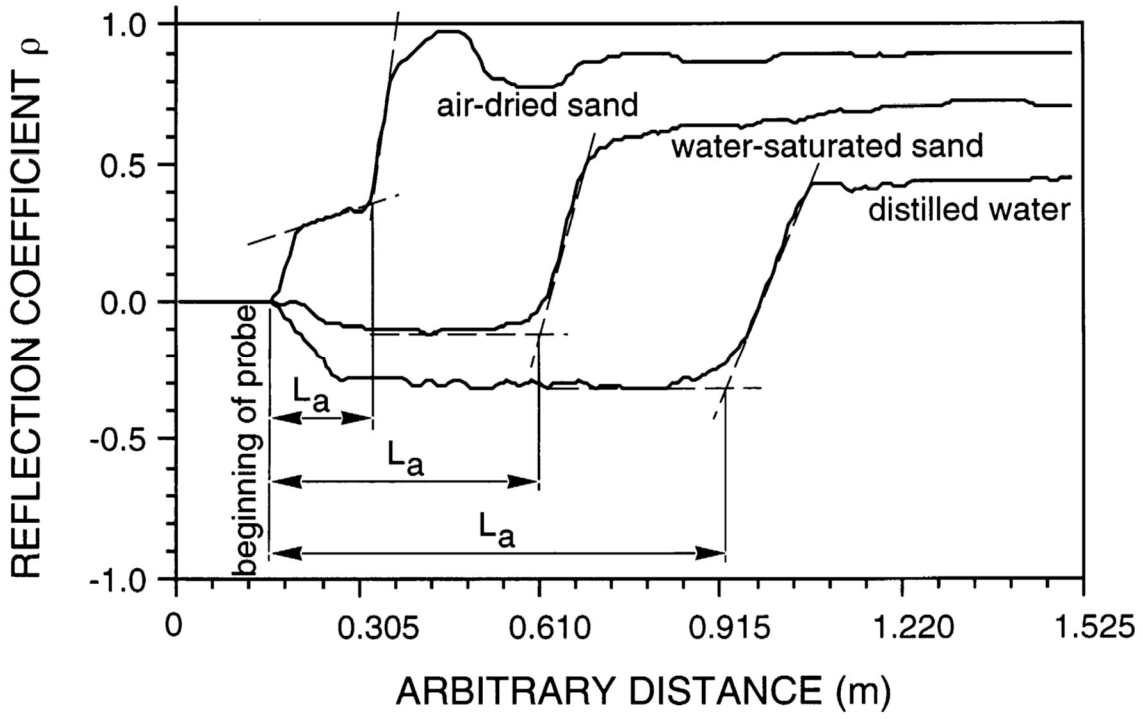


Figure 2.4 TDR waveforms examples provided by a three-probe sensor

The apparent distance $L_a$ between the start and end reflections can be obtained from waves reflected from a sensor. TDR waveforms examples from a three-probe sensor are shown in Figure 2.4.

## 2.4 Thermo-TDR Technique

Thermo-time-domain reflectometry (thermo-TDR) method might even be possible for monitoring the soil properties and thermal properties. Ren et al. (1999) came up with a design of the thermo-TDR sensor. The transient state method is used to measure thermal properties, such as dual-heat probes from the heat pulse theory (Jaeger 1965; Larson 1988; Lubimova et al. 1961). The dual-probe heat-pulse (DPHP) instrument was used to measure thermal properties, such as heat capacity, thermal conductivity, and thermal diffusivity, by several studies (Bristow et al. 1994; Campbell et al. 1991; Kluitenberg et al. 1995; Kluitenberg et al. 1993). The thermo-TDR sensor

is combined time-domain reflectometry (TDR) and a heat-pulse for soil properties and thermal property measurements within a similar volume (Ren et al. 1999). This thermo-TDR sensor is composed of three parallel probes; each is 1.3 mm in diameter and 40 mm long with 6 mm probe-to-probe spacing. However, the probes may be deflected when inserted into hard soil because of their narrow 1.3-mm diameter. The soil temperature, as well as the thermal and electrical properties, can be measured by the thermo-TDR sensor (Ren et al. 1999). Some researchers use the thermal-TDR sensor for monitoring soil physical properties comprehensively (Lu et al. 2007; Lu et al. 2014; Ochsner et al. 2001; Xie et al. 2018). Some researchers study coupled heat and water transfer in frozen and unfrozen soils using the thermo-TDR sensor (Heitman et al. 2008; Tian et al. 2015).

Many researchers have found that short probes will restrict the TDR measurements' accuracy and precision (Noborio 2001; Schwartz et al. 2014; Wang et al. 2016). The errors of volumetric moisture content using a TDR sensor with short probes were considerable at one time (Topp et al. 1984). Therefore, an improvement for a thermo-TDR sensor was to increase the length of probes appropriately. Several researchers tried to improve the precision of thermo-TDR sensors for soil thermal properties determination. A partial cylinder-shaped thermo-TDR sensor with a curved heater was provided by Olmanson and Ochsner (2008). Although this design raises the thermo-TDR sensor's strength, other problems arise, such as the curved heater, which affects the soil compaction (Olmanson and Ochsner 2008). An improved thermo-TDR sensor added pointed tips at the probe ends and increased the probe diameter to 2 mm and the probe-to-probe spacing to 8 mm (Liu et al. 2008). The benefit of the probe ends with pointed tips is that it reduces the difficulty of insertion. Yu et al. (2015) proposed a similar design with pointed tips. Some of the studies confirmed that higher accuracy would happen when increasing the length of the probes. In

addition, Lu et al. (2016) found that soil thermal conductivity measurements via a heat pulse technique are not impacted by needle deflection.

## 2.5 SWCC and TCDC

Buckingham (1907) created the first soil-water characteristic curve (SWCC). The SWCC is essential to the behavioral representations of unsaturated soils. The SWCC consists of a relationship between the soil matric suction and volumetric moisture content. SWCC can be rapidly determined in the field or laboratory. Most of the existing SWCC models are used for isothermal conditions. However, Zhou et al. (2014) provided an SWCC model for non-isothermal conditions. Sheng et al. (2008) proposed the initial framework considering the effects of temperature on SWCC in a thermo-hydro-mechanical (THM) theory.

A thermal conductivity dry-out curve (TCDC) presented a relationship between soil volumetric moisture content and soil thermal conductivity. The TCDC is characterized by capillary, funicular, and pendular regimes. At the capillary regime, thermal conductivity is mainly unaltered from the upper limit of thermal conductivity. However, at the funicular regime, the thermal conductivity decreases. This decrease is due to a more conductive water phase, which has shifted to a less conductive air phase. At a lower saturation, the thermal conductivity decreases rapidly at the critical saturation. In general, thermal conductivity is taken to reflect changes in the regime of pendular water retention.

## 2.6 Soil Thermal Properties and Applications

The soil thermal properties are soil physics components that have found essential uses in agriculture, climatology, and engineering. These properties impact how energy is divided into the

soil profile. Soil thermal properties deal with soil temperature more precisely, accompanying energy transfer throughout the soil by conduction, convection, and radiation. The primary soil thermal properties include volumetric heat capacity, thermal diffusivity, and thermal conductivity.

The thermal conductivity of a material is a measure of its ability to conduct heat. Heat transfer occurs at a lower rate in low thermal conductivity materials than in high thermal conductivity materials. For instance, metals typically have high thermal conductivity and are very efficient at conducting heat, while the opposite is true for insulating materials like styrofoam. Correspondingly, high thermal conductivity materials are used diffusely for heat sink applications. Conversely, low thermal conductivity materials are used as thermal insulation. In thermal resistivity is the reciprocal of thermal conductivity engineering practice; thus, it is common to work in terms of quantities, which are derivative to thermal conductivity, and implicitly consider design-specific features such as component dimensions.

## 2.7 Predicted Models

### 2.7.1 SWCC Modeling Parameters

Parameters used in mathematical models for the soil-water characteristic curve include fixed points pertaining to water content or suction at specific conditions (e.g., saturation, residual saturation, and air-entry pressure). Meanwhile, two or more empirical or semiempirical fitting constants are selected to capture the general shape of the curve between these fixed points. As illustrated in Figure 2.5, the saturated water content $\theta_s$ describes the point where all of the available pore space in the soil matrix is filled with water, usually corresponding to the curve's desorption branch. The air-entry or ‘‘bubbling,’’ pressure b describes the suction on the desorption branch where air first starts to enter the soil's largest pores, and desaturation commences. The residual water content $\psi_b$ describes the condition where the pore water resides primarily as

isolated pendular semilunar cartilage, and substantial alterations in suction are needed to eliminate additional water from the system. A reliable way to quantify the air-entry pressure and residual water content is to create pairs of tangent lines from inflection points on the characteristic curve.

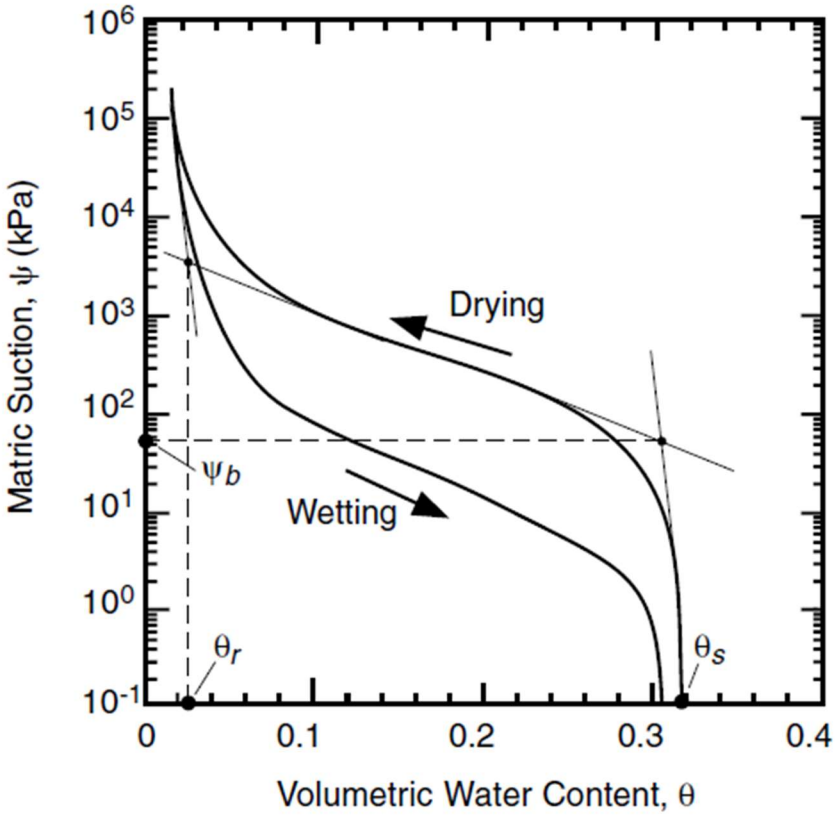


Figure 2.5 Example of a soil-water characteristic curve

### 2.7.2 Brooks and Corey (BC) Model

One of the earliest methods for modeling the soil-water characteristic curve is an equation devised by Brooks and Corey (1964). According to observations from an extensive group of experimental suction and water content measurements, Brooks and Corey suggested a two-part power-law relationship incorporating a "pore size distribution index," $\lambda$. The model is nonsmooth or open form about the air-entry pressure, $\psi_b$, and is written as

$$\Theta = S_e = \begin{cases} 1 & \psi < \psi_b \\ \left(\frac{\psi_b}{\psi}\right)^{\lambda} & \psi \geq \psi_b \end{cases} \tag{2.1}$$

Eq. (2.1) can also be written as:

$$\theta = \begin{cases} \theta_s & \psi < \psi_b \\ \theta_r + (\theta_s - \theta_r)\left(\frac{\psi_b}{\psi}\right)^{\lambda} & \psi \geq \psi_b \end{cases} \tag{2.2}$$

or in terms of suction head $h$ and air-entry head $h_b$:

$$\Theta = S_e = \begin{cases} 1 & h < h_b \\ \left(\frac{h_b}{h}\right)^{\lambda} & h \geq h_b \end{cases} \tag{2.3}$$

Figure 2.6 presents three models of soil-water characteristic curves using the Brooks and Corey model.

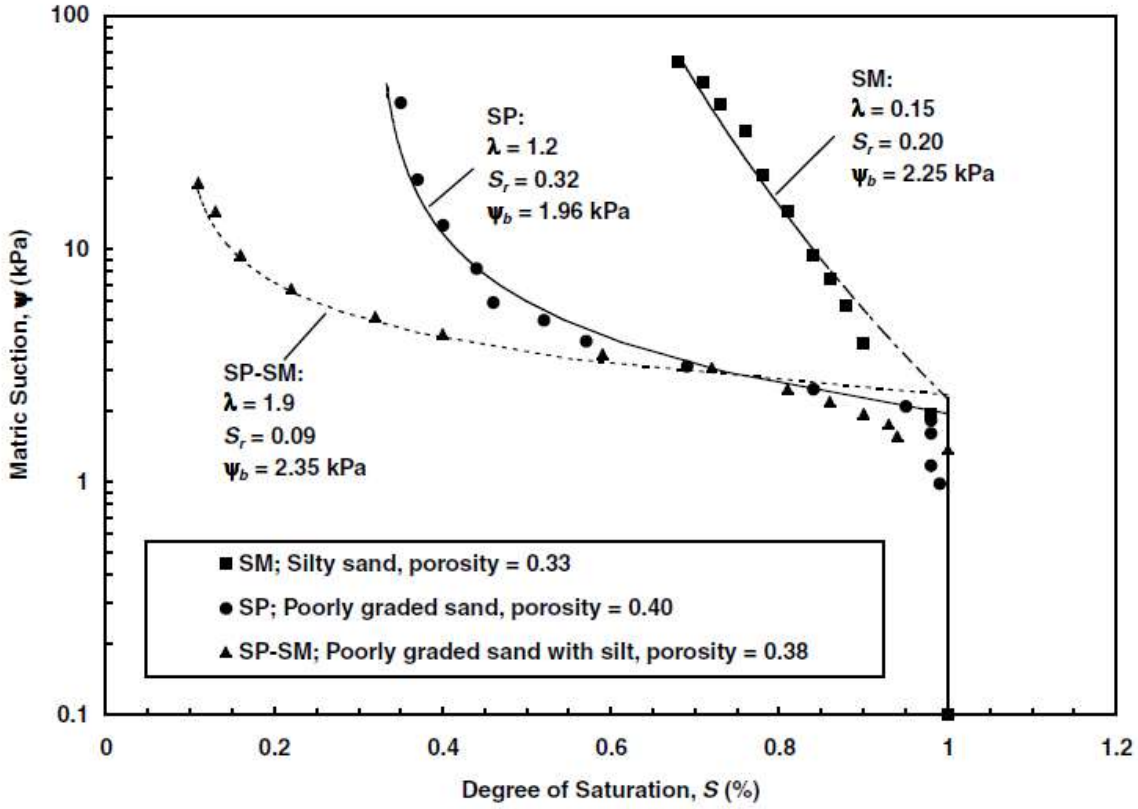


Figure 2.6 Models of soil-water characteristic curves based on the Brooks and Corey (1964) model (with experimental data obtained from Clayton (1996))

### 2.7.3 van Genuchten (VG) Model

van Genuchten (1980) came up with a closed-form, smooth, and three-parameter model for the SWCC expressed as:

$$\Theta = S_e = \left[\frac{1}{1 + (a\psi)^n}\right]^m \tag{2.4}$$

where

a, n, and m = parameters of fitting.

The VG model's mathematical expression gives reasons for a point of inflection, which agrees with more extensive adaptability than the Brooks and Corey model over a larger range of suction and overcomes the snatched typical curves' anaclastic shape.

### 2.7.4 Fredlund and Xing (FX) Model

Fredlund and Xing (1994) exploited a model based on consideration of pore size distribution in a form similar to the VG model calculating it as:

$$\theta = C(\psi)\theta_s \left[\frac{1}{\ln\left[e+(\psi/a)^n\right]}\right]^m \tag{2.5a}$$

where

$\psi$ = suction (kPa); $a$, $n$, and $m$ = fitting parameters; $e$ = the natural logarithmic constant; and $C(\psi)$ = a correction factor that forces the model through a prescribed suction value of $10^6$ kPa at zero water content; therefore:

$$C(\psi) = \left[1 - \frac{\ln(1+\psi/\psi_r)}{\ln(1+10^6/\psi_r)}\right] \tag{2.5b}$$

where

$\psi_r$ = the suction (kPa) estimated at the residual condition.

## 2.8 Summary

This chapter discusses the relevant background of literature pertaining to this research. It includes the soil moisture measurement, the time-domain reflectometry (TDR) technique, the soil-water characteristic curve (SWCC), and the thermal conductivity dry-out curve (TCDC), as well as soil thermal properties, applications, and predicted models.

# 3 CHAPTER 3 DESIGN, FABRICATION, AND EVALUATION OF THERMO-TDR SENSORS

## 3.1 Introduction

Geothermal energy has attained a lot of attention in recent years because it is renewable, clean, and sustainable features (Lei et al. 2019). It is widely used in geotechnical engineering relevant and includes borehole thermal energy storage (BTES), geothermal energy piles (GEPs), and ground source heat pumps (GSHPs) (Zhang et al. 2017). These underground energy-saving systems and devices utilize comprising the heat transfer process in soils as they depend on the soil thermal properties. Consequently, it is necessary to understand soil thermal properties, such as diffusivity, heat capacity, thermal conductivity, and influence factors (i.e., the soil's basic properties).

A mass number of historical and rising applications are considered for the thermal properties of soil. Historical applications include agricultural water management, artificial ground freezing, frost penetration in cold regions, and pipeline design. More recent applications include heat exchangers for geothermal cooling and heating systems (Johnston et al. 2011), nuclear waste repository applications, and the emergence of thermally-active geo-structures, such as heat-exchanger piles, thermo-active tunnels, bridge deck de-icing systems, and geo-synthetics integrated with heat exchangers (Adam and Markiewicz 2009; Brandl 2006; Knellwolf et al. 2011; Loveridge and Powrie 2013). The central heat transfer mechanism in sand-sized soil responds to conditions and is quantified by the multiphase system's effective thermal conductivity (Farouki 1981). The effective thermal conductivity of soil is not constant and relies on the soil's bulk density, mineralogy of the solid phase, particle and pore microstructure, as well as the soil moisture content.

Promotion of time-domain reflectometry (TDR) technological progress for soil water content monitoring is mainly ascribed to Topp et al. (1980). They found a connection between soil apparent dielectric constant and soil volumetric moisture content. Subsequently, Dalton et al. (1984) presented the dielectric/soil moisture relationship as able to determine bulk electrical conductivity from TDR waveforms. Zeglin et al. (1989) presented a seminal work showing unbalanced coaxial cells. Topp et al. (1982) and Baker and Lascano (1989) showed a balanced two-probe sensor with a balun. Malicki and Skierucha (1989) showed a balanced two-probe sensor without a balun. As an electrical device, balun can convert a balanced signal and an unbalanced signal. Heimovaara (1993) showed the symmetric multi-rod probes. An improvement was made to widen the TDR technique to geotechnical applications (Siddiqui and Drnevich 1995). TDR technology has been established as a fast, responsible, and tried technology for field monitoring of soil water content based on volumetric moisture content, as defined by Benson and Bosscher (1999) and Noborio (2001). Liu et al. (2008) tested four-probe designs for bulk density of soil, volumetric moisture content, and volumetric heat capacity measurement. The thermo-time-domain reflectometry (thermo-TDR) sensor incorporates the dual-probe heat pulse (DPHP) device with the TDR technique to obtain simultaneous soil moisture content, dry density, and thermal property measurements. Yu et al. (2015) utilized their newly developed thermo-TDR sensor for geothermal applications and demonstrated high accuracy in measuring geotechnical and soil thermal properties in compacted soil samples. Zhang et al. (2015) used the sensor to further study quartz sands and sand-kaolin clay mixtures thermal conductivity measurements. Yu et al. (2015)'s thermo-TDR sensor has measured moisture content, dry density, and thermal properties for both coarse-grained and fine-grained soils with reasonable accuracy. Wang and Yu (2018) reported a newer designed

thermo-TDR sensor, which was evaluated in stage compacted sands and had better performance than the previous thermo-TDR sensor.

This chapter introduces the design, fabrication, and evaluation of a new thermo-TDR sensor for simultaneous soil thermal properties, moisture content, and dry density measurements. The measurement performance of the thermo-TDR sensor was investigated by performing a series of laboratory tests using different types of soil. The constraints of the sensor designation are presented in this article. The thermo-TDR sensor was fabricated following a new design specification. Nine different chemical reagents, each with a known dielectric constant were utilized to perform calibration of the dielectric constant ($K_a$). Potassium chloride (KCl) and Sodium chloride (NaCl) solutions of different concentrations were used to implement the calibration of electrical conductivity ($EC_b$). The accuracy and precision of the new sensor were tested by thermal property measurements, which were evaluated by comparing and analyzing the measurement results from a KD2 Pro thermal properties analyzer. Laboratory tests on four standard sand, two site sand samples, one standard clay, and one site clay sample were also implemented for a comprehensive evaluation of the sensor. Experimental results from a newly designed thermo-TDR sensor were compared to a previous version sensor by analyzing calibration and experiment results.

## 3.2 Design of Thermo-TDR Sensors

The thermo-TDR sensor's contrivance must meet the dual-probe heat pulse (DPHP) requirements and those requirements of the TDR probes. The TDR sensor is based on the transmission line theory. The DPHP is based on the principle of radial heat conduction. The TDR moisture probes' primary design constraints include an effective sampling area, sensor assembly, and signal attenuation. The sensor probe's length is established by resolving recorded signals, analyzing the source voltage of the pulse generator, and the loss of the signal, controlled by soil's

electrical conductivity (Ren et al. 1999) who found that probe-to-probe spacing to probe diameter ratio should be less than or equal to 10, as shown in Eq. (3.1). The design of a DPHP requires a heat source to be close to the infinite line heat source. The design constraints are presented by Eqs. (3.2) to (3.4) (Blackwell 1956; Ren et al. 1999).

$$I/D \leq 10 \tag{3.1}$$

$$(L)/(2 \times I) > 2.2 \tag{3.2}$$

$$L/D > 25 \tag{3.3}$$

$$D/(2 \times I) < 0.13 \tag{3.4}$$

where

$L$ = length of sensor probe; $I$ = center-to-center interval between the center probe and the outer probe, and $D$ = diameter of the sensor probe.

An improved design of the thermo-TDR sensor was developed, as shown in Figure 3.1(B). The dimension of the previous sensor design is shown in Figure 3.1(A). One main change for both recent and previous designs is the center-to-center interval between the center probe and the outer probe. Another significant change is the height of epoxy. These two significant changes are based on previous experimentation. The advantages of the current design are described as follows:

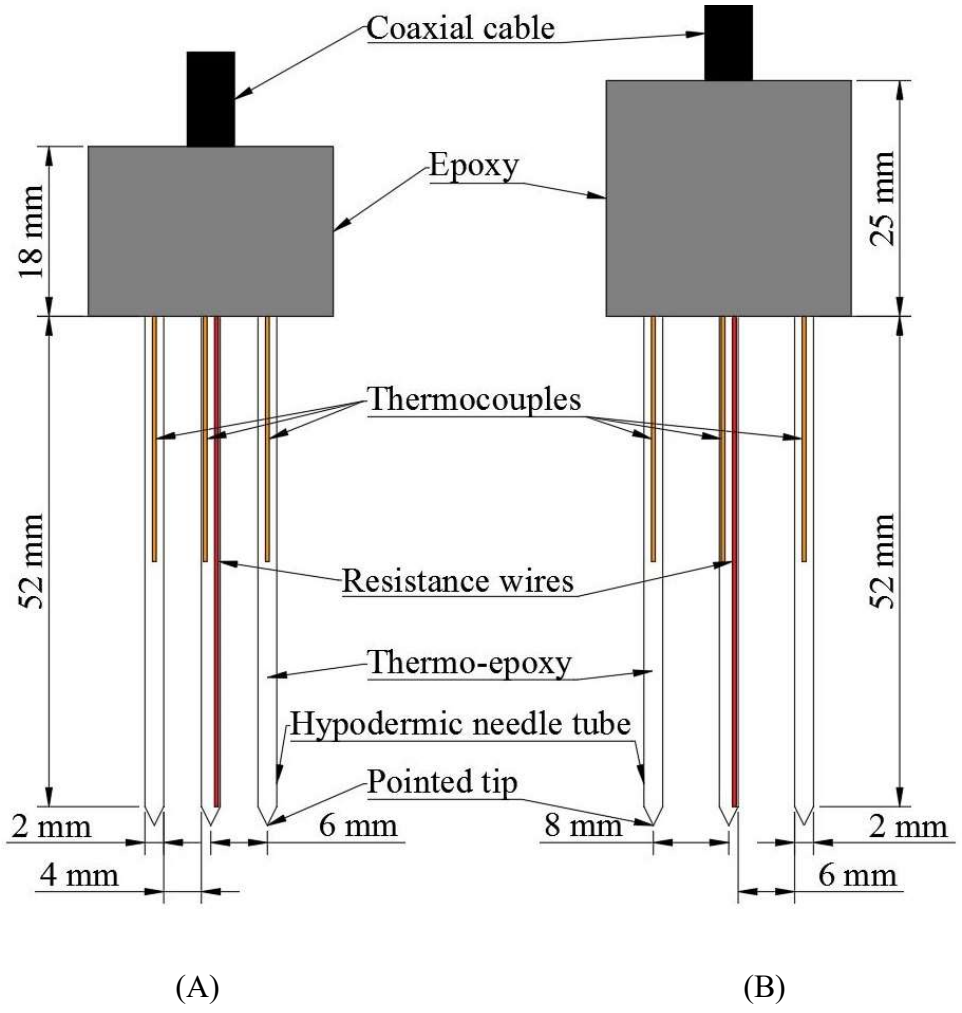


Figure 3.1 Schematic of thermo-TDR sensors: (A) previous design, (B) current design

3.3 Fabrication of Thermo-TDR Sensors

Based on the design requirements, the thermo-TDR sensor fabrication process is presented as follows: Three hypodermic needle tubes were used with inner and outer diameters of 1.7 mm and 2.0 mm, respectively. The tubes' length was 77.0 mm, and the tubes extending away from the head of the thermo-TDR sensor probes were 52.0 mm. The probes were filled with a mixture of thermal epoxy made up of an OMEGABOND 200 catalyst and an OMEGABOND 200 resin with a mix proportion by weight of 1 to 10. Mixed thermal epoxy is liquid at room temperature. Three type T thermocouples from OMEGA with a wire diameter of 0.076 mm and two loops of 38-gauge

Nichrome 80 resistance wire and a total length of 104 mm were coated with the thermal epoxy mixture and transferred into a muffle oven set at 204 °C for two hours to solidify the isolation between wires. Three type T thermocouples were inserted into three tubes, with the sensing element extending through each tubes' center core. The resistance wire was inserted into the center tube, extending the full length of the tube. The three tubes with thermocouples and resistance wire were transferred into the muffle oven again at the same temperature for two more hours. The thermal epoxy was cured, and the thermocouples and the resistance wire were immobilized. A multimeter was used to inspect the outputs to ensure that the resistance wire is appropriately functioning. The three completed tubes were clamped into a prefabricated mold, which held them in place with a center-to-center interval between the 8-mm tubes. The RG-58 coaxial cable was connected to the corresponding tubes by soldering. The CR-600 casting resin was poured into the mold, and the head was separated from the mold after 24 hrs. Three central tines were joined by soldering at the probes' ends to reduce soil perturbation during the insertion process.

### 3.4 Calibration of Thermo-TDR Sensors

The value of dielectric constant and electrical conductivity for measured soil can be directly determined by analyzing TDR waveforms. The dielectric constant is determined by Eq. (3.5) (Topp et al. 1980).

$$K_a = (L_a / L_p)^2 \tag{3.5}$$

where

$K_a$ = dielectric constant; $L_p$ = physical length of sensor probe, and $L_a$ = length of the sensor probe in the testing materials determined from TDR waveforms. The sensor probe's length in the TDR

waveform is determined by locating the electromagnetic wave reflection points at the probe head and end following the single tangent method proposed by Baker and Allmaras (1990).

The electrical conductivity measured by the TDR sensor can be determined by using the following expression developed by (Giese and Tiemann 1975).

$$EC_b\ (Sm^{-1}) = (\varepsilon_o c Z_o / L_p Z_c)(2V_o / V_f - 1) \quad (3.6)$$

where

$EC_b$ = electrical conductivity ($Sm^{-1}$); $\varepsilon_o$ = dielectric permittivity of free space; $c$ = speed of light in a vacuum ($3.0 \times 10^8$ m/s); $Z_o$ = characteristic probe impedance; $L_p$ = length of sensor probe; $Z_c$ = output impedance from TDR cable tester; $V_o$ = voltage of source; and $V_f$ = long-term voltage level of the signal reflection. Details of dielectric constant and electrical conductivity calculations can be found in Yu et al. (2015).

Nine standard chemical solutions with known dielectric constants were used for dielectric constant (Ka) calibration. The values of Ka for most testing soils are less than 20. Therefore, only three different chemicals were selected for dielectric constant calibration. TDR waveforms of the chemicals and air can be found in Wang and Yu (2018). Calibrations of dielectric constant for the optimal designed thermo-TDR sensor is shown in Figure 3.2 (A). A thermo-TDR sensor determined the measured dielectric constant. The actual dielectric constant was the known dielectric constant. The calibration of the thermo-TDR sensor for the electrical conductivity measurement was performed by measuring potassium chloride (KCl) and sodium chloride (NaCl) solutions with different concentrations using the thermo-TDR sensor and an electrical conductivity (EC) meter. The electrical conductivity by the thermo-TDR sensor is compared with the EC meter measurement, as shown in Figure 3.2 (B). The calibration results show that the thermo-TDR sensor

can satisfactorily measure both dielectric constant and electrical conductivity with a coefficient of determination ($R^2$) of 0.99.

The values of measured dielectric constant and electrical conductivity are dependent on the temperature. They need to be interpreted if the experiment was performed differently from the soils' temperature during calibration (Yu and Drnevich 2004). According to test results at small temperature differences (less than 20 °C), the temperature effects are minuscule.

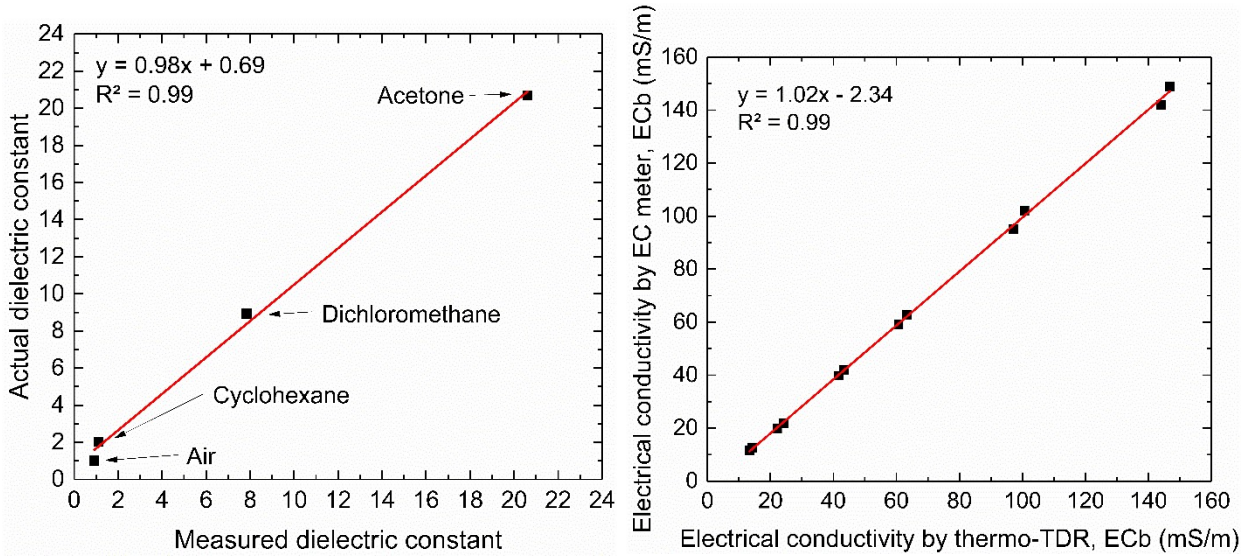


(A) (B)

Figure 3.2 Actual and measured value comparison from TDR waveforms: (A) dielectric constant and (B) electrical conductivity

3.5 Thermal Properties Determination

A direct current (DC) source was connected to the resistance wire in the thermo-TDR middle sensor probe to generate a heat pulse in the same sensor probe. The temperature variations of the three sensor probes were monitored using PicoLog Recorder software. The temperature

response can be predicted by the infinite line heat source theory, as shown in Eq. (3.7) (De Vries 1952; Kluitenberg et al. 1993).

$$T(r,t) = (Q / 4\pi\alpha) [Ei(-r^2 / 4\alpha(t - t_o)) - Ei(-r^2 / 4\alpha t)] \quad (3.7)$$

where

$T$ = temperature change; $Q$ = strength of line heat source; $\alpha$ = soil thermal diffusivity; $Ei(x)$ = exponential integral; $r$ = radial distance; $t$ = time, and $t_o$ = duration of the heat pulse.

The volumetric heat capacity, thermal diffusivity, and thermal conductivity were calculated using Eqs. (3.8) to (3.10).

$$\rho_c = (q / 4\pi\alpha T_m) [Ei(-r^2 / 4\alpha(t_m - t_o)) - Ei(-r^2 / 4\alpha t_m)] \quad (3.8)$$

$$\alpha = (r^2 / 4) [1 / (t_m - t_o)] / ln[tm / (t_m - t_o)] \quad (3.9)$$

$$k = \frac{q}{4\pi T_m} \left[ Ei\left(\frac{-ln\,[t_m / (t_m - t_o)]}{t_o / t_m}\right) - Ei\left(\frac{-ln\,[t_m\,(t_m - t_o)]}{t_o / (t_m - t_o)}\right)\right] \quad (3.10)$$

where

$r$ = radial distance between the center probe and outer probes; $t_m$ = time when the maximum temperature of the outer probes occurred; $T_m$ = maximum temperature increases of outer probes. Details of the analysis of heat pulse response curves can be found in Yu et al. (2015). Only thermal conductivity measurement is discussed in this dissertation. A thermal properties analyzer (KD2 Pro) with a TR1 probe was used for thermal conductivity measurement.

## 3.6 Effective Sampling Area for Thermo-TDR Probes

Theoretically, all the points in a cross-section of the electric field perpendicular to the thermo-TDR sensor contribute to the sensor response. Nevertheless, the overall response points'

contributions are continually dropping when they are farther away from the thermo-TDR sensor until they reach an insignificant level. One method used for the effective sampling area calculation is also given in Ferré et al. (1998).

$$f = \frac{100 \times \sum_{w_{h_i}}^{W} w_i A_i}{\iint w_i \, dA} \tag{3.11}$$

where

$A_i$ = elemental areas, $w_i$ = elemental spatial weighting functions, and $f$ = desired percentage of the total response. The recognized value of $f$ for the effective sampling area determination is 70% and 90%.

The electrical field distribution surrounding a thermo-TDR sensor can be perceived as an electrostatic problem, based on the transverse electromagnetic (TEM) propagation mode of the TDR wave (Ramo et al. 1965). Poisson's equation can be used to solve the electrical field distribution problem. The solution of Poisson's equation can be solved numerically by finite element analysis (Yu et al. 2013). COMSOL Multiphysics was used to solve this problem.

A finite element model was developed for the thermo-TDR sensor, as shown in Figure 3.3. The rectangular box around the sensor was created for numerical analysis. The TDR sensor model is based on the actual size and material distribution. The dielectric constant of air is set at 1.0. The electric displacement at the outer rectangular boundary is selected as 0. The center probe's electric potential is specified as 1 volt (V), and the electrical potential for outer probes are established as -1 V.

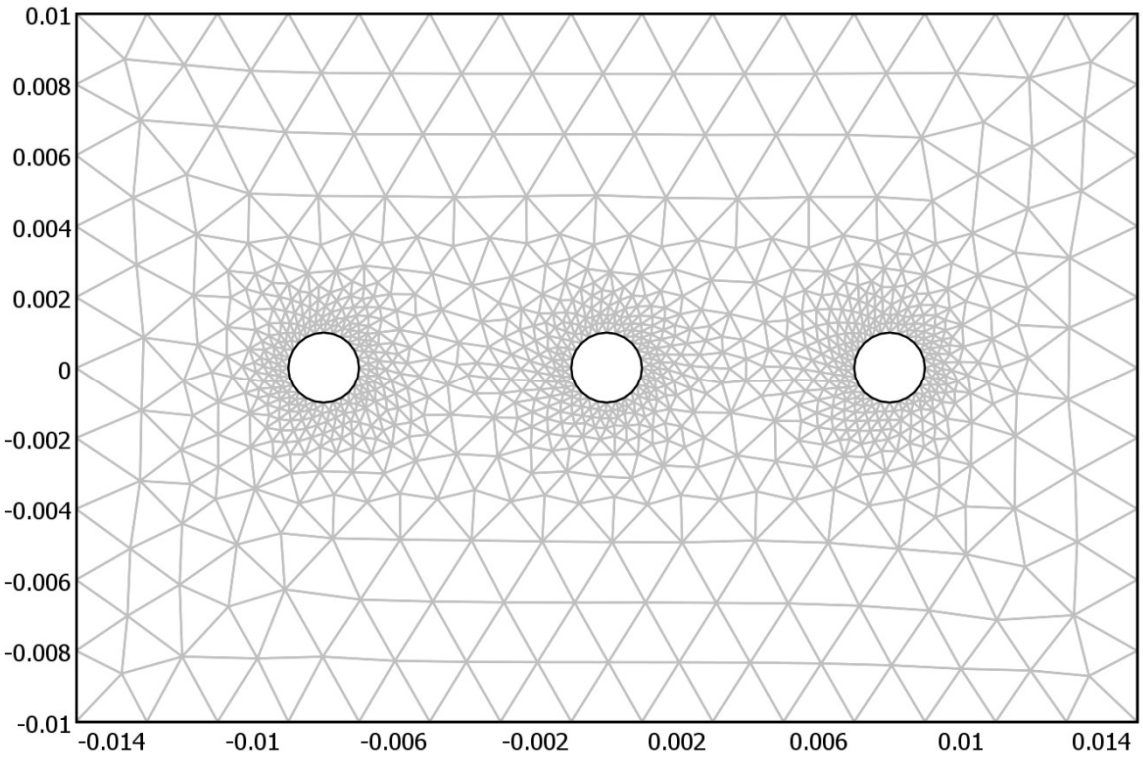


Figure 3.3 Finite element method model of the thermo-TDR sensor (units: m)

The electrical field distribution of the thermo-TDR sensor is submerged in water, as shown in Figure 3.4. The highest energy density occurs at the center sensor probe.

The sensor's effective sampling area was determined using areas that make a 70% and 90% contribution to the total electrical field energy (Eq. (3.11)). It was achieved by exporting FEM simulation results and further handling them with MATLAB. A code developed by MATLAB was used for searching the elements with high electric energy density values.

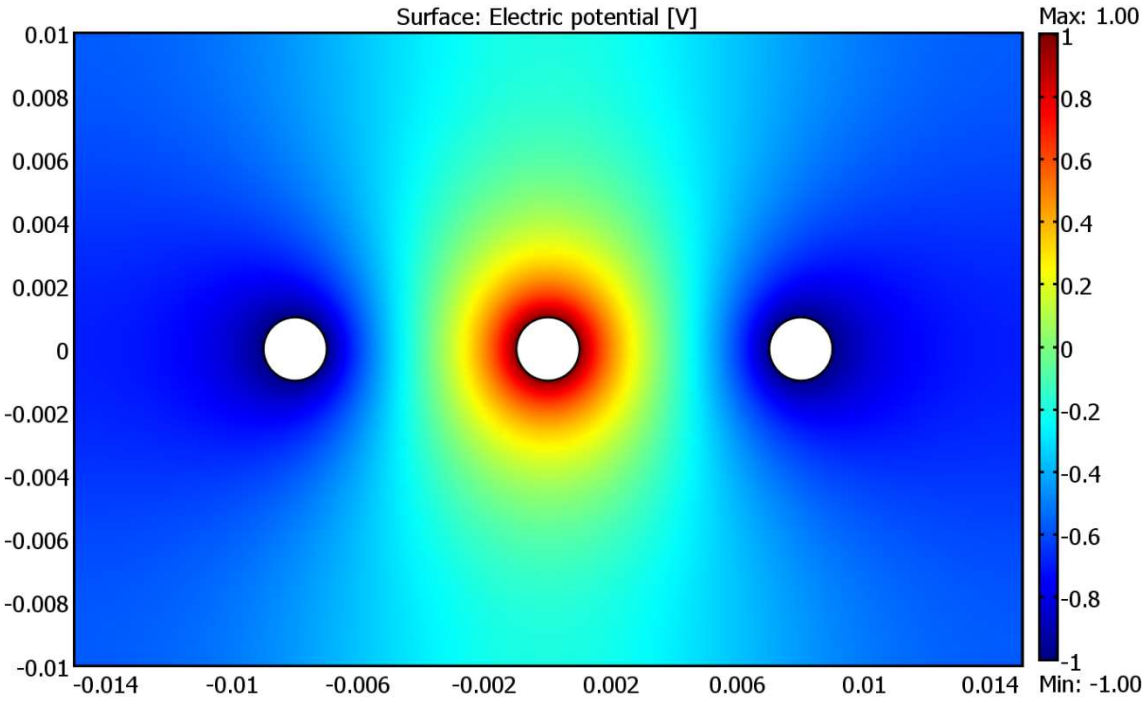


Figure 3.4 Electric potential (V) of the thermo-TDR sensor submerged in water

The first case is the thermo-TDR sensor embedded under water. A simulation was conducted when the sensor was placed in water with a dielectric constant (Ka) of 81. The electrical field energy distribution around the sensor, as shown in Figure 3.5 (the right side of the figure). The calculated total electrical field energy per unit length of the sensor is 1.948 e-6 J/m. The effective sampling area contributing to 70% and 90% of total energy (red and green line area) is shown in Figure 3.5 (on figure's right side) as well. The calculated effective sampling area is 1.69 $cm^2$. One similar simulation was conducted when the sensor was placed in the air with a dielectric constant of 1. The calculated total electrical field energy per unit length of the sensor is 2.403 e-6 J/m.

The second case is the thermo-TDR sensor embedded in saturated sand. A simulation was conducted when the sensor was placed in saturated sand with a dielectric constant of 26. The

electrical field energy distribution around the sensor is shown in Figure 3.6 (the left side of the figure). The sensor's total energy in saturated sand is 6.253 e-5 J/m, which is smaller than the sensor submerged in water. The calculated effective sampling area is 1.58 $cm^2$, which is very close to the sampling area, as shown in Figure 3.6 (left side of figure). The sample area is not highly sensitive to the relative dielectric constant. This conclusion was proved by Ferré et al. (1998).

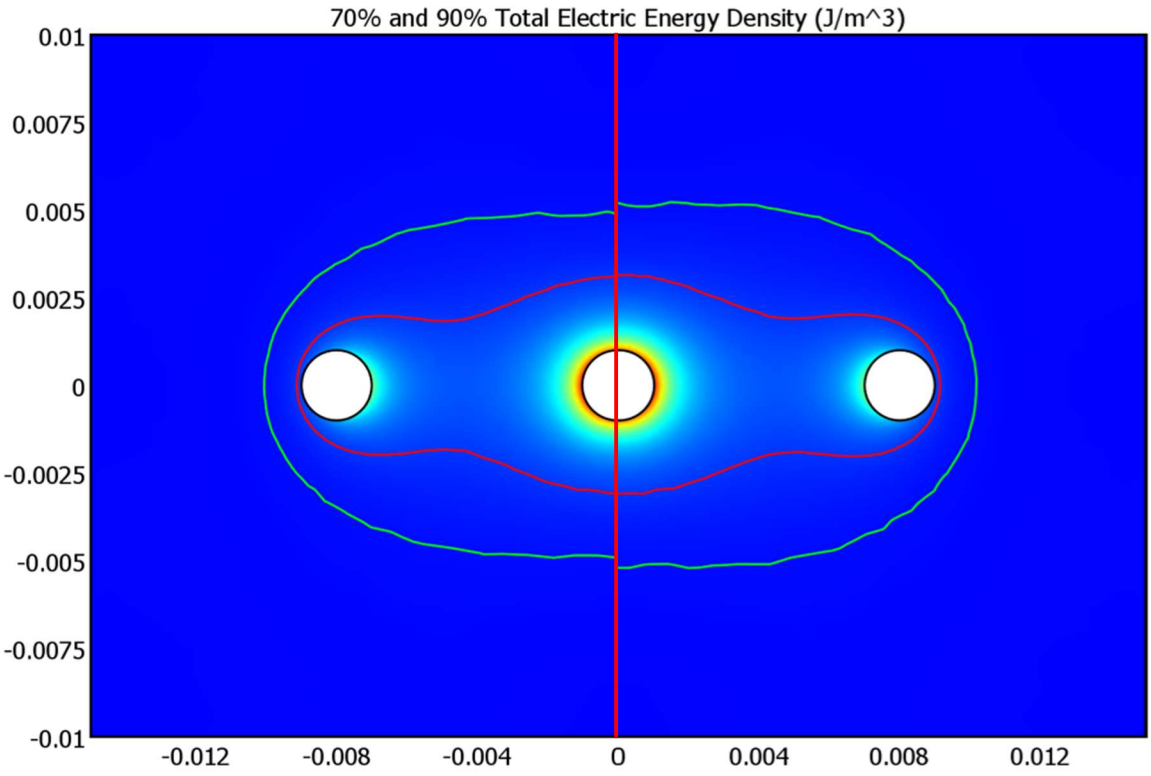


Figure 3.5 Electrical field energy distribution around the sensor with an indication of the effective sampling area when the sensor was installed in saturated sand (left) and water (right)

## 3.7 Evaluation of Thermo-TDR Sensors

### 3.7.1 Experimental Setup

A modified proctor test is needed to evaluate the thermo-TDR sensor in the multistage compacted specimen. Figure 3.6 shows a schematic of the experiment setup. To acquire TDR

waveforms, the thermo-TDR sensor stick in the soil inside the compaction mold is connected through a coaxial cable to a time-domain reflectometer (Campbell Scientific TDR100). The resistance wire is connected to direct current (DC) electronic loads (BK PRECISION 17850B) for resistance heating. Three thermocouple plugs are connected to the thermocouple data logger (Pico USB TC-08) to monitor the temperature variations of three sensor probes every second. The compaction mold is in a vertical position, which can slow down the evaporation process.

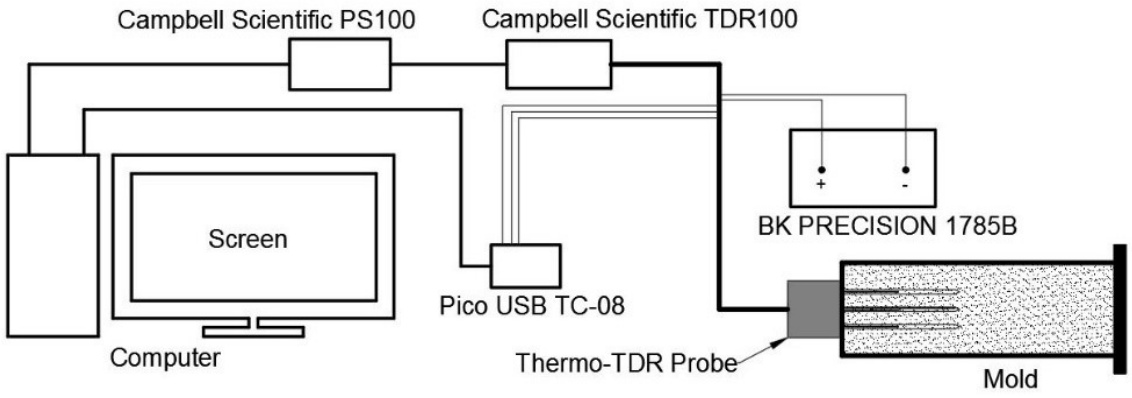


Figure 3.6 Schematic of the experimental setup

### 3.7.2 Test Materials, Test Plan, and Experimental Procedures

There are eight different soil types to be appraised by the thermo-TDR sensor to measure basic soil properties and thermal properties. The eight different types of soils include (1) 12-20 filter sand, (2) A.F.S. 50-70 sand, (3) ASTM 20-30 sand, (4) ASTM fine graded sand, (5) Calcined kaolin clay, (6) Hazy Meadow Park sand, (7) UTA F11 parking lot sand, and (8) UTA residence hall clay. Figure 3.7 shows the particle size distributions of these soils except for minuscule calcined kaolin clay and UTA residence hall clay. Table 3.1 lists the soil classification of the eight different types of soils selected for testing.

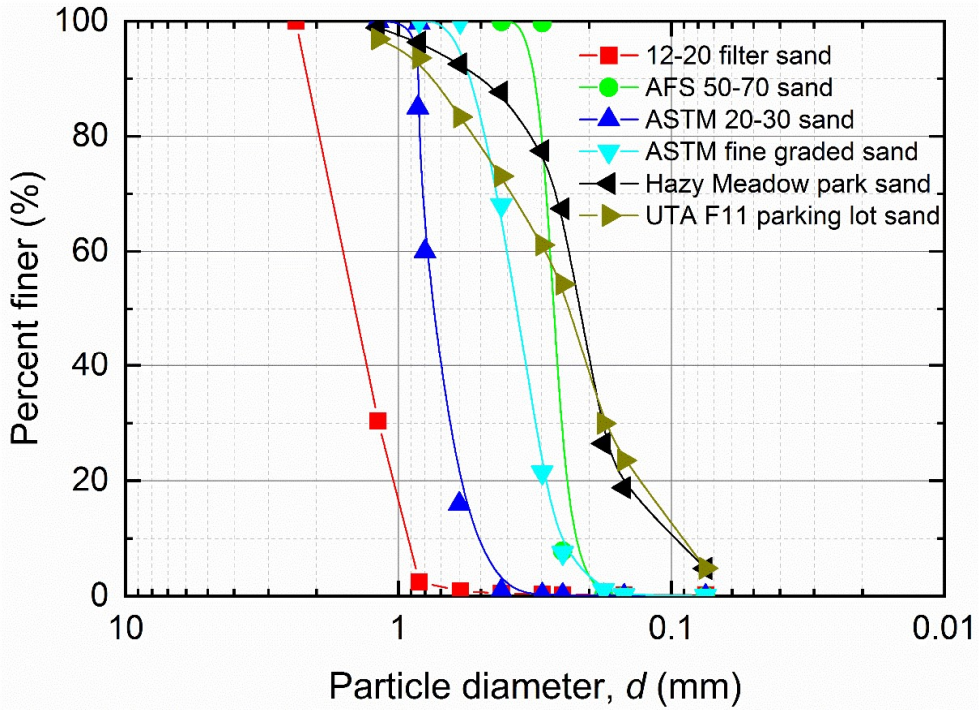


Figure 3.7 Particle size distributions of sands

Table 3.1 Soil classification for testing soils

| No. | Soil Name | $F_{200}$ (%) | Unified Soil Classification | Group Name |
|---|---|---|---|---|
| 1 | 12-20 filter sand | 0.21 | SP | Poorly graded sand |
| 2 | AFS 50-70 sand | 0.01 | SP | Poorly graded sand |
| 3 | ASTM 20-30 sand | 0.03 | SP | Poorly graded sand |
| 4 | ASTM fine graded sand | 0.03 | SP | Poorly graded sand |
| 5 | Calcined kaolin clay | 100 | CL-ML | Silty clay |
| 6 | Hazy Meadow Park sand | 4.79 | SP | Poorly graded sand |
| 7 | UTA F11 parking lot sand | 4.84 | SP | Poorly graded sand |
| 8 | UTA residence hall clay | 5.81 | SP-SC | Sandy fat clay |

One group test was set up for each type of soil to appraise the consequence of the sample primary method and reproducibility of experimental results. Each test group included compaction of soil at various expected moisture content levels using custom-designed PVC compaction molds. The dimensions of the extension collar and compaction mold are shown in Figure 3.8.

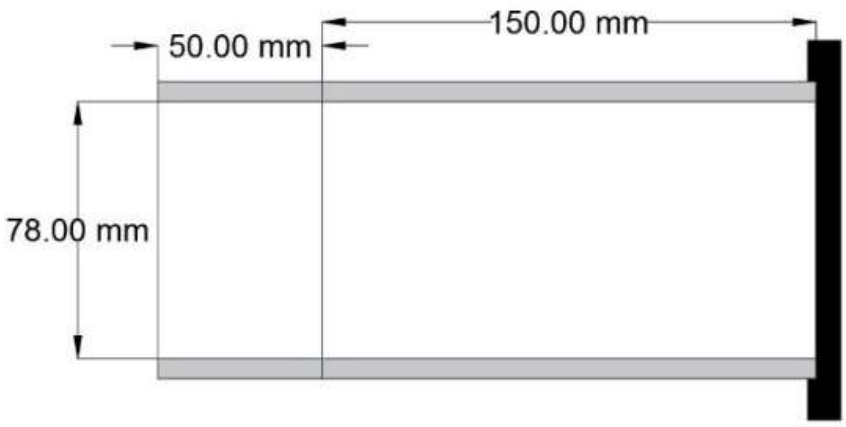


Figure 3.8 Dimensions of the extension collar and compaction mold

A successful appraisal requires that the dry soil samples be mixed with tap water at an expected mass mixing ratio in a metal bowl and kept for 30 minutes before compaction. The prepared soil samples are compacted at three equal lifts to achieve the compaction mold's height with the rammer at its highest 30 cm height. The soil compaction method is illustrated in Figure 3.9.

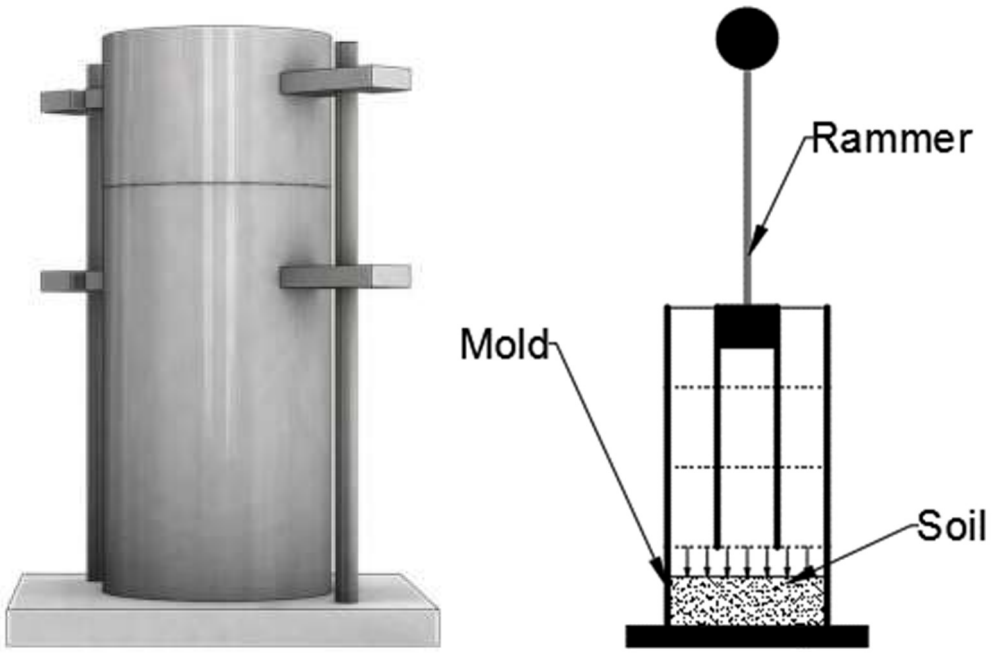


Figure 3.9 Methods of soil compression for tests

The soil sample is compacted by utilizing the process represented in the previous section. The thermo-TDR sensor must be inserted into the soil with the probe head in close contact with the soil surface. During insertion, the probe should be kept vertical to maintain the probe closely aligned with surrounding soils. Two TDR waveforms must be acquired consecutively using a TDR waveform collection software (PM-TDR SM Version 1.7). Then the DPHP test is performed by supplying a direct current of 0.15 A for 15 s. The thermocouple readings are acquired using a PicoLog Recorder. The above measurements are repeated one more time, and a total of four TDR waveforms and two heat pulse responses are recorded. After the thermo-TDR sensor tests, a KD2 Pro TR-1 heat probe is inserted into the specimens separately for heat pulse tests following the operation manual's procedure. Two readings are taken for each probe. After all the measurements are taken, two soil samples are collected from the top third of the compaction mold to determine

oven-dry moisture content. The test must be conducted with the mold kept in a horizontal position to maintain uniform moisture and height.

### 3.7.3 Calibration Relationships for Dielectric Constant and Electrical Conductivity

Yu and Drnevich (2004) proposed the one-step method to develop calibration equations to measure the gravimetric moisture content and dry density. This method adopts two calibration equations shown in Eqs. (3.12) and (3.13) based on the measured dielectric constant and electrical conductivity of the measured soils.

$$\sqrt{K_a}\frac{\rho_w}{\rho_d} = a + bw \tag{3.12}$$

$$\sqrt{EC_b}\frac{\rho_w}{\rho_d} = c + dw \tag{3.13}$$

where

$a$, $b$, $c$, and $d$ = specific calibration constants; $\rho_d$ = dry density of soil, kg/m$^3$; $\rho_w$ = density of water, kg/m$^3$, and $\omega$ = gravimetric moisture content, (based on percentage).

Hence, gravimetric moisture content and dry density can be evaluated by solving Eqs. (3.14) and (3.15).

$$\omega = \frac{c\sqrt{K_a} - a\sqrt{EC_b}}{b\sqrt{EC_b} - d\sqrt{K_a}} \tag{3.14}$$

$$\rho_d = \frac{d\sqrt{K_a} - b\sqrt{EC_b}}{ad - c}\,\rho_\omega \tag{3.15}$$

The calibration relationships for the thermo-TDR sensor are presented in Figures 3.10 and 3.11 and are based on the dielectric constant measurement and electrical conductivity, respectively.

Tables 3.2 and 3.3 show the eight different types of soils tested and provide the specific calibration constants for Eqs. (3.12) and (3.13), respectively.

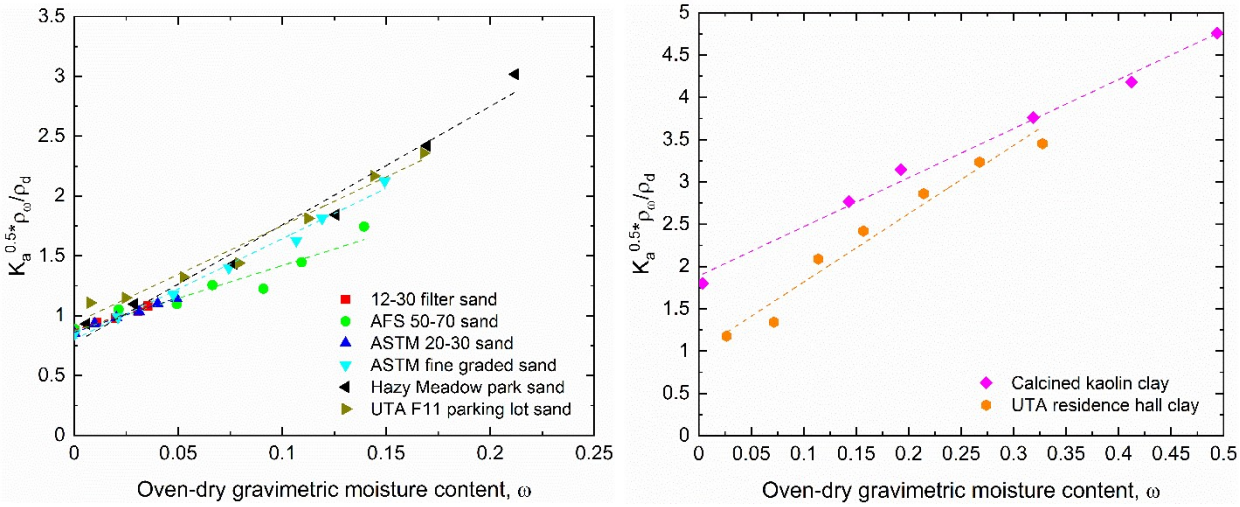


(A) (B)

Figure 3.10 Calibration relationship using the measured dielectric constant: (A) sand and (B) clay

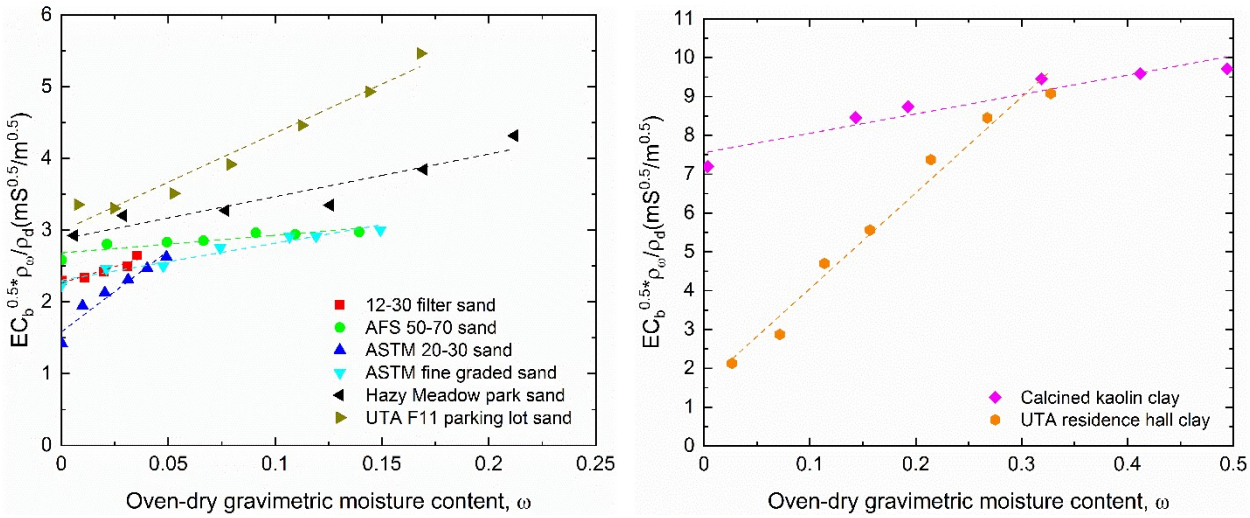


(A) (B)

Figure 3.11 Calibration relationship using measured electrical conductivity: (A) sand and (B) clay

From the summary of specific calibration contents (Table 3.2), the coefficient of determination ($R^2$) value for dielectric constant is over 95% for most of the soils, even close to 1, except for AFS 50-70 sand, which is 92%. The summary of specific calibration contents for electrical conductivity (Table 3.3) of the $R^2$ is close or above 90 %, except for the AFS 50-70 sand, which is above 80%. The plot for the AFS 50-70 sand is shown in Figure 3.11 as the green, solid circle, and the lowest point is a little bit away from the trend line. This point may lead to a lower value of $R^2$. The plot for the 12-20 filter sand is shown in Figure 3.11 and appears as a red, solid square the highest point is away from the trend line. The results indicate that the thermo-TDR sensor has a good performance for sand and clay. From the plots of the calibration relationships (Figure 3.11 and 3.12), both dielectric constant and electrical conductivity tend to increase moisture content. Whether the soil is standard soil or field soil, trend curves for these soils have outstanding performances.

Table 3.2 Summary of specific calibration constants for dielectric constant

| Soil Name | Calibration Equation | | Specific calibration constants | |
|---|---|---|---|---|
| | Equation | $R^2$ | a | b |
| 12-20 filter sand | y = 0.88 + 5.41x | 0.99 | 0.88 | 5.41 |
| AFS 50-70 sand | y = 0.87 + 5.50x | 0.92 | 0.87 | 5.50 |
| ASTM 20-30 sand | y = 0.86 + 5.83x | 0.99 | 0.86 | 5.83 |
| ASTM fine graded sand | y = 0.80 + 8.41x | 0.99 | 0.80 | 8.41 |
| Calcined kaolin clay | y = 1.89 + 5.80x | 0.99 | 1.89 | 5.80 |
| Hazy Meadow Park sand | y = 0.77 + 9.90x | 0.98 | 0.77 | 9.90 |
| UTA F11 parking lot sand | y = 0.94 + 8.15x | 0.97 | 0.94 | 8.15 |

| | | | | |
|---|---|---|---|---|
| UTA residence hall clay | y = 1.01 + 8.08x | 0.96 | 1.01 | 8.08 |

Table 3.3 Summary of specific calibration constants for electrical conductivity

| Soil Name | Calibration Equation | | Specific calibration constants | |
|---|---|---|---|---|
| | Equation | $R^2$ | c | d |
| 12-20 filter sand | y = 2.26 + 9.19x | 0.89 | 2.26 | 9.19 |
| AFS 50-70 sand | y = 2.68 + 2.47x | 0.81 | 2.68 | 2.47 |
| ASTM 20-30 sand | y = 1.58 + 22.57x | 0.93 | 1.58 | 22.57 |
| ASTM fine graded sand | y = 2.30 + 5.15x | 0.96 | 2.30 | 5.15 |
| Calcined kaolin clay | y = 7.55 + 5.00x | 0.91 | 7.55 | 5.00 |
| Hazy Meadow Park sand | y = 2.87 + 5.93x | 0.89 | 2.87 | 5.93 |
| UTA F11 parking lot sand | y = 2.99 + 13.66x | 0.96 | 2.99 | 13.66 |
| UTA residence hall clay | y = 1.58 + 24.67x | 0.98 | 1.58 | 24.67 |

### 3.7.4 Calibration for Thermal Conductivity Measurement

A comparison of measured thermal conductivity between the thermo-TDR sensor and thermal properties analyzer (KD2 Pro) is shown in Figure 3.12. The relative deviation was within 10% for thermal conductivity.

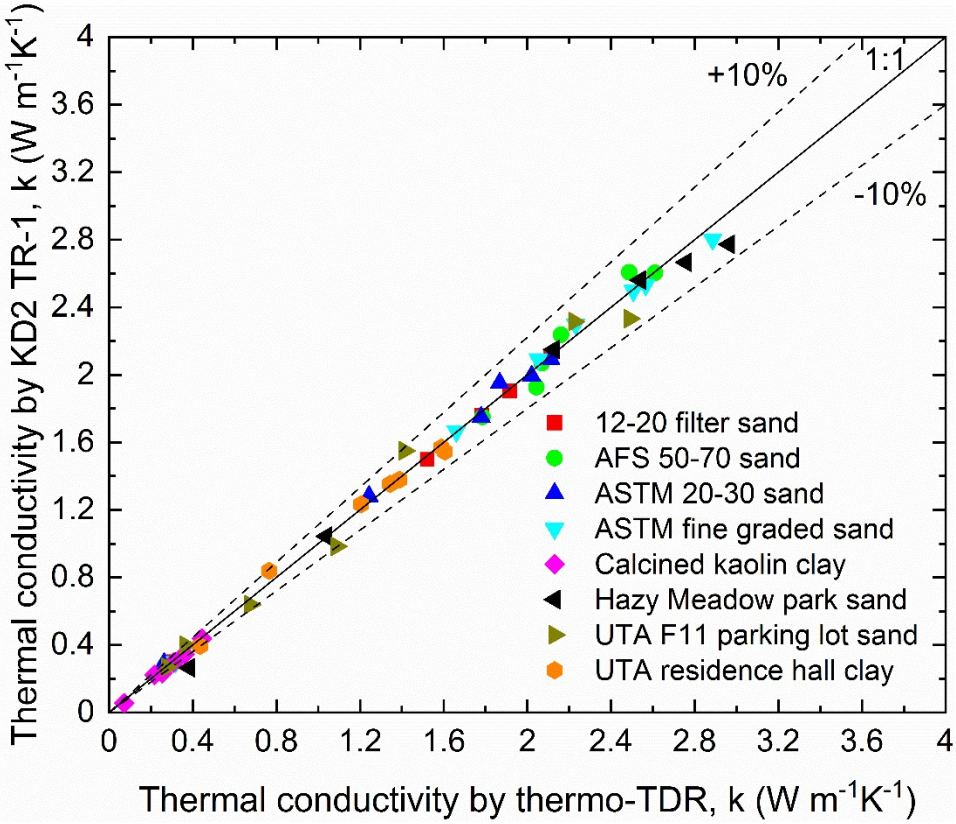


Figure 3.12 Thermal conductivity comparison between the thermo-TDR sensor and KD2 Pro

The coefficient of determination for all the soils is close to 1. The gradient or slope (specific calibration constant b values) are near to 1. And the y-intercept (specific calibration constant values) are negligibly small when comparing the eight different soil types in Table 3.4. This means the fabricated thermo-TDR sensor has excellent performance and precision in the thermal conductivity measurement.

### 3.7.5 Moisture Content and Dry Density

The actual volumetric moisture content using the oven-dry method and the calculated values from Topp's equation (Eq. (3.16)) (Topp et al. 1980) are shown in Figure 3.13.

$$\theta = 4.3 \times 10^{-6} K_a^3 - 5.5 \times 10^{-4} K_a^2 + 2.92 \times 10^{-2} K_a - 5.3 \times 10^{-2} \qquad (3.16)$$

where

$\theta$ = the volumetric moisture content, $m^3/m^3$, and

$K_a$ = the measured apparent dielectric constant from TDR waveforms.

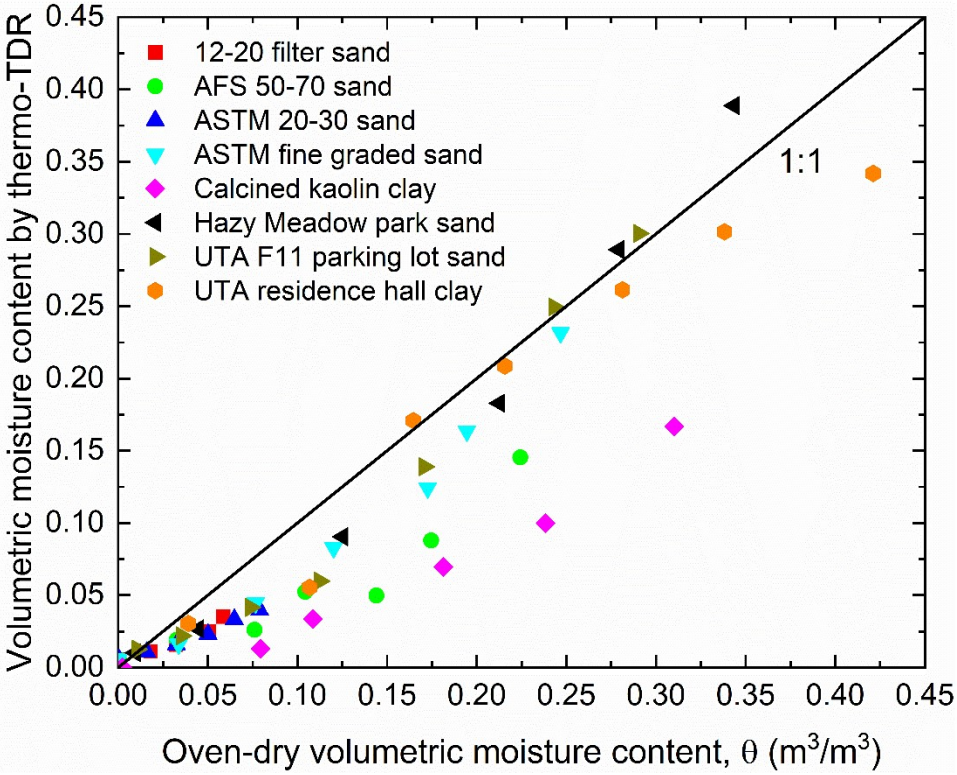


Figure 3.13 Actual volumetric moisture content and calculated value from Topp's equation (Topp et al. 1980)

The relationship between the measured apparent dielectric constant using the thermo-TDR sensor and the actual volumetric moisture content using the drying oven method is shown in Figure 3.14. A slight inconsistency was presented between the predicted values by Topp's equation (black line) and the measured volumetric moisture content for sand (red dash line). Besides, a massive difference exists between the predicted values in Topp's equation (black line) and the measured volumetric moisture content for clay (purple dash line). The divergence can be input as due to the

effects of the mineral component, particle size, and soil texture. Figure 3.14 shows that the $\theta - K_a$ relationships do not correspond with Topp's equation for sand or clay. The new fitted relationships for sand and clay are shown in Eq. (3.17) and (3.18), respectively.

$$Sand: \theta = 8.0 \times 10^{-5} K_a^3 - 3.6 \times 10^{-3} K_a^2 + 6.05 \times 10^{-2} K_a - 9.77 \times 10^{-2} \quad (3.17)$$

$$Clay: \theta = 4.0 \times 10^{-5} K_a^3 - 4.1 \times 10^{-3} K_a^2 + 7.94 \times 10^{-2} K_a - 9.56 \times 10^{-2} \quad (3.18)$$

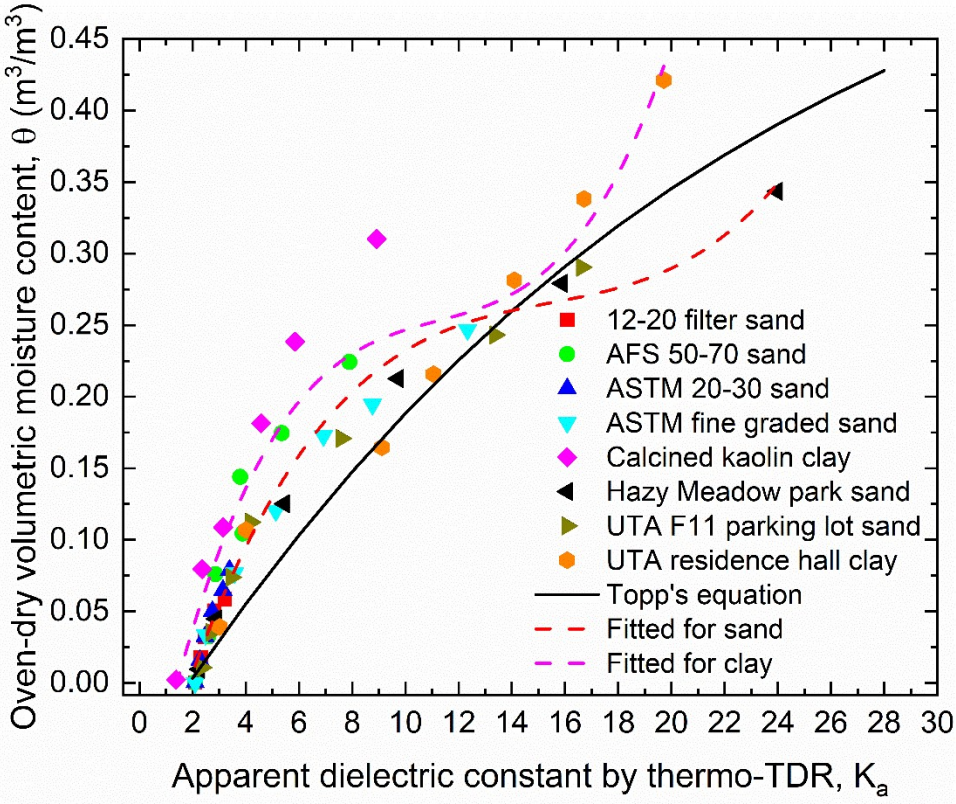


Figure 3.14 Relationship between volumetric moisture content and apparent dielectric constant

Based on the calibration relationships of the apparent dielectric constant and electrical conductivity determined from TDR waveforms, Eqs. (3.14) and (3.15) were used to predict soil gravimetric moisture content and dry density. A comparison between the oven-dry and thermo-TDR determined values of gravimetric moisture content and dry density for sand and clay is shown

in Figure 3.15. The relative deviation for both gravimetric moisture content and dry density prediction is within 10%. Since Eqs. (3.14) and (3.15) were derived from calibrated equations for the dielectric constant (Table 3.2) and electrical conductivity (Table 3.3), which represent an excellent linear relationship in the two calibrated equations with expectations of high accuracy in predicting soil gravimetric moisture content and dry density. Therefore, the superb performance of the thermo-TDR sensor was observed in measuring soil moisture content and dry density.

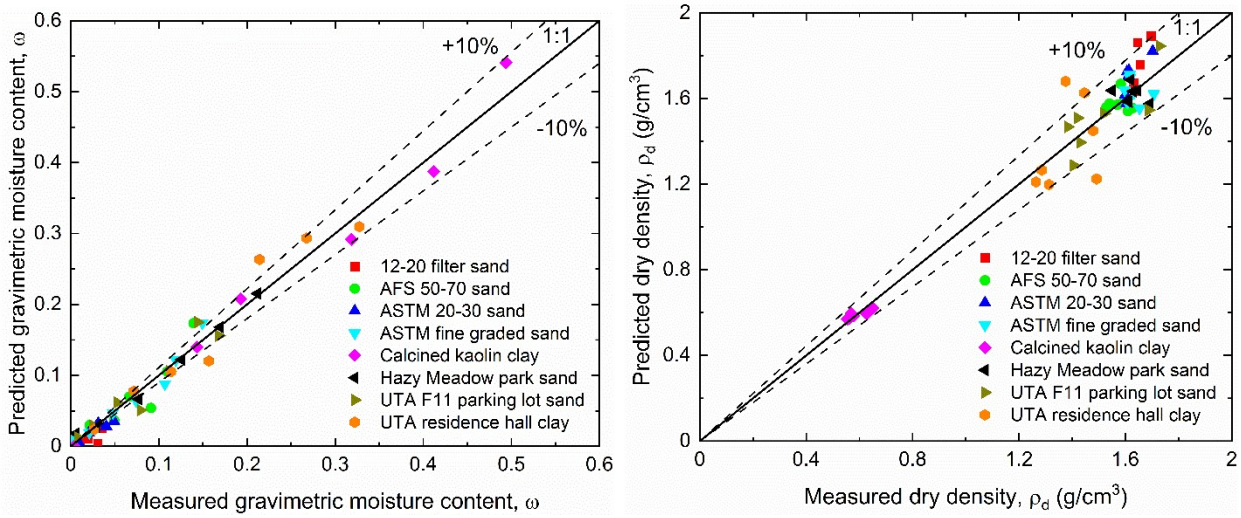


Figure 3.15 Comparison of oven-dry and thermo-TDR determined gravimetric moisture content and dry density

## 3.8 Experiment for Effects of Temperature on Apparent Dielectric Constant and Electrical Conductivity with Distilled Water

A temperature effect test for distilled water was performed to explore the effects of temperature on the apparent dielectric constant and electrical conductivity. The experiment related materials were placed in an environmental chamber for 24 hours. The experiment includes a beaker, distilled water, a thermo-TDR sensor, a thermocouple, and a data logger with an automatic recording code. The experimental setup is very similar to Figure 3.7. The thermocouple is used for

ambient temperature measurement. The recorded ambient temperature and thermo-TDR sensor measured temperature is shown in Figure 3.16. The recorded temperatures range from nearly 22 °C to around 12 °C.

Pepin et al. (1995) confirmed the formula for determining the dielectric constant of water based on the temperatures. The formula characterized as

$$\varepsilon_w = 78.54 \times (1 - 4.579 \times 10^{-3}\,\Delta + 1.19 \times 10^{-5}\,\Delta^2 - 2.8 \times 10^{-8}\,\Delta^3) \quad (3.19)$$

where

$\varepsilon_w$ = the dielectric constant of water at the corresponding temperature; thus

$\Delta$ = 25 °C (the temperature of distilled water).

Stogryn (1971) proposed a formula for determining water's electrical conductivity at the corresponding temperature shown below.

$$\sigma_w = \sigma_{w(25\,°C)}\, EXP(-\Delta'(2.033 \times 10^{-2} + 1.266 \times 10^{-4}\Delta' + 2.464 \times 10^{-6}\,\Delta'^2) \quad (3.20)$$

where

$\sigma_w$ = the electrical conductivity of water at the corresponding temperature (dS/m).

$\Delta'$ = 25 °C (i.e., the temperature of distilled water under ambient conditions).

The corresponding measured and predicted dielectric constant with various temperatures for distilled water is shown in Figure 3.17. The measured dielectric constant was obtained using a thermo-TDR sensor. The predicted dielectric constant was determined by Eq. (3.19). Figure 3.17 presents the apparent dielectric constant decreasing linearly from a lower temperature to a higher temperature. The corresponding measured and predicted electrical conductivity with the

temperature for distilled water is shown in Fig. 3.18. The measured electrical conductivity was obtained using a thermo-TDR sensor. The predicted electrical conductivity was determined from Eq. (3.20). Fig. 3.18 shows the electrical conductivity increasing linearly from a lower temperature to a higher temperature. Therefore, the temperature slightly affects both the apparent dielectric constant and the electrical conductivity measurement.

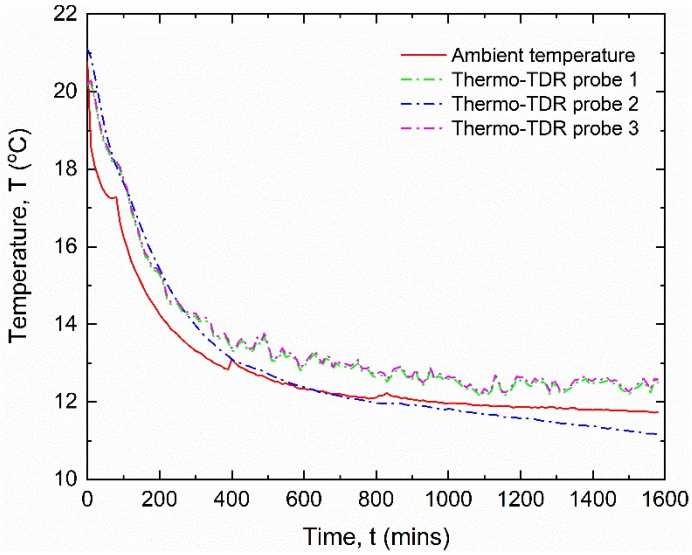


Figure 3.16 Recorded temperature variation for temperature effects test

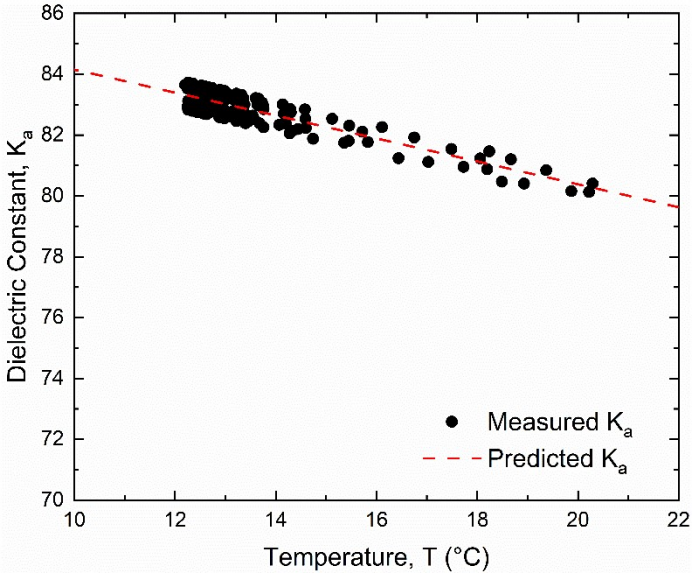


Figure 3.17 Apparent and predicted dielectric constant variation with temperature for distilled water

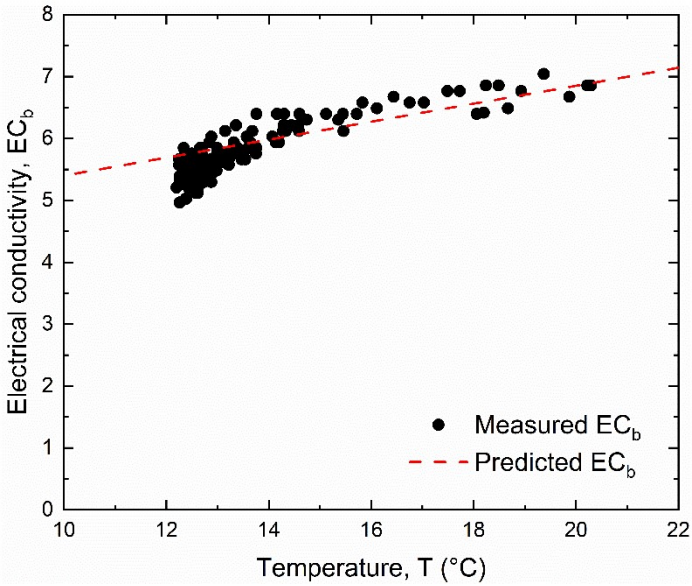


Figure 3.18 Measured and predicted electrical conductivity variation with temperature for distilled water

3.9 Validation of Temperature Compensation for One-Step Method

Measured apparent dielectric constant and bulk electrical conductivity are affected by ambient temperature. A formula for dielectric constant correction as Eq. (3.21) is provided by Yu and Drnevich (2004).

$$K_{a,20°C} = K_{a,T} \times TCF \tag{3.21}$$

where

TCF = temperature compensation function

$= 0.97 + 0.0015\, T_{test,℃}$ for cohesionless soils, $4\ ℃ \leq T_{test,℃} \leq 40\ ℃$

$= 1.10 - 0.005\, T_{test,℃}$ for cohesive soils, $4\ ℃ \leq T_{test,℃} \leq 40\ ℃$

In order to validate the performance of this dielectric constant correction formula, temperature effect tests for sand were performed with ASTM fine graded sand at two different moisture contents. Experiment related materials were placed in a commercial freezer box for 12 hours. The experiment includes oven-dried ASTM fine graded sand, 7.8% moisture content ASTM fine graded sand, a thermo-TDR sensor, two thermocouples with results recorded by a Pico TC-08 USB thermocouple data logger, and a data logger with an automatic recording code. The experimental setup is very similar to Figure 3.6. Two thermocouples were used for ambient temperature and the bottom part of soil (Figure 3.19 red circles) measurements. The recorded ambient temperature, the temperature at the bottom of the sand, thermo-TDR sensor measured temperature, and the dielectric constant is shown in Figure 3.20. The actual gravimetric moisture content for the dry sand and wet sand was 0.13% and 7.80%, respectively. The recorded temperatures ranged from nearly 20 °C to around 1 °C. Figure 3.20 shows the ambient temperature measurement as lower than the thermo-TDR sensor measurement. The temperature at the bottom part of the sand is higher than the other two locations because the thermocouple at the bottom of

the sand was the least affected. The simulated and measured dielectric constant comparison plots for dry and wet sand are shown in Figure 3.21. The comparison between measured and simulated dielectric constant for dry sand had a better match than that found for wet sand. Based on Figure 3.17 and Figure 3.21, water is the primary factor affecting temperatures of the apparent dielectric constant.

Figure 3.19 Thermocouple at the bottom of the compaction mold

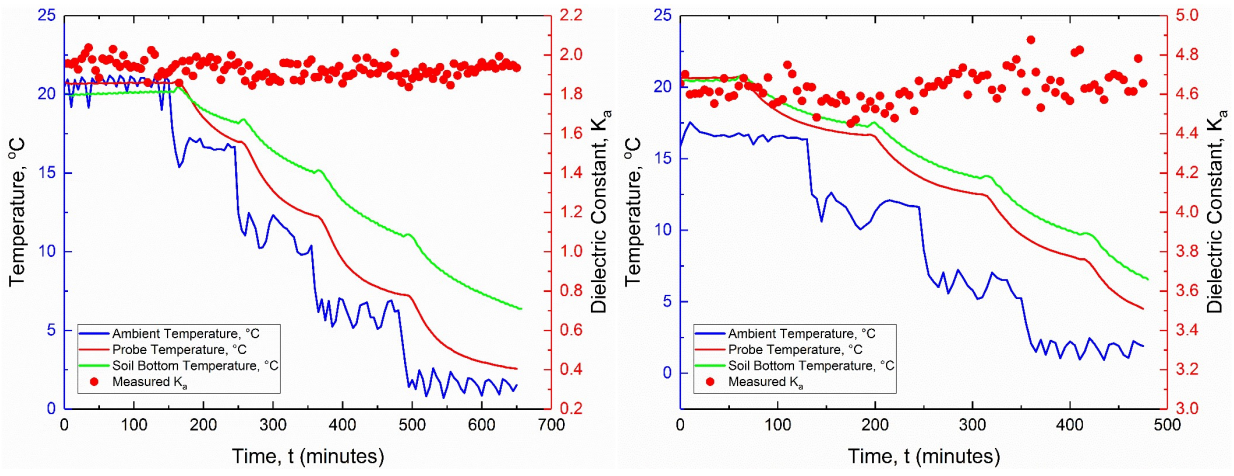


(A) (B)

Figure 3.20 Temperature variations for ambient soil, sensor probes, and soil bottom section temperatures and measured dielectric constant values: (A) for dry sand and (B) for wet sand

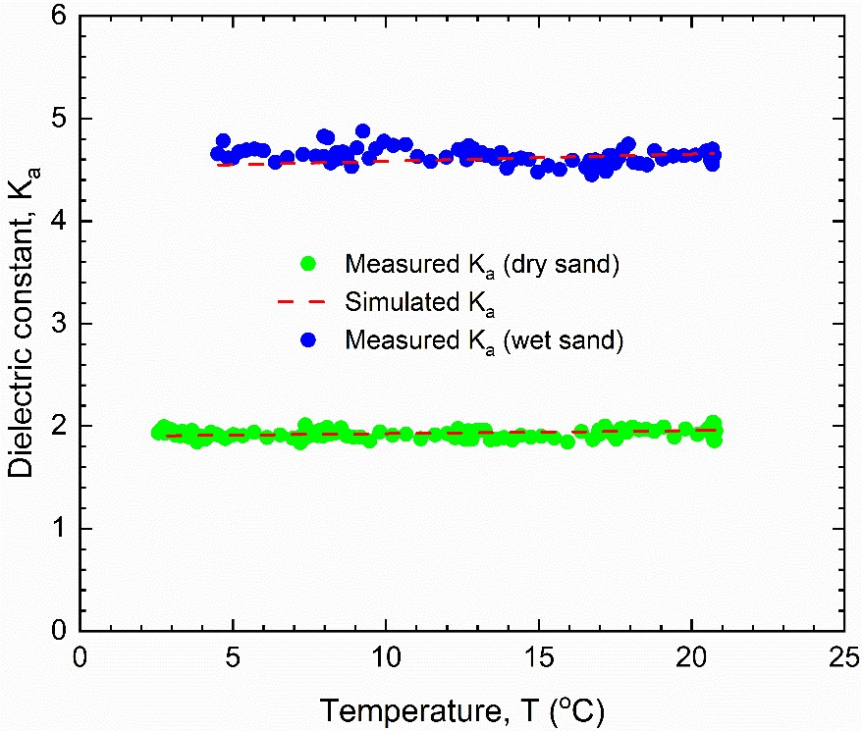


Figure 3.21 Measured and simulated dielectric constant ($K_a$) comparison

Persson and Berndtsson (1998) proposed a temperature compensation function for bulk electrical conductivity and compensated the effects of temperature on bulk electrical conductivity in TDR measurements.

Figure 3.22 presents the measured electrical conductivity for dry sand and wet sand. A simulated electrical conductivity trendline with a temperature dependence factor of 0.1580 (inspired by Persson and Berndtsson (1998)) for both dry sand and wet sand is shown in Figure 3.22. It was observed that the electrical conductivity values increase with the increase of temperature from Figure 3.22. Based on Figure 3.18 and Figure 3.22, water is the minor factor for

the temperature effects on electrical conductivity. Persson and Berndtsson (1998) found no significant differences depending on the temperatures between the different soils.

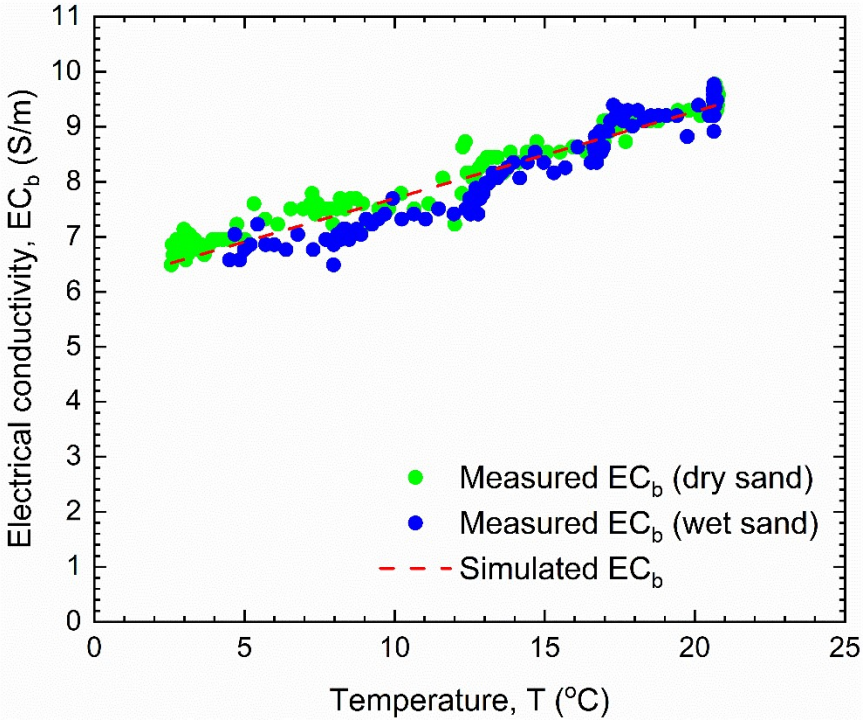


Figure 3.22 Measured electrical conductivity versus temperature

## 3.10 Conclusions

In this chapter, an overview of the performance of the optimal thermo-TDR sensor was provided. The optimal sensor satisfied all the requirements and was improved by previous experiences. The author learned from the successes and failures of earlier sensor fabrication, such as the soldering process, probe immobilizing, and wire connection. Later on, the new sensor was fabricated. This paper provides a kind of improved process for sensor calibration. Mastering the procedure of sensor calibration is essential. A way to achieve or improve the sensor calibration of soil is presented in this study.

Seven types of sands and one clay were used for laboratory experiments for the thermo-TDR sensor evaluation performance. Sensor evaluations include the dielectric constant, electrical conductivity, and thermal conductivity. The calibrated results illustrate that the sensor had a brilliant performance for the measurement of thermal conductivity. The performance of the dielectric constant and electrical conductivity were also exceptional. Through a comparison could be made between results from the optimal sensor and the previous sensor, the optimal thermo-TDR sensor had a better demonstration in many ways.

# 4 CHAPTER 4 MODIFIED HANGING COLUMN DEVICE (MHCD) TEST

## 4.1 Introduction

Awareness of soil thermal conductivity and matric suction, together with soil moisture and density, is fundamental to understanding the coupled thermal-hydro-mechanical (THM) processes in soils. THM processes have dominated the soil behavior in active geothermal structures (Zhang et al. 2015). Brandl (2006) demonstrated and explained the effects of soil thermal properties in the design of energy piles. When heat carrier fluid is circulated inside the energy piles, heat exchange occurs between the surrounding soils and the fluid. However, it is widely known that moisture migration and heat transfer at shallow depths near the land-atmosphere interface are strongly coupled processes that create spatial and temporal temperature and water content distributions or gradients (Smits et al. 2010). Hence, the study of soil moisture, suction, and thermal conductivity is indispensable to understanding these conjugated processes. Furthermore, it capacitates the design of more efficient geothermal systems.

Thermo-time-domain reflectometry (thermo-TDR) sensors incorporate the dual-probe heat pulse (DPHP) device with the TDR technique for simultaneous measurements of soil water content, dry density, and thermal properties. Yu et al. (2015) presented a newly designed thermo-TDR sensor for geothermal applications and demonstrated high accuracy in measuring soil thermal and geotechnical properties in compacted soil samples. Zhang et al. (2015) used the sensor to further study quartz sands and sand-kaolin clay mixtures and to measure their thermal conductivity. The thermo-TDR has shown that the probe has a reasonable accuracy for measuring moisture content, dry density, and thermal properties for both coarse-grained and fine-grained soils. However, in former studies, the thermo-TDR sensor has mainly been used to measure soil properties under

static moisture situations (Zhang et al. 2018). The performance of the sensor under dynamic moisture situations was tested in the initial stage.

A newer designed thermo-TDR sensor was tested in stage compacted sands and showed better performance over the former sensors presented by Zhang et al. (2015) and Wang and Yu (2018). The objective of this chapter is to verify the performance of the newer designed thermo-TDR sensors to measure the sand's thermal conductivity with a complete moisture spectrum during the dry-out processes and to determine the soil-water characteristic curve (SWCC) and the thermal conductivity dry-out curve (TCDC) during the drainage and evaporation processes. MHCD tests were implemented with the thermo-TDR sensor, a suction sensor, and a thermal properties analyzer on three sands in different temperature environment.

## 4.2 Materials and Methods

### 4.2.1 Modified Hanging Column Device (MHCD)

In this research, dry-out tests were conducted on sand via a modified hanging column device (MHCD) to monitor water content, matric suction, and sand thermal conductivity during drainage and evaporation processes. The device includes a top cap, a perforated bottom plate, an acrylic Tempe cell, and a standpipe. The cell has an external diameter of 13.4 cm, a wall thickness of 0.7 cm, and a height of 8.0 cm. The bottom brass plate was covered with a high-air-entry nylon membrane (pore size = 0.2 μm, air-entry pressure = 340 kPa), across which suction is effected by way of an external hanging-column water system (ASTM D6836-16). Three sensors were assembled radially into a soil sample at approximately the same height in the cell to determine the corresponding soil moisture content, matric suction, and thermal conductivity measurements in the same situation. With the utilization of the modified hanging column device, soil suction is slowly and sustainably increased by bottom drainage and then an evaporation phase (Yao et al. 2014).

During the drainage and evaporation processes, the sand thermal conductivity measurement used the newer designed thermo-TDR sensor, designed and manufactured by Wang and Yu (2018). A thermal properties analyzer with a TR-1 thermal needle manufactured by Decagon Devices was also used for the sand thermal conductivity measurement.

### 4.2.2 Sensors for Tests

The installed sensors include one thermo-TDR sensor, one thermal properties analyzer with a TR-1 thermal needle probe, and one suction sensor (T5x). The thermo-TDR sensor integrates the dual-probe heat pulse (DPHP) device with the time domain reflectometry (TDR) technique. It can be used for water content, dry density, and thermal properties measurements. The newly designed thermo-TDR sensor improved by Wang and Yu (2018) was selected for the modified hanging column device (MHCD) tests. The length of the needles of the fabricated thermo-TDR sensor, including the tips, is 54 mm; the diameter of the probe is 2 mm, and the probe-to-probe spacing is 6 mm. The thermo-TDR sensor was calibrated and demonstrated improved accuracy and reliability when compared to the previous ones (Wang and Yu 2018).

A KD2 standard pro thermal property analyzer, i.e., a KD2 (TR-1) single probe, was selected to measure the thermal conductivity as a standard comparison base. The TR-1 thermal needle probe, 100 mm in length and 2.4 mm in diameter, is able to measure thermal conductivity with an accuracy of ± 0.02 $Wm^{-1}K^{-1}$ from 0.1 to 0.2 $Wm^{-1}K^{-1}$, and ± 10 % from 0.2 to 4.0 $Wm^{-1}K^{-1}$. T5x is a piezoresistive pressure transducer that can measure the soil water tension against the atmospheric pressure up to - 85 kPa transmitted via the ceramic cup into the tensiometer. The maximum overpressure for this sensor is ± 300 kPa. The shaft diameter is 5 mm. The shaft material is acrylic glass. The body diameter is 20 mm. The reference atmospheric air pressure is performed to the pressure transducer via the air-permeable Teflon membrane and through the cable.

4.2.3 Determination of Volumetric Moisture Content, Matric Suction, and Thermal Conductivity

A heat pulse in the central probe of the thermo-TDR sensor is generated by connecting a direct current (DC) source to the resistance wire located in the central probe. The temperature variation of the three probes is monitored using a thermocouple data logger manufactured by Pico Technology. A theory of infinite line heat source predicts the temperature response of three probes and is shown in Eq. (5.1) (De Vries 1952; Kluitenberg et al. 1993).

$$T(r,t) = (Q/4\pi\alpha)[Ei(-r^2/4\alpha(t-t_0)) - Ei(-r^2/4\alpha t)] \quad (5.1)$$

where

$T$ = the influence in temperature; $Q$ = the line heat source strength; $\alpha$ = soil thermal diffusivity; $Ei(x)$ = the exponential integral; $r$ = the radial distance between the central probe and the external probes; $t$ = the traveling time; and $t_0$ = the heat pulse duration.

The volumetric heat capacity, the thermal diffusivity, and the thermal conductivity can be determined as follows:

$$\rho_c = (q/4\pi\alpha T_m)[Ei(-r^2/4\alpha(t_m-t_0)) - Ei(-r^2/4\alpha t_m)] \quad (5.2)$$

$$\alpha = (r^2/4)[1/(t_m - t_0)]/\ln[t_m/(t_m - t_0)] \quad (5.3)$$

$$k = \frac{q}{4\pi T_m}\left[Ei\left(\frac{-\ln\left[\frac{t_m}{t_m - t_0}\right]}{t_0/t_m}\right) - Ei\left(\frac{-\ln[t_m(t_m - t_0)]}{t_0/(t_m - t_0)}\right)\right] \quad (5.4)$$

where

$r$ = the radial distance between the central probe and the external probes; $t_m$ = the time recorded at the maximum temperature of the external probes; $T_m$ = the maximum temperature difference of the external probes.

Yu et al. (2015) presented detailed calculations of the volumetric heat capacity, the thermal diffusivity, and the thermal conductivity via Eqs. (5.2) to (5.4), which support or verify the recorded heat pulse response curve. Only the measurement of thermal conductivity is demonstrated in this study.

Topp's equation (Topp et al. 1980) used the apparent dielectric constant obtained from TDR waveforms. Zhang et al. (2015) determined the volumetric moisture content of soil samples. A relationship between the apparent dielectric constant and volumetric moisture content can be expressed as:

$$\theta = 4.3 \times 10^{-6} K_a^3 - 5.5 \times 10^{-4} K_a^2 + 2.92 \times 10^{-2} K_a - 5.3 \times 10^{-2} \quad (5.5)$$

where

$\theta$ = the volumetric moisture content, $m^3/m^3$; and $K_a$ = the apparent dielectric constant, determined from the thermo-TDR sensor.

The soil matric suction measurement was determined by a pressure transducer tensiometer (T5x). A calibration equation is offered from the manufacturer, in which 1 mV equals 1 kPa suction.

### 4.2.4 MHCD Tests

The American Society for Testing and Materials (ASTM) fine-graded sand, ASTM 20-30 sand, and AFS 50-70 sand was chosen for the MHCD tests. The ASTM fine-graded sand, ASTM 20-30 sand, and AFS 50-70 sand have particles ranging from 150 μm to 600 μm, 600 μm to 850 μm, and 210 μm to 300 μm, respectively. This exceptionally fine graded sand for ASTM tests are naturally rounded silica sands of nearly pure quartz, mined from the Ottawa, Illinois area. A sieve

analysis test was performed on each of the three sands. The grain size distribution curves for the three testing sands are shown in Figure 4.1.

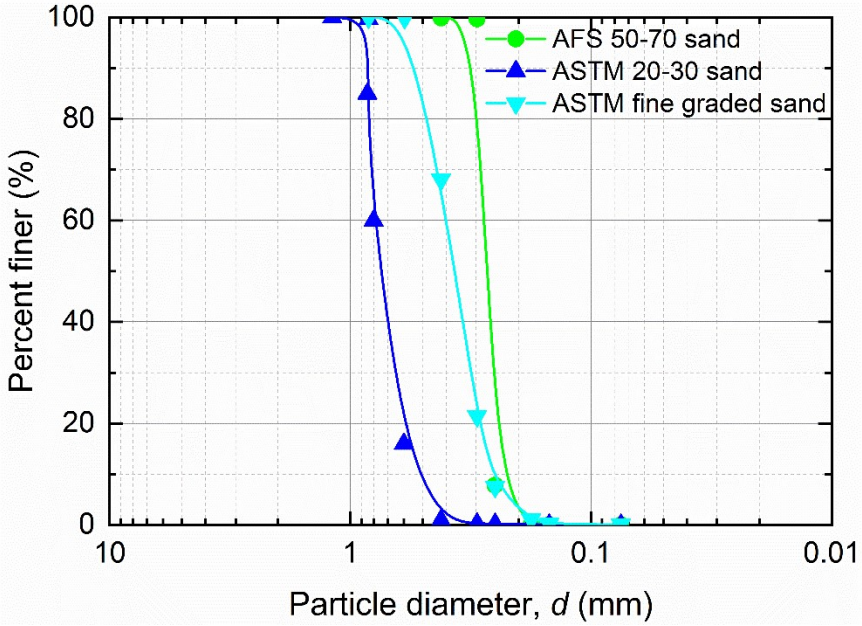


Figure 4.1 Grain size distribution curves of testing soils

A thermo-TDR sensor was used for the sand's temperature, moisture content, and thermal conductivity measurements during the tests. A thermal properties analyzer with a TR-1 thermal needle was also used for thermal conductivity measurements. The sand matric suction measurements utilized a suction sensor (T5x). The testing sands were first dried in the oven at 105°C for one day; then, the sample was put into the Tempe cell in four uniform layers, using a funnel and a tripod, at the free fall height of 38 cm for each layer. The top of the sand sample was 1.0 cm below the cell's top edge. The height of the sand sample was infinitely close to 7.0 cm. Probes of Thermo-TDR, TR-1, and T5x were horizontally embedded in the Tempe Cell just when the second layer was filled. It is around 3.5 cm above the bottom of the cell, as demonstrated in Figure 4.2. The three sensors were installed with the TR-1 thermal needle at the top, the shaft of T5x at the middle, and Thermo-TDR probes at the bottom with a slight overlap of their tips and a

gap between the ends of around 4 mm. Because the tip has less effect on the sensor measurement, the disturbance was not significant. The height of the standby column is 76 cm. The dimensions of the Tempe cell are 13.4 cm (external diameter) 0.7 cm (wall thickness) 8.0 cm (height).

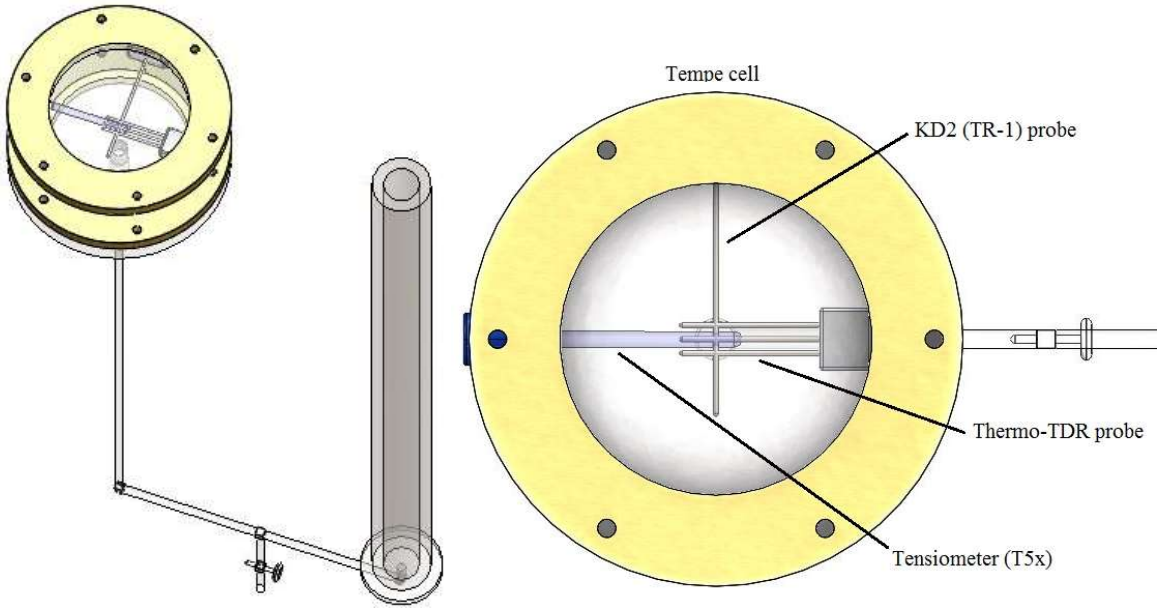


(A) (B)

Figure 4.2 Schematic diagram of modified hanging column device (MHCD): (A) trimetric view and (B) top view

The soil matric suction, moisture content, thermal conductivity, and temperature were initially measured at a completely dry condition. The standpipe was then filled with distilled water to saturate the soil sample from bottom to top until around 0.5 cm of water ponded on the sand sample's top surface. Then, a top cap was placed on top of the Tempe cell. The valve was opened to lower the water level (in both cell and standpipe) to the cell's midpoint at the height where the sensor probes were located. The valve was partially closed to generate a very slow water drip at a rate of 3 to 5 seconds per drip to discharge the water from the sand sample. Then, the suction,

moisture content, and thermal conductivity were measured concurrently by the sensors, which recorded continuously using data loggers at 1-h intervals. The time interval between the thermal properties analyzer and thermo-TDR sensor measurements was 5 minutes to afford time for the equilibrium of local temperatures. After that, a direct current of 0.15 A was delivered to each thermal properties analyzer to affect the resistance wire of the thermo-TDR sensor for 15 seconds to heat the sand sample. To determine the thermal conductivity, temperature variations at the center probe and the two side probes were recorded every second during the heating and following the cooling process. After the water in the standpipe was utterly drained, the cell's top cap was removed from the cell. An electrical fan was located near the cell's top edge to evaporate the sand sample continuously. The test was terminated when the thermal properties analyzer's reading remained constant for at least 4 h. Small pieces of the sand sample were collected, weighed, oven-dried, and weighed again to obtain the gravimetric moisture content at the end of the test. A summary of the MHCD tests is shown in Table 4.1.

Table 4.1 Summary of MHCD tests

| Soil Type | Target Temperature, T (°C) | Initial dry density ($g/cm^3$) | Initial void ratio |
|---|---|---|---|
| ASTM fine graded sand | Room temperature (24) | 1.73 | 0.53 |
| | 10 | 1.73 | 0.53 |
| | 2 | 1.73 | 0.53 |
| ASTM 20-30 sand | Room temperature (24) | 1.71 | 0.55 |
| | 10 | 1.71 | 0.55 |
| AFS 50-70 sand | Room temperature (24) | 1.73 | 0.54 |

## 4.3 Results and Discussion

### 4.3.1 Measurements of Thermal Conductivity

Figure 4.3 demonstrates a comparison of thermal conductivities measured by the thermo-TDR and thermal properties analyzer as a function of time during the drying processes. Soil Matric suction was determined by a tensiometer (T5x) and is also plotted in this figure.

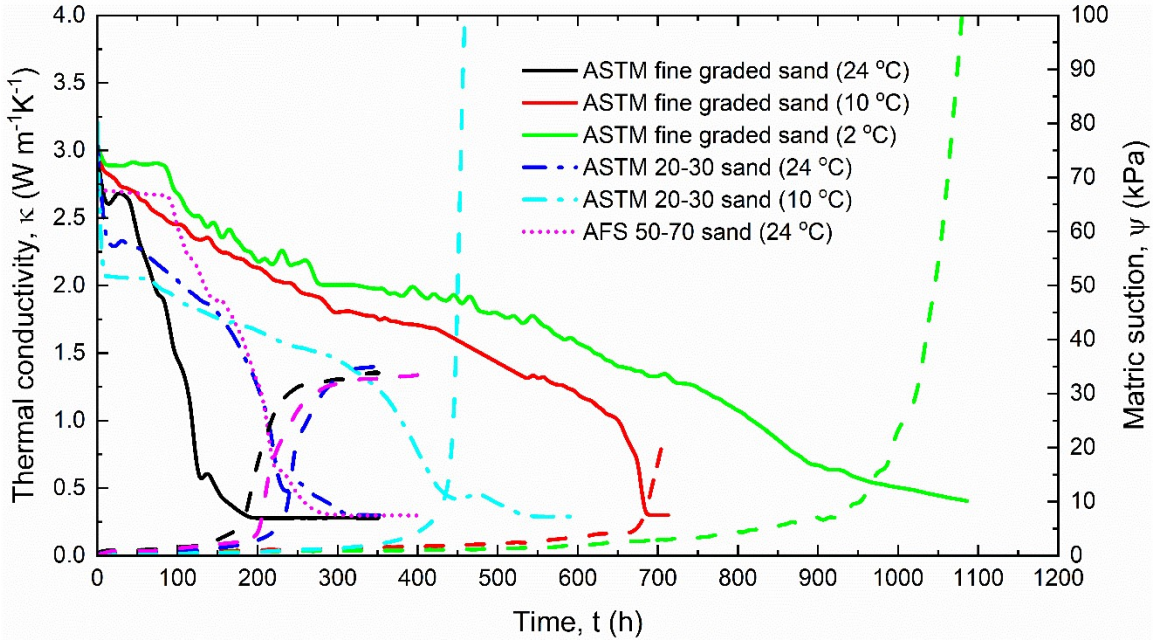


Figure 4.3 Soil thermal conductivity and matric suction as a function of time during the dry-out processes for three sands under different temperature conditions

Figure 4.4 presents a comparison of thermo-TDR measured volumetric moisture content during the drainage and evaporation processes. When the test was started, distilled water was continuously drained from the sand sample through an opened valve at the bottom of the Tempe Cell. The fully saturated sand specimen lost its water content with time. Air then occupied the pore space initially occupied by water. As a result, the extremely low air thermal conductivity led to increased sand particles' thermal contact resistance. The thermal conductivity of air is from 0.02

to 0.03. The thermal conductivity for water is from 0.5 to 0.8, and the thermal conductivity for solid sand is between 2.3 and 3.8. This explains the reason for the sudden drop in thermal conductivity in the first two to four hours, as shown in Figure 4.3. The measurement from the valve shows that it had just been turned on, as shown in Figure 4.4.

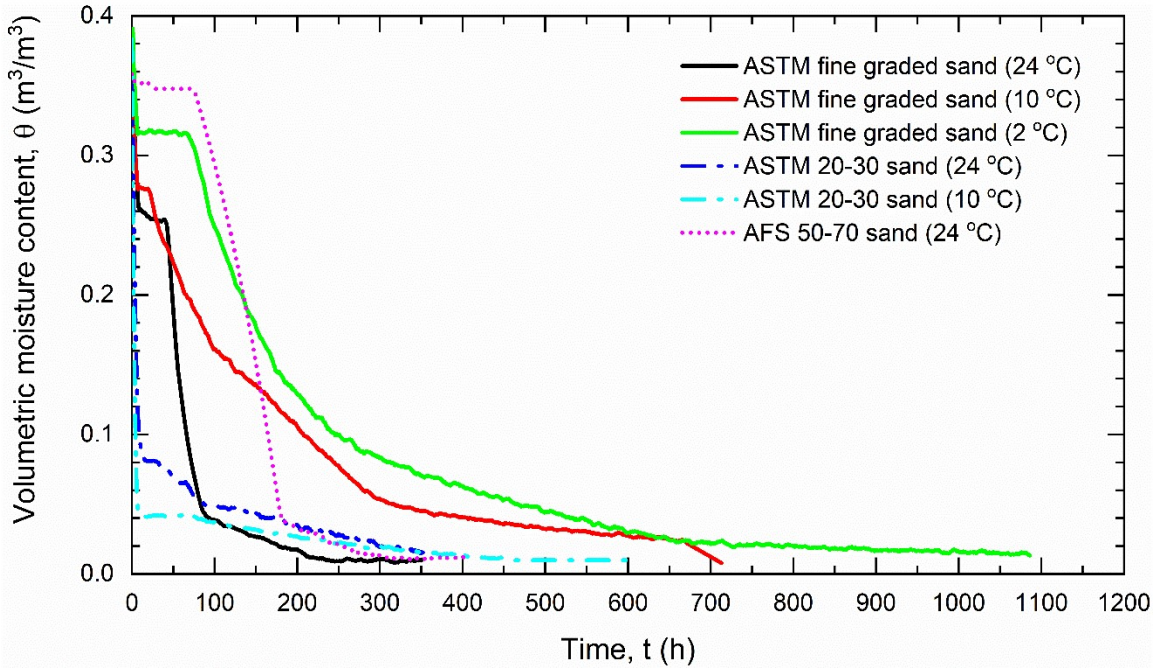


Figure 4.4 Volumetric moisture content (Topp's equation) as a function of time during dry-out processes for three sands under different temperature conditions

Figure 4.5 demonstrates a recorded temperature variation in time during the dry-out processes. ASTM fine graded sand, ASTM 20-30 sand, and AFS 50-70 sand were tested at a room temperature of around 21.1°C (70.0 °F). ASTM fine graded sand was also tested in the environmental chamber at 10°C and 2°C. ASTM 20-30 sand was tested at 10°C in the environmental chamber as well. The probes to monitor temperature were located in the middle layer of the testing sand sample.

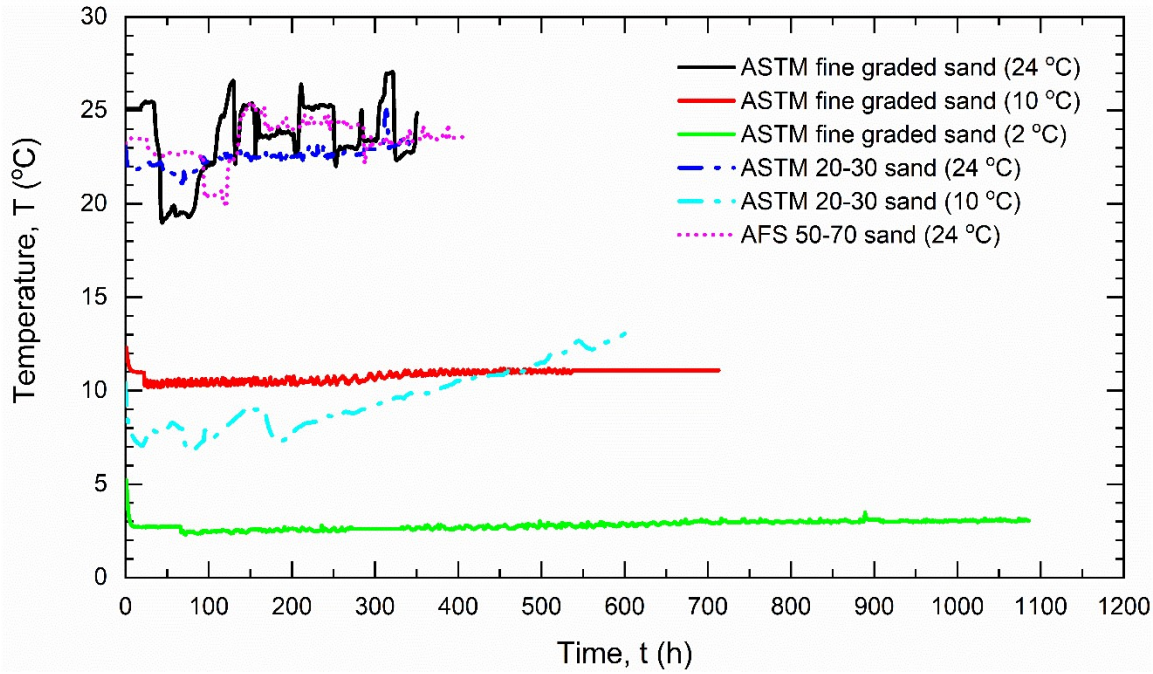


Figure 4.5 Recorded temperature variations with time during the dry-out processes

A comparison of the measured thermal conductivity between the thermo-TDR and thermal properties analyzer is shown in Figure 4.6. Figures 4.6 (A) and (B) demonstrate the thermal conductivity results for the ASTM fine graded and ASTM 20-30 sand at room temperature, respectively. The coefficient of determination for the trend-line is near 1.00 for both tests. This shows that the Thermo-TDR sensor results were very similar to the thermal properties analyzer with a TR-1 thermal needle. The KD2 Pro Thermal Properties Analyzer Manual indicates that the accuracy for the 10-cm long single needle probe of the TR-1 is ±10%.

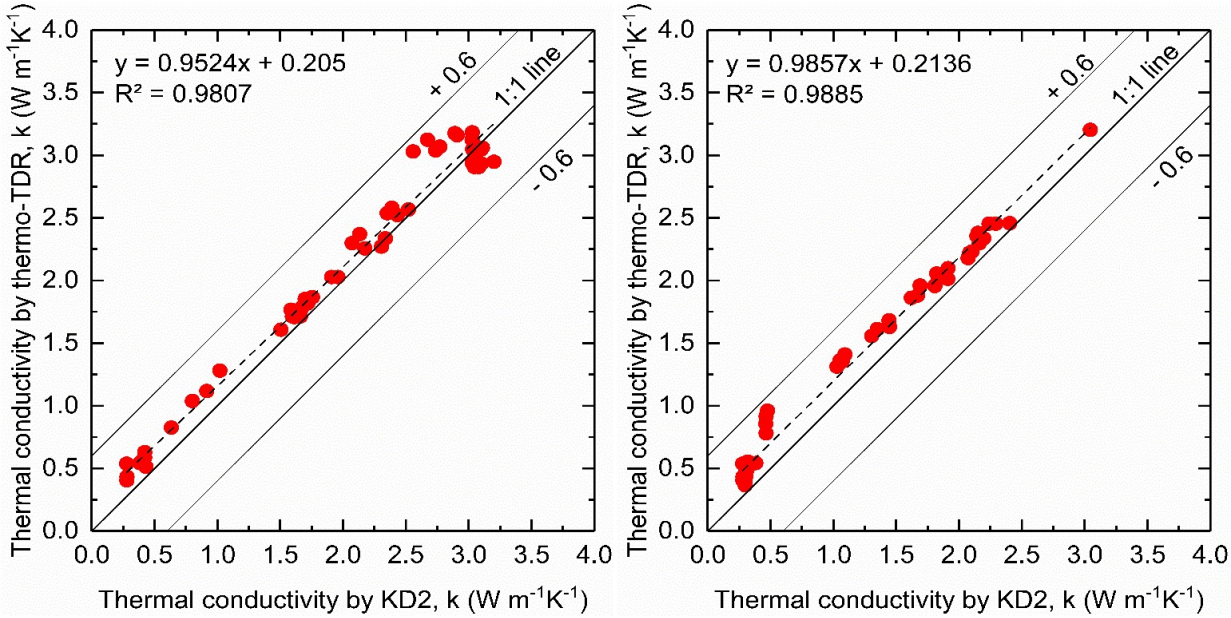


(A) (B)

Figure 4.6 Comparison of the measured thermal conductivity from a thermo-TDR sensor and a KD2 Pro thermal properties analyzer with a TR-1 probe at room temperature: (A) ASTM fine graded sand and (B) ASTM 20-30 sand

### 4.3.2 Soil-Water Characteristic Curve (SWCC)

Figure 4.7 demonstrates the soil-water characteristic curve (SWCC) for ASTM fine graded sand, ASTM 20-30 sand, and AFS 50-70 sand. Figure 4.7 presents the matric suction and volumetric moisture content measured at the same start time. By comparing ASTM 20-30 sand and ASTM fine graded sand at different temperature situations, sand has a higher maximum volumetric moisture content at a lower temperature. Because of the increased water viscosity at low temperatures (Toselli et al. 1999), the three sands had very close values of the maximum matric suction at room temperature, and as shown in Figure 4.7, it is around 36 kPa. The ASTM fine graded sand has a larger matric suction value than the ASTM 20-30 sand under the same moisture content. In addition, the AFS 50-70 sand had a larger matric suction value than the ASTM

fine graded sand. The soils' matric suction for the same moisture content is more significant for soils with small particles. The values obtained from the Tempe cell are the average values of the whole soil sample, while the results from the suction sensor (T5x) are point measurements. Moreover, the soil fabric for the three tests is not the same.

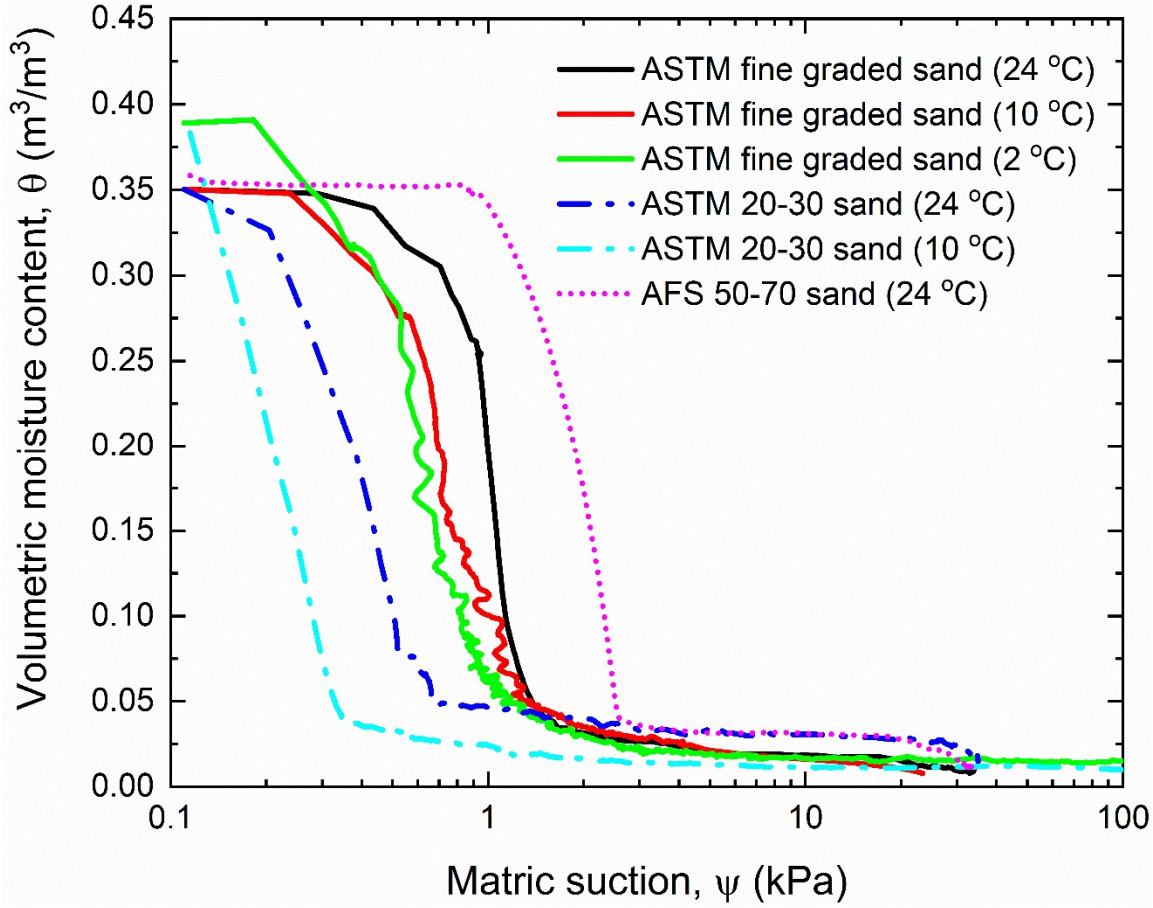


Figure 4.7 Soil-water characteristic curves during the drainage and evaporation processes for three sands at different temperatures condition

### 4.3.3 Thermal Conductivity Dry-Out Curve (TCDC)

Figure 4.8 demonstrates the thermal conductivity dry-out curve for ASTM fine graded sand and ASTM 20-30 sand. Simultaneously, ASTM fine graded sand has a higher thermal conductivity value at the same volumetric moisture content situation. The soils' thermal conductivity for the

same moisture content is greater for soils with small particles. At the low moisture content (regime I), thermal conductivity shows a very pronounced decrease in moisture content. In regime II, water is displaced by air leading to more water in a pendular form. The grain/water paths decrease, heat flows partially through less-conductive air/water/grain or air/grain paths, and apparent thermal conductivity decreases.

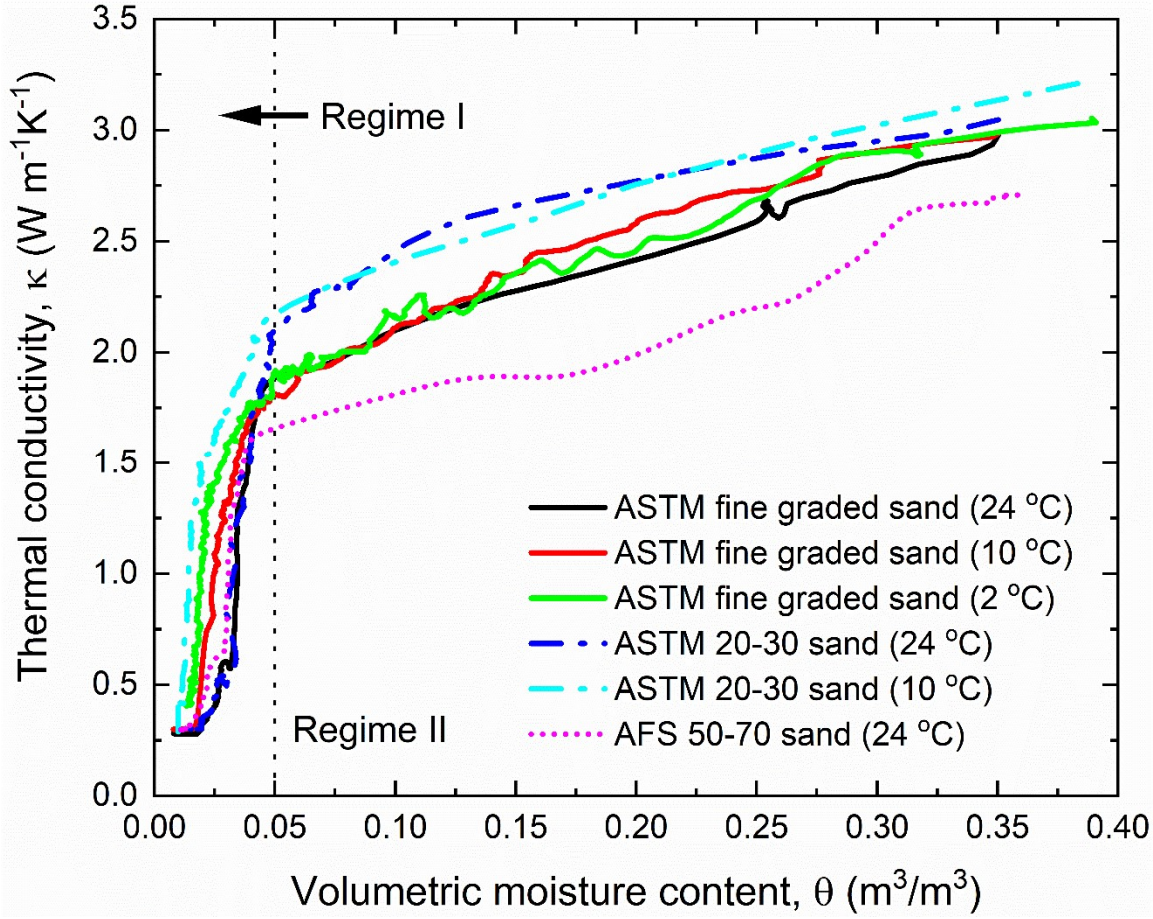


Figure 4.8 Thermal conductivity dry-out curve for three different types of sands under different temperature conditions

# 5 CHAPTER 5 DEVELOPMENT OF SWCC AND TCDC MODELS

## 5.1 Introduction

This chapter introduces a new continuum soil thermal conductivity model development and validation. Laboratory experiments were tested on ASTM fine graded sand, ASTM 20-30 sand, and AFS 50-70 sand using a modified hanging column device at different temperature conditions. Chapter 4 detailed the present test materials, methods, and relevant results. The model was developed based on the thermal conductivity dry-out curve (TCDC). The purpose of this model is to evaluate relevant thermal conductivity values at corresponding volumetric moisture content for different soil types and temperature conditions. This chapter also presents the validation of the soil-water characteristic curve (SWCC) via the MHCD test method. Three SWCC models developed by (Brooks and Corey (1964), van Genuchten (1980), and Fredlund and Xing (1994) were used for SWCC validation.

## 5.2 Validation for SWCC Models

Chapter 2 introduced SWCC models in detail, such as the Brooks and Corey (BC) model, van Genuchten (VG) model, and Fredlund and Xing (FX) model. This section presents the results of the MHCD tests fitted with three SWCC models. Chapter 5 shows the MHCD test in detail.

Figures 5.1 to 5.6 show measured SWCC and fitted models for three different soil types at three different temperature settings. The fitted curves using the FX model were better than the comparative (BC and VG models).

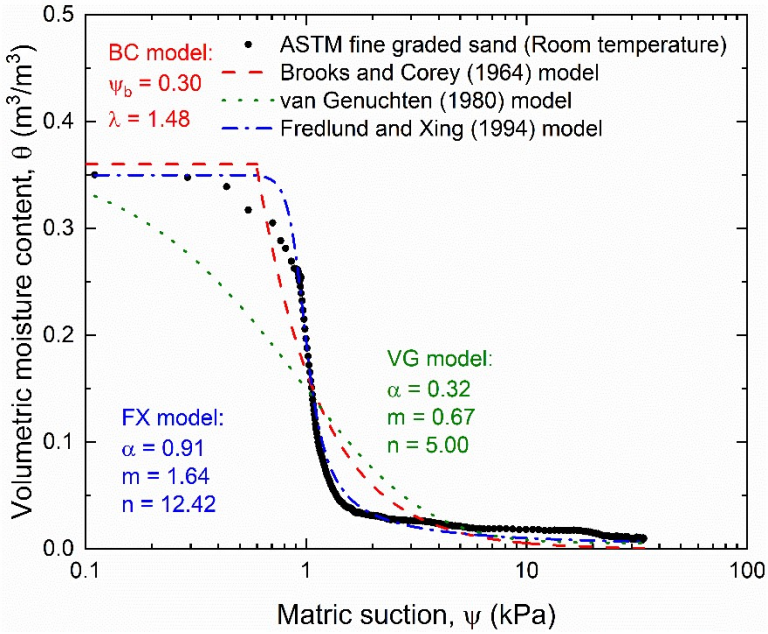


Figure 5.1 Measured SWCC and fitted SWCC models for ASTM fine graded sand at room temperature

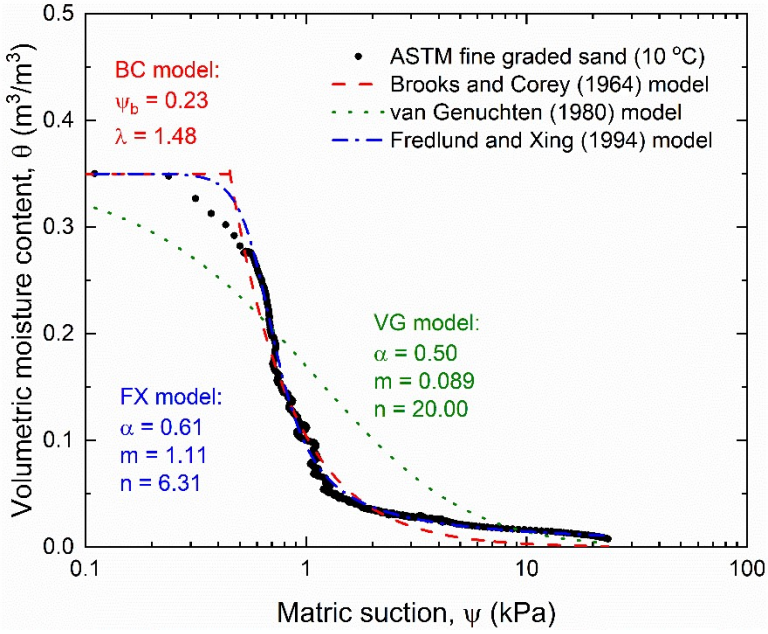


Figure 5.2 Measured SWCC and fitted SWCC models for ASTM fine graded sand at 10 °C temperature setting

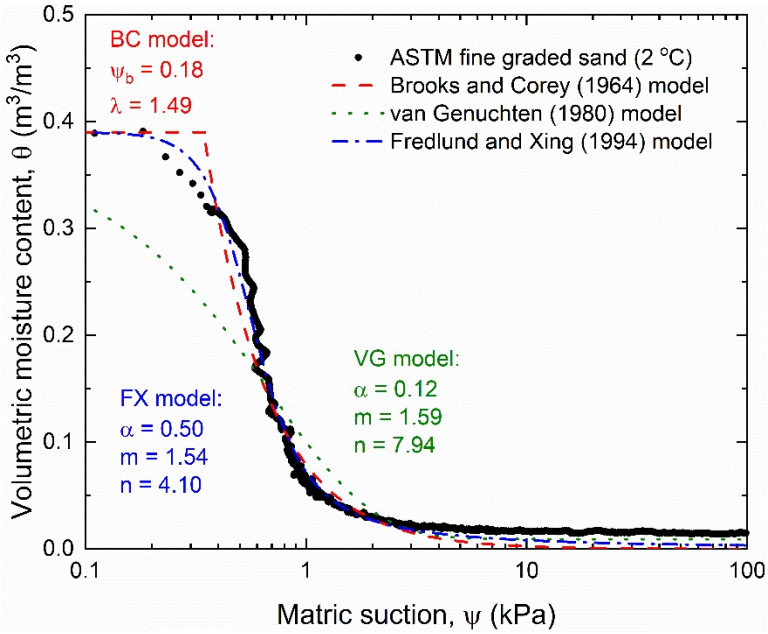


Figure 5.3 Measured SWCC and fitted SWCC models for ASTM fine graded sand at 2 °C temperature setting

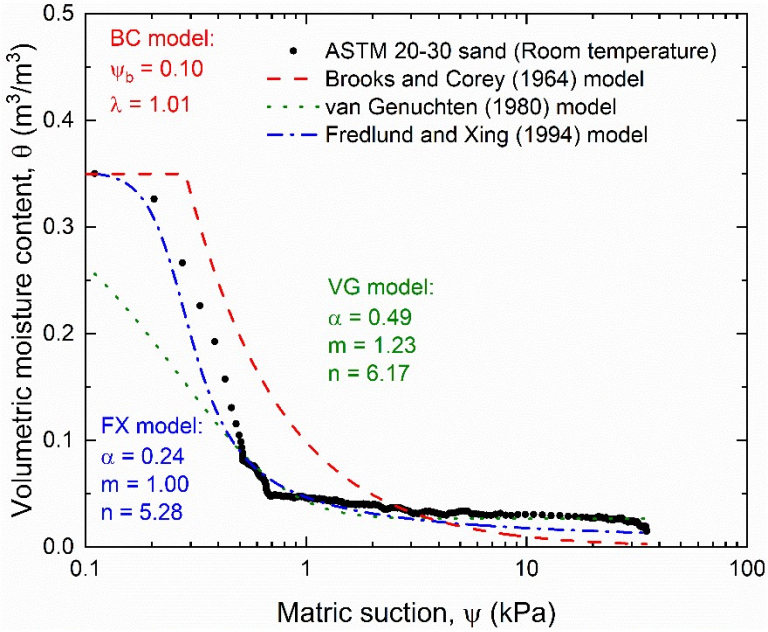


Figure 5.4 Measured SWCC and fitted SWCC models for ASTM 20-30 sand at room temperature

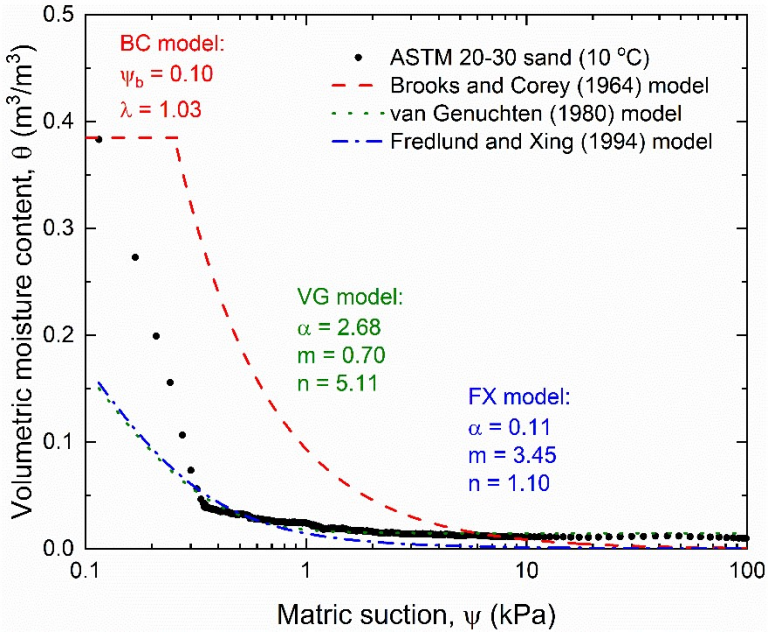


Figure 5.5 Measured SWCC and fitted SWCC models for ASTM 20-30 sand at 10 °C temperature setting

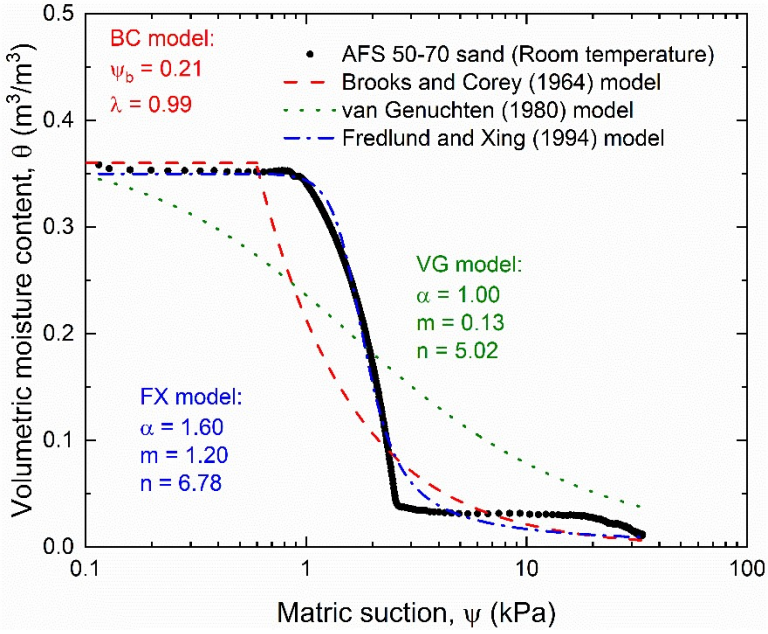


Figure 5.6 Measured SWCC and fitted SWCC models for AFS 50-70 sand at room temperature

5.3 Model for TCDC

This section presents the measured TCDCs and developed TCDC models.

Figures 5.7 to 5.12 show measured TCDCs and fitted curves for three different sand types at different temperature settings.

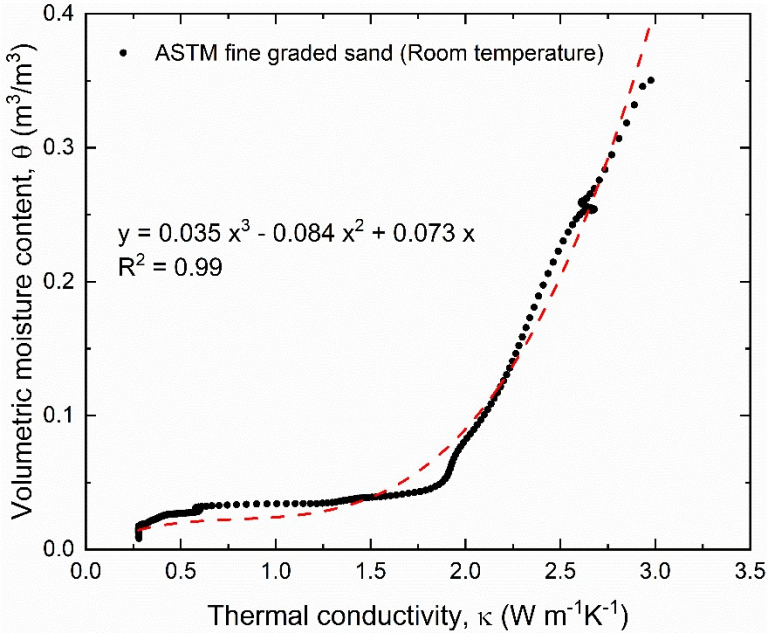


Figure 5.7 Measured TCDC and fitted curves for ASTM fine graded sand at room temperature

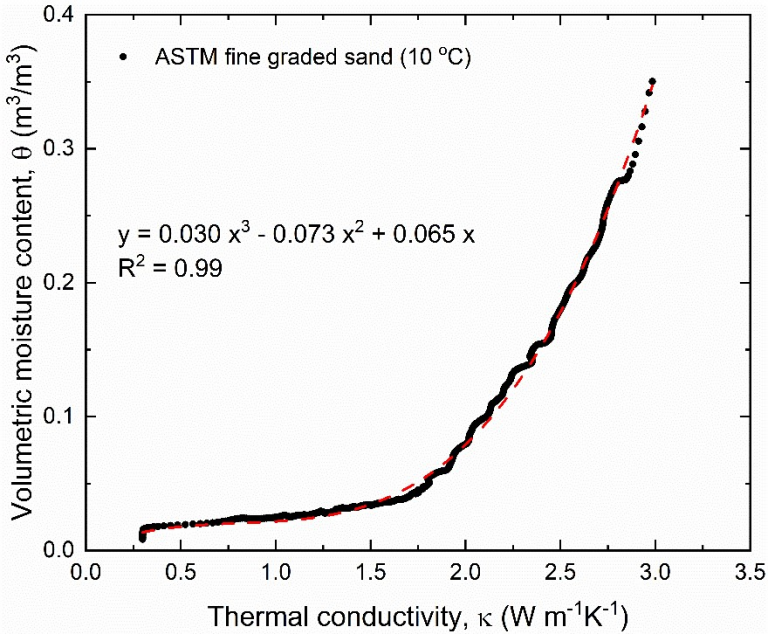


Figure 5.8 Measured TCDC and fitted curves for ASTM fine graded sand at 10 °C temperature setting

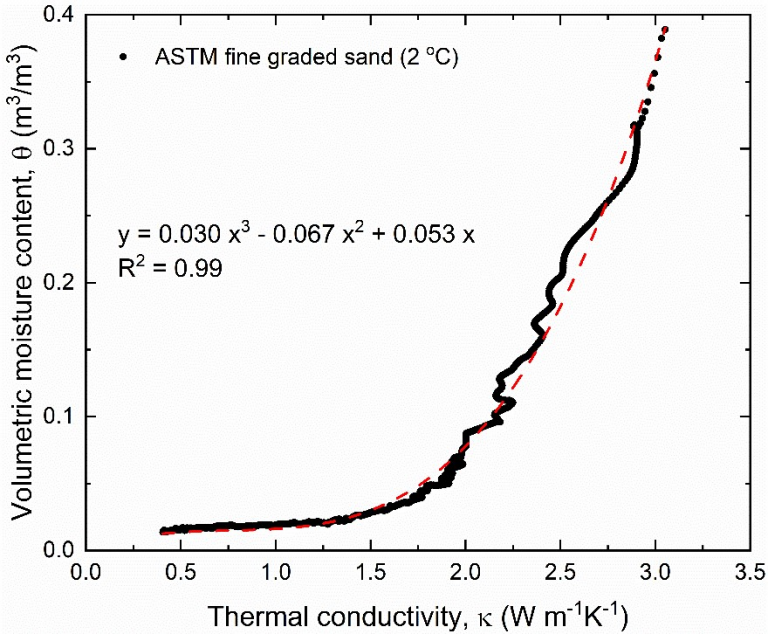


Figure 5.9 Measured TCDC and fitted curves for ASTM fine graded sand at 2 °C temperature setting

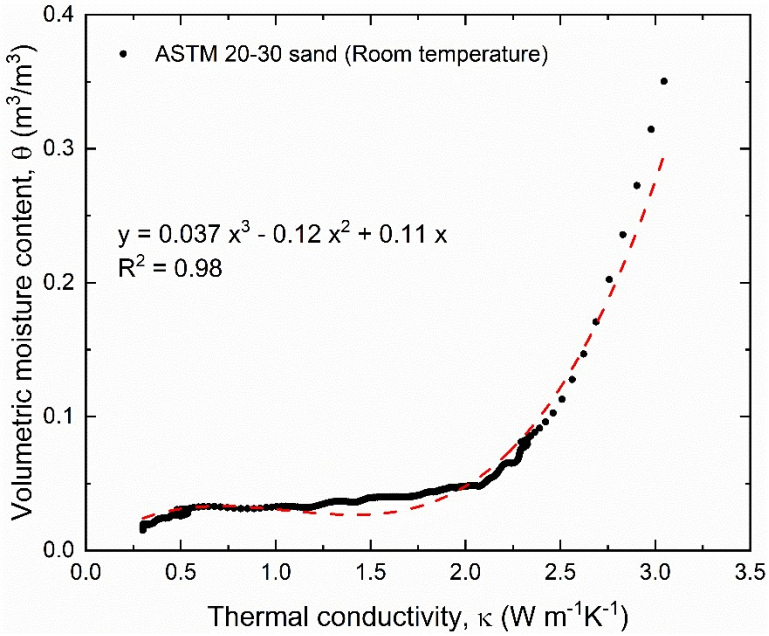


Figure 5.10 Measured TCDC and fitted curves for ASTM 20-30 sand at room temperature

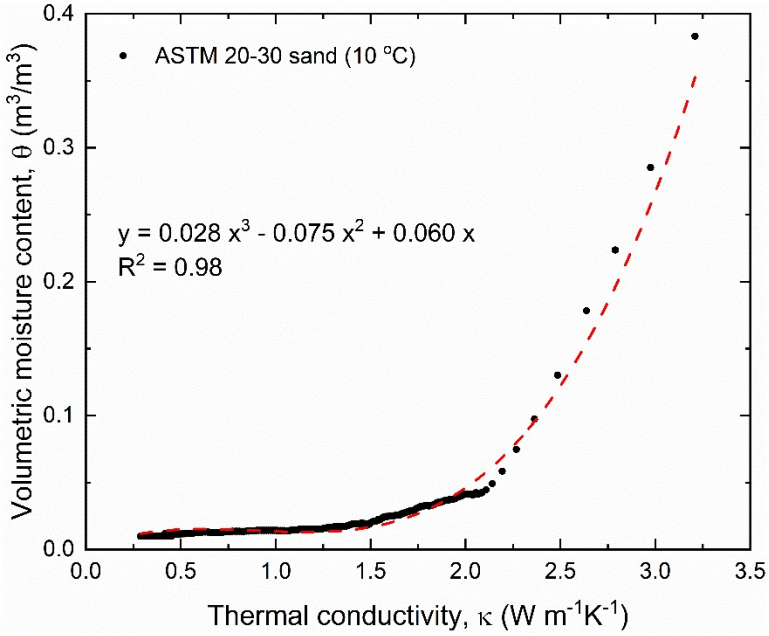


Figure 5.11 Measured TCDC and fitted curves for ASTM 20-30 sand at 10 °C temperature setting

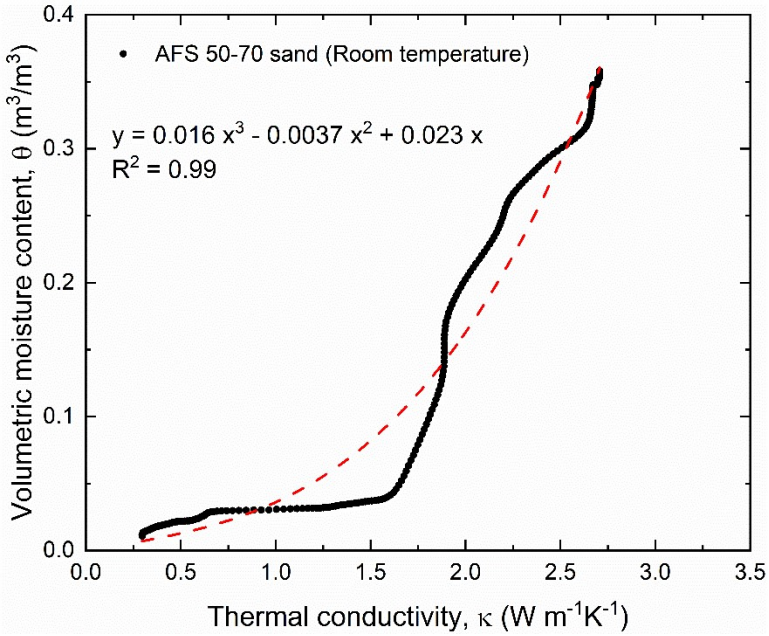


Figure 5.12 Measured TCDC and fitted curves for AFS 50-70 sand at room temperature

Table 5.1 summarizes the TCDC model's best-fit parameters. The coefficient of determination ($R^2$) for all the test results had a good performance.

Table 5.1 Summary of best-fit parameters for the TCDC model

| **Soil Type** | **Temperature, T (°C)** | **$\theta = a\kappa^3 - b\kappa^2 + c\kappa$** | | | |
|---|---|---|---|---|---|
| | | a | b | c | $R^2$ |
| **ASTM fine graded sand** | 24 | 0.035 | 0.084 | 0.073 | 0.99 |
| | 10 | 0.030 | 0.073 | 0.065 | 0.99 |
| | 2 | 0.030 | 0.067 | 0.053 | 0.99 |
| **ASTM 20-30 sand** | 24 | 0.037 | 0.12 | 0.11 | 0.98 |
| | 10 | 0.028 | 0.075 | 0.06 | 0.98 |
| **AFS 50-70 sand** | 24 | 0.016 | 0.0037 | 0.023 | 0.99 |

Based on the fitted curves from Figure 5.7 to 5.12. A TCDC model was developed and is written as

$$\theta = a\,\kappa^3 - b\,\kappa^2 + c\,\kappa \tag{6.1}$$

where

$\theta$ = volumetric moisture content ($m^3\ m^{-3}$); $\kappa$ = thermal conductivity ($W\ m^{-1}K^{-1}$); $a$, $b$, and $c$ = fitting parameters.

## 5.4 Summary

Based on the measured TCDCs, a model was developed. According to the fitting performance, the developed model shows an excellent match to the measured values. The TCDC model can predict the volumetric moisture content value from thermal conductivity. Also, it can expect thermal conductivity values from volumetric moisture content.

# 6 CHAPTER 6 Summary, Conclusion, and Recommendation

## 6.1 Introduction

This research primarily focused on understanding the soil thermal and hydraulic properties of sands during dry-out processes by determining how temperature affects the soil-water characteristics curve. Sensors are needed to accurately measure the soil thermal and hydraulic properties over the complete saturation regime and account for temperature. However, no verified sensors can provide accurate soil moisture measurements and density when the soil is subjected to moisture loss from saturation to dry and significant density change. Experimental techniques for precise simultaneous measuring soil suction, moisture content, and thermal properties were attempted. The soil-water characteristic curve (SWCC) and thermal conductivity dry-out curve (TCDC) are recognized methods used to present a relationship between soil matric suction and moisture content. However, research on this information gap was almost non-existent in the geotechnical literature. In this case, we were seeking soil moisture measurements that can directly and simultaneously measure the volumetric water content, soil matric suction, and thermal conductivity. Notably, studies on soil volume change during drainage were minuscule at best.

In this research, a newly designed thermo-TDR sensor was used for simultaneous soil thermal properties, moisture content, and dry density measurements. The measurement performance of the thermo-TDR sensor was investigated by performing a series of laboratory tests using different types of soil. The constraints of the sensor designation are presented in this article. The thermo-TDR sensor was fabricated following the design specifications. Nine different chemical reagents with known dielectric constant were utilized to perform calibration of the dielectric constant (Ka). Potassium chloride (KCl) and sodium chloride (NaCl) solutions of different concentrations were used to implement the calibration of electrical conductivity (ECb).

The accuracy and precision of the thermal properties measurement were evaluated by comparing and analyzing the measurement results from a thermal properties analyzer (KD2 Pro). Laboratory tests were performed on four standard sand, two site sand, one standard clay, and one site clay were implemented for a comprehensive evaluation of the sensor as well. Experimental results from a newly designed thermo-TDR sensor were compared to a previous version sensor by analyzing calibration and experiment results.

Laboratory experiments, using the newer designed thermo-TDR sensor and modified hanging column device (MHCD), were performed on sands for measuring thermal conductivity with the complete moisture spectrum during dry-out processes. These tests also determined the soil-water characteristic curve (SWCC) and thermal conductivity dry-out curve (TCDC) during drainage and evaporation processes at different temperatures. MHCD tests implemented with the thermo-TDR sensor, a suction sensor, and a thermal properties analyzer were conducted on three sands in different temperature environments.

A new continuum soil thermal conductivity model was developed and validated in this research. Laboratory experiments were tested on ASTM fine graded sand, ASTM 20-30 sand, and AFS 50-70 sand using a modified hanging column device at different temperature conditions. Chapter 4 details the present test materials, methods, and relevant results. The model was developed based on the thermal conductivity dry-out curve (TCDC). The purpose of this model is to evaluate relevant thermal conductivity values at corresponding volumetric moisture contents for different soil types and temperature conditions. The validation of the soil-water characteristic curve (SWCC) via the MHCD test method was demonstrated as well. Three SWCC models developed by (Brooks and Corey (1964), van Genuchten (1980), and Fredlund and Xing (1994) were used for SWCC validation.

## 6.2 Summary and Conclusion

A modified hanging column device with a newly designed thermo-TDR sensor, tensiometer, and thermal property analyzer was used in this study as competent tools that can accurately and rapidly attain soil moisture content, dry density, thermal properties, and matric suction measurements during drainage and evaporation processes. The primary summaries and conclusions of this research are listed below:

1) This research provides an overview of the performance of a newly designed thermo-TDR sensor, which has satisfied all the requirements with improvements based on previous experiences with the traditional TDR sensor. Lessons from earlier sensor fabrication successes and failures were used in the author's new approach to procedures such as soldering process, probe immobilizing, and wire connections.
2) Nine standard chemical solutions with known dielectric constants were used for the dielectric constant ($K_a$) calibration. The coefficient of determination ($R^2$) from the comparison of the known and thermo-TDR measured dielectric constant plot is 0.99 (1.00 is the best case in which the modeled values match the observed values). The calibrations of the thermo-TDR sensor for the electrical conductivity ($EC_b$) measurements were performed by measuring sodium chloride (NaCl) and potassium chloride (KCl) solutions of six different concentrations using electrical conductivity (EC) meter to establish references. The calibration results verified that the thermo-TDR sensor could satisfactorily measure both dielectric constant and electrical conductivity with the coefficient of determination ($R^2$) determined at 0.99 (1.00 is the best case). Note that the modeled values exactly match the observed values.

3) The effective sampling area of the newly designed thermo-TDR sensor was determined using the areas that make 70% and 90% contribution to the total electrical field energy. This was achieved by exporting FEM simulation results and further processing with MATLAB. A code developed by MATLAB was used for searching the elements with high electric energy density values. When the thermo-TDR sensor is embedded in water (with a dielectric constant of 81), the calculated total electrical field energy per unit length of the sensor is 1.948 e-6 J/m. The calculated effective sampling area is 1.69 $cm^2$. When the thermo-TDR sensor is embedded in saturated sand (with a dielectric constant of 26), the calculated total electrical field energy per unit length of the sensor is 6.253 e-5 J/m, which is smaller than the sensor submerged in water. The calculated effective sampling area is 1.58 $cm^2$, which is very close to the sampling area. The thermo-TDR sensor embedded in water is just slightly larger than the sensor embedded in saturated sand. The sample area is not highly sensitive to the relative dielectric constant.
4) Eight types of soils (seven sands and one clay) were selected for laboratory experiments for the thermo-TDR sensor performance evaluation. The coefficient of determination ($R^2$) value for the calibration relationship of the dielectric constant is over 0.95 for most of the soils, even close to 1, except for AFS 50-70 sand, which is 0.92. The coefficient of determination value for the calibration relationship of electrical conductivity is close to or above 0.9. The calibration relationship results of dielectric constant and electrical conductivity indicated that the newly designed thermo-TDR sensor has a good performance for both sand and clay. The calibration results illustrate that the sensor has an excellent performance for the measurement of thermal conductivity with a relative

deviation within 10%. A one-step method was used to predict soil gravimetric moisture content and dry density. A comparison between the measured and predicted values of gravimetric moisture content and dry density for sand and clay presented the relative deviation for both gravimetric moisture content and dry density prediction at 10%. Calibration equations for dielectric constant (Table 3.2) and electrical conductivity (Table 3.3) had an excellent linear relationship in two calibration equations in expectations of high accuracy of soil gravimetric moisture content and dry density. Therefore, the excellent performance of the thermo-TDR sensor was observed in measuring soil moisture content and dry density.

5) Dry-out tests were performed on sand via a modified hanging column device (MHCD) to monitor water content, matric suction, and sand thermal conductivity during drainage and evaporation processes. The device includes a top cap, a perforated bottom plate, an acrylic Tempe cell, and a standpipe. The bottom brass plate was covered with a high-air-entry nylon membrane, across which suction was affected by way of an external hanging-column water system. Three sensors were assembled radially into a soil sample at approximately the same height in the cell to determine corresponding soil moisture content, matric suction, and thermal conductivity measurements in the same situation. The installed sensors include one thermo-TDR sensor, one KD2 Pro thermal properties analyzer with a TR-1 thermal needle probe, and one T5x tensiometer.
6) Thermal conductivity dry-out curves (TCDCs) and soil water characteristic curves (SWCCs) during drainage and evaporation processes were determined using a modified hanging column device (MHCD) for three types of sands in different temperature environments (24 °C, 10 °C, and 2 °C). By comparing the soil-water characteristic

curves of ASTM 20-30 sand and ASTM fine graded sand at different temperatures, sand was determined to have a higher maximum volumetric moisture content at a lower temperature. Because of the increased water viscosity at low temperatures (Toselli et al. 1999). The three sands have very close values of the maximum matric suction at room temperature. The ASTM fine graded sand has a larger matric suction value than the ASTM 20-30 sand for the same moisture content. In addition, the AFS 50-70 sand has a larger matric suction value than the ASTM fine graded sand. The soils' matric suction for the same moisture content is more significant for soils with small particles. The values obtained from the Tempe cell are the average values of the whole soil sample, while the results from the T5x tensiometer are point measurements.

7) Soil water characteristic curves (SWCCs) were validated using the Brooks and Corey (BC) model, van Genuchten (VG) model, and Fredlund and Xing (FX) model for three different types of sands at three different temperature settings. The performance of fitted curves using the FX model was better than the other two models (BC and VG models).

8) A thermal conductivity dry-out curve (TCDC) model was developed based on laboratory experiments on sands at different temperatures. The TCDC model was written as a cubic polynomial function with three parameters. The TCDC model can predict the volumetric moisture content value from thermal conductivity. It can also predict thermal conductivity values from volumetric moisture content. The determination coefficient for the TCDC model fitted with three sands (ASTM fine graded sand, ASTM 20-30 sand, and AFS 50-70 sand) at different temperature environments (24 °C, 10 °C, and 2 °C) and are equal or greater than 0.98 in most cases.

## 6.3 Recommendations for Future Work

The recommendations for future work are listed below:

1) Functions from the thermo-TDR sensor and tensiometer can be combined. A new thermo-suction-TDR sensor may be designed and fabricated in the future. The current designed thermo-TDR sensor's main change is to replace the block material from epoxy to high-grade porous ceramic.
2) The developed thermal conductivity dry-out curve (TCDC) model needs to be validated by more different types of soils and larger temperature setting ranges.

# REFERENCES


Adam, D., and Markiewicz, R. (2009). "Energy from earth-coupled structures, foundations, tunnels and sewers." *Géotechnique*, 59(3), 229-236.

Alsherif, N. A., and McCartney, J. S. (2016). "Yielding of silt at high temperature and suction magnitudes." *Geotechnical and Geological Engineering*, 34(2), 501-514.

Amoozegar, A., Martin, K., and Hoover, M. (1989). "Effect of access hole properties on soil water content determination by neutron thermalization." *Soil Science Society of America Journal*, 53(2), 330-335.

Arulanandan, K. (1991). "Dielectric method for prediction of porosity of saturated soil." *Journal of Geotechnical Engineering*, 117(2), 319-330.

ASTM, D. (2008). "4944–11. Standard Test Method for Field Determina tion of Water (Moisture) Content of Soil By The Calcium Carbide Gas Pressure Tester." *ASTM D*, 425-488.

Bachmann, J., and van der Ploeg, R. R. (2002). "A review on recent developments in soil water retention theory: interfacial tension and temperature effects." *Journal of Plant Nutrition and Soil Science*, 165(4), 468-478.

Baker, J., and Allmaras, R. (1990). "System for automating and multiplexing soil moisture measurement by time-domain reflectometry." *Soil Science Society of America Journal*, 54(1), 1-6.

Baker, J., and Lascano, R. (1989). "The spatial sensitivity of time-domain reflectometry." *Soil Science*, 147(5), 378-384.

Benson, C. H., and Bosscher, P. J. (1999). "Time-domain reflectometry (TDR) in geotechnics: a review." *Nondestructive and automated testing for soil and rock properties*, ASTM International.

Bhat, A. M., and Singh, D. (2007). "A generalized relationship for estimating dielectric constant of soils." *Journal of ASTM International*, 4(7), 1-17.

Blackwell, J. (1956). "The axial-flow error in the thermal-conductivity probe." *Canadian Journal of Physics*, 34(4), 412-417.

Brandl, H. (2006). "Energy foundations and other thermo-active ground structures." *Géotechnique*, 56(2), 81-122.

Bristow, K. L., Kluitenberg, G. J., and Horton, R. (1994). "Measurement of soil thermal properties with a dual‐probe heat‐pulse technique." *Soil Science Society of America Journal*, 58(5), 1288-1294.

Brooks, R., and Corey, A. (1964). "Hydraulic properties of porous media, Hydrology Papers, No. 3, Colorado State University, Ft." *Collins, Colo*.

Buckingham, E. (1907). "Studies on the movement of soil moisture." *US Dept. Agic. Bur. Soils Bull.*, 38.

Burghignoli, A., Desideri, A., and Miliziano, S. (2000). "A laboratory study on the thermomechanical behaviour of clayey soils." *Canadian Geotechnical Journal*, 37(4), 764-780.

Campbell, G., Calissendorff, C., and Williams, J. (1991). "Probe for measuring soil specific heat using a heat‐pulse method." *Soil Science Society of America Journal*, 55(1), 291-293.

Campbell, J. E. (1990). "Dielectric properties and influence of conductivity in soils at one to fifty megahertz." *Soil Science Society of America Journal*, 54(2), 332-341.

Childs, E. C. (1969). "An introduction to the physical basis of soil water phenomena."

Clayton, W. S. (1996). "Relative permeability-saturation-capillary head relationships for air sparging in soils." Colorado School of Mines.

Craig, R. F. (2004). *Craig's soil mechanics*, CRC press.

Dalton, F. N., Herkelrath, W. N., Rawlins, D. S., and Rhoades, J. D. (1984). "Time-Domain Reflectometry: Simultaneous Measurement of Soil Water Content and Electrical Conductivity with a Single Probe." *Science*, 224(4652), 989.

Das, B. M., and Sobhan, K. (2013). *Principles of geotechnical engineering*, Cengage learning.

Davis, J. "Electrical property measurements of sea ice in situ using a wide-band borehole radar and a time-domain reflectometer." *Proc., Proc. Int. Workshop on the Remote Estimation of Sea Ice Thickness, St. John's Newf*, 80-85.

De Vries, D. (1952). "A nonstationary method for determining thermal conductivity of soil in situ." *Soil Science*, 73(2), 83-90.

Elder, A., and Rasmussen, T. C. (1994). "Neutron probe calibration in unsaturated tuff." *Soil Science Society of America Journal*, 58(5), 1301-1307.

Evett, S. (2000). "Some aspects of time domain reflectometry, neutron scattering, and capacitance methods for soil water content measurement."

Farouki, O. T. (1981). "Thermal properties of soils." COLD REGIONS RESEARCH AND ENGINEERING LAB HANOVER NH.

Fellner-Feldegg, H. (1969). "Measurement of dielectrics in the time domain." *The Journal of Physical Chemistry*, 73(3), 616-623.

Ferré, P. A., Knight, J. H., Rudolph, D. L., and Kachanoski, R. G. (1998). "The sample areas of conventional and alternative time domain reflectometry probes." *Water Resources Research*, 34(11), 2971-2979.

Fredlund, D. G., and Xing, A. (1994). "Equations for the soil-water characteristic curve." *Canadian geotechnical journal*, 31(4), 521-532.

Gardner, C., Dean, T., and Cooper, J. (1998). "Soil water content measurement with a high-frequency capacitance sensor." *Journal of Agricultural Engineering Research*, 71(4), 395-403.

Gaskin, G., and Miller, J. (1996). "Measurement of soil water content using a simplified impedance measuring technique." *Journal of agricultural engineering research*, 63(2), 153-159.

Giese, K., and Tiemann, R. (1975). "Determination of the complex permittivity from thin-sample time domain reflectometry improved analysis of the step response waveform." *Advances in Molecular Relaxation Processes*, 7(1), 45-59.

Heimovaara, T. J. (1993). "Design of Triple-Wire Time Domain Reflectometry Probes in Practice and Theory." *Soil Science Society of America journal*, 1993 v.57 no.6(no. 6), pp. 1410-1417.

Heitman, J., Horton, R., Sauer, T., and DeSutter, T. (2008). "Sensible heat observations reveal soil-water evaporation dynamics." *Journal of Hydrometeorology*, 9(1), 165-171.

Hernandez-Mejia, J. C., and Perkel, J. (2016). "Partial Discharge (PD) HV and EHV Power Cable Systems." *Cable Diagnostic Focused Initiative (CDFI); Georgia Tech Research Corporation: Atlanta, GA, USA*, 1-88.

Hilhorst, M., Dirksen, C., Kampers, F., and Feddes, R. (2001). "Dielectric relaxation of bound water versus soil matric pressure." *Soil Science Society of America Journal*, 65(2), 311-314.

Hilhorst, M. A. (2000). "A Pore Water Conductivity Sensor." *Soil Science Society of America Journal*, 64(6), 1922-1925.

Hillel, D. (2013). *Introduction to soil physics*, Academic press.

Huang, W., Fityus, S., and Wells, T. (2011). "Water content measurement in expansive soils using the neutron probe." *Geotechnical Testing Journal*, 34(3), 255-264.

Hueckel, T., François, B., and Laloui, L. (2009). "Explaining thermal failure in saturated clays." *Géotechnique*, 59(3), 197-212.

Jackson, T., Mansfield, K., Saafi, M., Colman, T., and Romine, P. (2008). "Measuring soil temperature and moisture using wireless MEMS sensors." *Measurement*, 41(4), 381-390.

Jacobsen, O. H., and Schjønning, P. (1993). "Field evaluation of time domain reflectometry for soil water measurements." *Journal of Hydrology*, 151(2-4), 159-172.

Jaeger, J. C. (1965). "Application of the theory of heat conduction to geothermal measurements." *Terrestrial heat flow*, 8, 7-23.

Jayawardane, N., Meyer, W., and Barrs, H. (1984). "Moisture measurement in a swelling clay soil using neutron moisture meters." *Soil Research*, 22(2), 109-117.

Johnston, I. W., Narsilio, G. A., and Colls, S. (2011). "Emerging geothermal energy technologies." *KSCE Journal of Civil Engineering*, 15(4), 643-653.

Kelly, S. F., Selker, J. S., and Green, J. L. (1995). "Using short soil moisture probes with high‐bandwidth time domain reflectometry instruments." *Soil Science Society of America Journal*, 59(1), 97-102.

Kluitenberg, G., Bristow, K. L., and Das, B. (1995). "Error analysis of heat pulse method for measuring soil heat capacity, diffusivity, and conductivity." *Soil Science Society of America Journal*, 59(3), 719-726.

Kluitenberg, G., Ham, J., and Bristow, K. L. (1993). "Error analysis of the heat pulse method for measuring soil volumetric heat capacity." *Soil Science Society of America Journal*, 57(6), 1444-1451.

Knellwolf, C., Peron, H., and Laloui, L. (2011). "Geotechnical Analysis of Heat Exchanger Piles." *Journal of Geotechnical and Geoenvironmental Engineering*, 137(10), 890-902.

Kupfer, K., Trinks, E., Wagner, N., and Hübner, C. (2007). "TDR measurements and simulations in high lossy bentonite materials." *Measurement Science and Technology*, 18(4), 1118.

Larson, T. H. (1988). "Thermal measurement of soils using a multineedle probe with a pulsed-point source." *Geophysics*, 53(2), 266-270.

Ledieu, J., De Ridder, P., De Clerck, P., and Dautrebande, S. (1986). "A method of measuring soil moisture by time-domain reflectometry." *Journal of Hydrology*, 88(3-4), 319-328.

Lei, G., Yu, X., and Li, T. "Design and Numerical Analysis of an Externally Heated Geothermal Bridge Deck." Springer International Publishing, 150-159.

Lekshmi, S., Singh, D. N., and Shojaei Baghini, M. (2014). "A critical review of soil moisture measurement." *Measurement*, 54, 92-105.

Li, J., Smith, D. W., and Fityus, S. G. (2003). "The effect of a gap between the access tube and the soil during neutron probe measurements." *Soil Research*, 41(1), 151-164.

Liu, X., Ren, T., and Horton, R. (2008). "Determination of soil bulk density with thermo-time domain reflectometry sensors." *Soil Science Society of America Journal*, 72(4), 1000-1005.

Loveridge, F., and Powrie, W. (2013). "Pile heat exchangers: thermal behaviour and interactions." *Proceedings of the ICE-Geotechnical Engineering*, 166(2), 178-196.

Lu, N., and Likos, W. J. (2004). *Unsaturated soil mechanics*, Wiley.

Lu, S., Ren, T., Gong, Y., and Horton, R. (2007). "An improved model for predicting soil thermal conductivity from water content at room temperature." *Soil Science Society of America Journal*, 71(1), 8-14.

Lu, Y., Liu, X., Heitman, J., Horton, R., and Ren, T. (2016). "Determining soil bulk density with thermo‐time domain reflectometry: A thermal conductivity‐based approach." *Soil Science Society of America Journal*, 80(1), 48-54.

Lu, Y., Lu, S., Horton, R., and Ren, T. (2014). "An empirical model for estimating soil thermal conductivity from texture, water content, and bulk density." *Soil Science Society of America Journal*, 78(6), 1859-1868.

Lubimova, H., Lusova, L., Firsov, F., Starikova, G., and Shushpanov, A. (1961). "Determination of surface heat flow in Mazesta (USSR)." *Annals of Geophysics*, 14(2), 157-167.

Malicki, M., Plagge, R., Renger, M., and Walczak, R. (1992). "Application of time-domain reflectometry (TDR) soil moisture miniprobe for the determination of unsaturated soil water characteristics from undisturbed soil cores." *Irrigation Science*, 13(2), 65-72.

Malicki, M. A., and Skierucha, W. M. (1989). "A manually controlled TDR soil moisture meter operating with 300 ps rise-time needle pulse." *Irrigation Science*, 10(2), 153-163.

Minet, J., Lambot, S., Delaide, G., Huisman, J. A., Vereecken, H., and Vanclooster, M. (2010). "A generalized frequency domain reflectometry modeling technique for soil electrical properties determination." *Vadose zone journal*, 9(4), 1063-1072.

Mittelbach, H., Lehner, I., and Seneviratne, S. I. (2012). "Comparison of four soil moisture sensor types under field conditions in Switzerland." *Journal of Hydrology*, 430, 39-49.

Noborio, K. (2001). "Measurement of soil water content and electrical conductivity by time domain reflectometry: a review." *Computers and Electronics in Agriculture*, 31(3), 213-237.

Ochsner, T. E., Horton, R., and Ren, T. (2001). "A new perspective on soil thermal properties." *Soil science society of America Journal*, 65(6), 1641-1647.

Olmanson, O. K., and Ochsner, T. E. (2008). "A partial cylindrical thermo‐time domain reflectometry sensor." *Soil Science Society of America Journal*, 72(3), 571-577.

Pepin, S., Livingston, N., and Hook, W. (1995). "Temperature‐dependent measurement errors in time domain reflectometry determinations of soil water." *Soil Science Society of America Journal*, 59(1), 38-43.

Persico, R., Cataldo, A., and De Benedetto, E. (2019). "Chapter 3 - Time-domain reflectometry: Current uses and new possibilities." *Innovation in Near-Surface Geophysics*, R. Persico, S. Piro, and N. Linford, eds., Elsevier, 59-96.

Persson, M., and Berndtsson, R. (1998). "Texture and electrical conductivity effects on temperature dependency in time domain reflectometry." *Soil Science Society of America Journal*, 62(4), 887-893.

Rajkai, K., and Ryden, B. (1992). "Measuring areal soil moisture distribution with the TDR method." *Geoderma*, 52(1-2), 73-85.

Ramo, S., Whinnery, J. R., and Van Duzer, T. (1965). *Fields and waves in communication electronics*, J. Wiley.

Rao, B. H., and Singh, D. (2011). "Moisture content determination by TDR and capacitance techniques: a comparative study." *Int. J. Earth Sci. Eng*, 4(6), 132-137.

Ren, T., Noborio, K., and Horton, R. (1999). "Measuring soil water content, electrical conductivity, and thermal properties with a thermo-time domain reflectometry probe." *Soil Science Society of America Journal*, 63(3), 450-457.

Rinaldi, V., and Francisca, F. (1999). "Impedance analysis of soil dielectric dispersion (1 MHz–1 GHz)." *Journal of Geotechnical and Geoenvironmental Engineering*, 125(2), 111-121.

Robert, A. (1998). "Dielectric permittivity of concrete between 50 MHz and 1 GHz and GPR measurements for building materials evaluation." *Journal of applied geophysics*, 40(1-3), 89-94.

Robinson, D. A., Campbell, C. S., Hopmans, J. W., Hornbuckle, B. K., Jones, S. B., Knight, R., Ogden, F., Selker, J., and Wendroth, O. (2008). "Soil Moisture Measurement for Ecological and Hydrological Watershed-Scale Observatories: A Review." *Vadose Zone Journal*, 7(1), 358-389.

Robinson, M., and Dean, T. (1993). "Measurement of near surface soil water content using a capacitance probe." *Hydrological Processes*, 7(1), 77-86.

Rohini, K., and Singh, D. N. (2004). "Methodology for determination of electrical properties of soils." *Journal of Testing and Evaluation*, 32(1), 62-68.

Schwartz, B. F., Schreiber, M. E., and Yan, T. (2008). "Quantifying field-scale soil moisture using electrical resistivity imaging." *Journal of Hydrology*, 362(3-4), 234-246.

Schwartz, R., Casanova, J., Bell, J., and Evett, S. (2014). "A reevaluation of time domain reflectometry propagation time determination in soils." *Vadose Zone Journal*, 13(1), 1-13.

Selig, E. T., and Mansukhani, S. (1975). "Relationship of soil moisture to the dielectric property." *Journal of Geotechnical and Geoenvironmental Engineering*, 101(ASCE# 11517 Proceeding).

Selker, J. S., Graff, L., and Steenhuis, T. (1993). "Noninvasive time domain reflectometry moisture measurement probe." *Soil Science Society of America Journal*, 57(4), 934-936.

Sheng, D., Fredlund, D. G., and Gens, A. (2008). "A new modeling approach for unsaturated soils using independent stress variables." *Canadian Geotechnical Journal*, 45(4), 511-534.

Siddiqui, S., and Drnevich, V. (1995). "Use of Time Domain Reflectometry for Determination of Water Content in Soil." *Joint Transportation Research Program*, 219.

Smits, K. M., Sakaki, T., Limsuwat, A., and Illangasekare, T. H. (2010). "Thermal Conductivity of Sands under Varying Moisture and Porosity in Drainage–Wetting Cycles." *Vadose Zone Journal*, 9(1), 172-180.

Sreedeep, S., Reshma, A., and Singh, D. (2004). "Measuring soil electrical resistivity using a resistivity box and a resistivity probe." *Geotechnical testing journal*, 27(4), 411-415.

Stein, J., and Kane, D. L. (1983). "Monitoring the unfrozen water content of soil and snow using time domain reflectometry." *Water Resources Research*, 19(6), 1573-1584.

Stogryn, A. (1971). "Equations for calculating the dielectric constant of saline water (correspondence)." *IEEE transactions on microwave theory and Techniques*, 19(8), 733-736.

SU, S. L., Singh, D., and Baghini, M. S. (2014). "A critical review of soil moisture measurement." *Measurement*, 54, 92-105.

Terhoeven-Urselmans, T., Schmidt, H., Joergensen, R. G., and Ludwig, B. (2008). "Usefulness of near-infrared spectroscopy to determine biological and chemical soil properties: Importance of sample pre-treatment." *Soil Biology and Biochemistry*, 40(5), 1178-1188.

Tian, Z., Heitman, J., Horton, R., and Ren, T. (2015). "Determining soil ice contents during freezing and thawing with thermo‐time domain reflectometry." *Vadose Zone Journal*, 14(8), 1-9.

Topp, G., Davis, J., and Annan, A. (1982). "Electromagnetic Determination of Soil Water Content Using TDR: I. Applications to Wetting Fronts and Steep Gradients 1." *Soil Science Society of America Journal*, 46(4), 672-678.

Topp, G., Zebchuk, W., Davis, J., and Bailey, W. (1984). "The measurement of soil water content using a portable TDR hand probe." *Canadian Journal of Soil Science*, 64(3), 313-321.

Topp, G. C., Davis, J. L., and Annan, A. P. (1980). "Electromagnetic determination of soil water content: Measurements in coaxial transmission lines." *Water Resources Research*, 16(3), 574-582.

Topp, G. C., Zegelin, S., and White, I. (2000). "Impacts of the Real and Imaginary Components of Relative Permittivity on Time Domain Reflectometry Measurements in Soils." *Soil Science Society of America Journal*, 64(4), 1244-1252.

Toselli, M., Flore, J., Marangoni, B., and Masia, A. (1999). "Effects of root-zone temperature on nitrogen accumulation by non-bearing apple trees." *The Journal of Horticultural Science and Biotechnology*, 74(1), 118-124.

Uchaipichat, A., and Khalili, N. (2009). "Experimental investigation of thermo-hydro-mechanical behaviour of an unsaturated silt." *Géotechnique*, 59(4), 339-353.

Van Genuchten, M. T. (1980). "A closed‐form equation for predicting the hydraulic conductivity of unsaturated soils." *Soil science society of America journal*, 44(5), 892-898.

Wang, X., and Yu, X. "Evaluation of Two Thermo-TDR Probes for Soil Moisture, Density, and Thermal Conductivity." Springer Singapore, 44-55.

Wang, Z., Lu, Y., Kojima, Y., Lu, S., Zhang, M., Chen, Y., and Horton, R. (2016). "Tangent line/second‐order bounded mean oscillation waveform analysis for short TDR probe." *Vadose Zone Journal*, 15(1), 1-7.

Whalley, W., Dean, T., and Izzard, P. (1992). "Evaluation of the capacitance technique as a method for dynamically measuring soil water content." *Journal of Agricultural Engineering Research*, 52, 147-155.

Xie, X., Lu, Y., Ren, T., and Horton, R. (2018). "An empirical model for estimating soil thermal diffusivity from texture, bulk density, and degree of saturation." *Journal of Hydrometeorology*, 19(2), 445-457.

Yao, J., Oh, H., Likos, W. J., and Tinjum, J. M. (2014). "Three laboratory methods for measuring thermal resistivity dryout curves of coarse-grained soils." *Geotechnical Testing Journal*, 37(6), 1056-1067.

Yu, X., and Drnevich, V. P. (2004). "Soil water content and dry density by time domain reflectometry." *Journal of Geotechnical and Geoenvironmental Engineering*, 130(9), 922-934.

Yu, X., Zhang, B., Tao, J., and Yu, X. (2013). "A new time-domain reflectometry bridge scour sensor." *Structural Health Monitoring*, 12(2), 99-113.

Yu, X., Zhang, N., Pradhan, A., Thapa, B., and Tjuatja, S. (2015). "Design and evaluation of a thermo-TDR probe for geothermal applications." *Geotechnical Testing Journal*, 38(6), 864-877.

Zazueta, F. S., and Xin, J. (1994). "Soil moisture sensors." *Soil Sci*, 73, 391-401.

Zegelin, S. J., White, I., and Jenkins, D. R. (1989). "Improved field probes for soil water content and electrical conductivity measurement using time domain reflectometry." *Water Resources Research*, 25(11), 2367-2376.

Zhang, N., Yu, X., and Li, T. (2017). "Numerical simulation of geothermal heated bridge deck." *DEStech Transactions on Materials Science and Engineering*(ictim).

Zhang, N., Yu, X., Pradhan, A., and Puppala, A. J. (2015). "Thermal conductivity of quartz sands by thermo-time domain reflectometry probe and model prediction." *Journal of Materials in Civil Engineering*, 27(12), 04015059.

Zhang, N., Yu, X., and Wang, X. (2018). "Validation of a Thermo–Time Domain Reflectometry Probe for Sand Thermal Conductivity Measurement in Drainage and Drying Processes." *Geotechnical Testing Journal*, 41(2), 403-412.

Zhou, A.-N., Sheng, D., and Li, J. (2014). "Modelling water retention and volume change behaviours of unsaturated soils in non-isothermal conditions." *Computers and Geotechnics*, 55, 1-13.

# VITA

Xuelin Wang was born on July 31st, 1992, in China. He completed his Bachelor of Science in civil engineering and computer science with a minor in mathematics at the University of Mount Union, Alliance, OH, in 2015.

In August 2015, he began his work in the graduate program of the Department of Civil Engineering at the University of Texas at Arlington, majoring in Geotechnical Engineering with a supervisor, Dr. Xinbao Yu. Under Dr. Yu's guidance, he pursued his research focus on the use of thermo-TDR for monitoring heat and moisture in geothermal applications. He finished all the course work and research tasks for the Doctor of Philosophy in Civil Engineering in December 2020.

This dissertation was written and presented by Xuelin Wang.